博士論文

Comparative pathological study on brain lesions relating to dementia of human

ヒトの認知症に関連する脳病変の比較病理学的研究

チェンバーズ　ジェームズ

Table of contents

Abbreviations

Aβ: amyloid β

AD: Alzheimer's disease

AGD: argyrophilic grain disease

ApoE: apolipoprotein E

APP: amyloid precursor protein

BB: Berlin blue

CAA: cerebral amyloid angiopathy

CBD: corticobasal degeneration

CL: ceroid-lipofuscin

FA: formic acid

HE: hematoxylin and eosin

HRP: horseradish peroxidase

LFB: luxol fast blue

LOAD: late onset Alzheimer's disease

MAPT: microtubule-associated protein tau

MBP: myelin basic protein

MCI: mild cognitive impairment

MRI: magnetic resonance imaging

MS: multiple sclerosis

MVAA: microvascular amyloid angiopathy

NA: normal aging

NEP: neprilysin

NFT: neurofibrillary tangle

PAM: periodic acid methenamine silver

PAS: periodic acid-Schiff

PBS: phosphate buffered saline

PiD: Pick's disease

PSEN: presenilin

PSP: progressive supranuclear palsy

RT: room temperature

SP: senile plaque

TBS: Tris-buffered saline

VD: vascular dementia

WM: white matter

Preface

The number of dementia patients is rapidly increasing in accordance with aging of the global population [Abbott 2011]. It is becoming a social problem due to its economical impact to the nations and a burden of care welfare to the family with a dementia patient. There are more than 30 dementing disorders in human. AD and vascular dementia VD covers more than 90% of the dementia cases. There is a substantial overlap between the pathology of AD and VD and thus there are patients with mixed type dementia in which lesions of both AD and VD are observed in their brain [Attems J 2014]. Though some risk factors of AD have been indicated, the most critical cause of this disease is aging. Curative treatment for AD is yet to be established, and once the pathological cascade starts, the disease will slowly progress until the patient dies.

The definitive diagnosis of AD relies on histopathological examination of postmortem brain tissues. SPs and NFTs are the two major lesions observed in the AD brain together with severe neuronal loss. The major components of SP and NFT are β amyloid (Aβ) and hyperphosphorylated tau, respectively. These lesions, especially SP that is considered to be the initial step of AD pathogenesis, are also seen in cognitively normal elderly people. However recent studies have revealed that the deposition of N-terminal subtype of Aβ is different between AD and normal aging brains. Various transgenic mouse strains that harbor the mutated gene responsible for the familial form of AD have been developed, although the familial form of AD accounts for less than 1% of AD cases. These mice develop numerous SPs within one year. In many

non-transgenic animal species, SPs develop age-dependently. For instance, SPs are often seen in dogs over 10 years old. However, neither in transgenic mouse models nor in non-transgenic animals, NFTs and subsequent neuronal loss had been reported before.

VD can be caused by various vasculopathies, such as arteriosclerosis, thrombosis and also Aβ angiopathy. Cerebral arteriosclerosis and thrombosis rarely occur in animals, while Aβ deposition in the cerebral blood vessel wall have been observed in various animal species. As mentioned above, cerebral accumulation of Aβ is also responsible for the pathogenesis of AD. Age-dependent accumulation of Aβ is attributed to a decrease in cerebral Aβ excretion or degradation rather than an increase in Aβ production. Therefore, a recent strategy for developing therapeutic application is focused on enhancing cerebral Aβ excretion and degradation.

In the present study, the author examined AD- and VD-related lesions in brains of various animal species, not only to seek for a suitable animal model, but also to compare the age-related changes in the brain among different animal species and to reveal common aging changes and species-specific changes of the aging brain in mammalian species. In chapter 1, the N-terminal subtypes of Aβ is examined in the brains of various animal species in order to determine whether Aβ deposition in the animal brains are normal aging phenomenon or related to AD pathology. In chapter 2, the pattern of vascular deposition of Aβ subtypes is discussed in association with the perivascular drainage system of the brain in squirrel monkeys. Also, the distribution of neprilysin (NEP), a major Aβ degradation enzyme, is demonstrated. In chapter 3,

WM lesions that are related to VD in humans, are examined in dogs in relation with capillary Aβ angiopathy. In chapter 4 and 5, pathogenesis of the felid-type Aβ deposition and NFTs are studied in the domestic cat and the leopard cat.

Chapter 1

Characterization of AβpN3 Deposition in the Brains of Dogs of Various Ages and Other Animal Species

1. Introduction

SPs are argyrophilic aggregates of Aβ fibrils formed in the brain parenchyma and are characteristic histopathological manifestations of AD [Masters 1985; Selkoe 1991]. However, SPs also develop in non-AD senescent brain tissues; i.e., "normal aging (NA)" brains [Aizenstein 2008; Armstrong 1996]. Recent studies have clinically described individuals in the non-AD group that displayed MCI, and whether MCI is a pre-AD state or a pathologically independent event is yet to be elucidated [Gauthier 2006; Petersen 1999].

Aβ deposits have been detected in the brains of dogs [Czasch 2006; Shimada 1991; Uchida 1991], cats [Brellou 2005; Nakamura 1996], monkeys [Nakamura 1995; Struble 1985; Walker 1990; Wisniewski 1973], bears [Cork 1988; Uchida 1995], wolverines [Roertgen 1996], camels [Nakamura 1995], and woodpeckers [Nakayama 1999]. In dogs, partial histopathological changes of AD are observed [Papaioannou 2001; Rofina 2003; Rofina 2004], but these animals do not develop the full pathology of AD of the human type including numerous NFTs and progressive neuronal loss, which cause concomitant dementia. Hence, transgenic mouse strains are usually used as experimental models of AD [Janus 2001; Wisniewski 2010]. Although the usefulness of transgenic mice is undisputed, these animals only replicate some aspects

of the disease and do not represent its systemic pathological features, especially the effects of aging [Philipson 2010; Sarasa 2009]. On the other hand, Aβ is deposited in the dog brain during aging at regions similar to those seen in aging humans [Head 2000]. Although dogs do not exhibit AD pathology *in toto*, some researchers think that aged canines display a pre-AD state and are therefore suitable models for studying age-dependent Aβ deposition [Papaioannou 2001; Cummings 1996; Nakayama 2004; Pugliese 2006].

Several subtypes of Aβ, which differ in the lengths of the peptides at their C- and N-terminals, are found in SP [Saido 1996]. Although AD and NA SP cannot be differentiated from each other using the C-terminal properties of their Aβ peptides [Fukumoto 1996], the Aβ species with an N-terminal pyroglutamate residue at position 3 (AβpN3) is the dominant N-terminal subtype in AD, and so can be used to discriminate AD from NA [Piccini 2005; Schilling 2008]. Hence, AβpN3 has recently received attention as a diagnostic marker and a therapeutic target for AD treatment [Gunn 2010; Marcello 2011]. In Down's syndrome, a congenital disease that leads to AD-like pathology early in life [Reeves 2001], the ratio of AβpN3 to AβN1 increases with age [Russo 1997]. However, the shift from AβN1-dominant to AβpN3-dominant deposition is under-represented in transgenic mouse models of AD [Gunn 2010].

In the present chapter, the author characterized AβN1 and AβpN3 deposition in canine brains of various ages in order to clarify whether the appearance of AβpN3 is an age-dependent phenomenon also in non-human animals and to examine brain pathology of human NA is detected in these animals. Furthermore, by comparing the

AβpN3 deposition observed in some species that are known to develop Aβ deposits (namely, cats, monkeys, bears, and woodpeckers) this study shows that Aβ N-terminal truncation at amino acid residue 3 is common among various animals and discuss the relevance of this peptide and the age-dependent formation of SP in vertebrates.

2. Materials and Methods

Canine Brains

Retrospective analysis was performed using paraffin-embedded tissues from 47 canine brains. The frontal cortex was selected for examination because this area is initially and consistently affected by Aβ deposition in an age-dependent manner in dogs [Yoshino 1996]. Dogs of various breeds and ages (ranging from 1 to 20 years old) were included in the materials (Table 1). The animals were euthanized or died spontaneously from various disorders. Brains were obtained from routine necropsies performed at the Department of Veterinary Pathology, Graduate School of Agricultural and Life Science, the University of Tokyo, or at the Department of Veterinary Pathology, Faculty of Agriculture, Kagoshima University. Individuals with major brain lesions, such as neoplasia or inflammatory disease that had been confirmed grossly or microscopically using hematoxylin and eosin (HE)-stained sections were excluded from the study. All brains were fixed in 10% phosphate-buffered formalin, coronally sliced, and then conventionally embedded in paraffin.

Brains of Other Species and AD

Additionally, paraffin-embedded brain tissue samples from a cat (*Felis catus*), an American black bear (*Ursus americanus*) [Uchida 1995], a greater spotted woodpecker (*Dendrocopos major*) [Nakayama 1999], and a Japanese macaque (*Macaca fuscata*), were examined (Table 2). The brains were obtained from routine necropsies performed at our laboratory. The brain tissue of an AD patient (73-year-old female, generously provided by Dr. Takao Makibuchi of the Saigata National Hospital) and a B6SJL APP-Tg mouse harboring human APP gene with the Swedish, Florida, and London familial AD mutations and human Presinilin1 gene with two familial AD mutations (purchased from the Jackson Laboratory, Bar Harbor, MA, USA) were also used.

Histopathology

The paraffin-embedded tissues were cut into 4-μm-thick serial sections. The deparaffinized sections were then stained with HE and PAM. The severity of SP formation was evaluated in the PAM-stained sections by counting the number of argyrophilic plaques under a microscope in 10 randomly chosen fields in the cortex (×100 power field). The mean number of plaques per field was graded into four: none (no argyrophilic plaque); mild (1-10 argyrophilic plaques); moderate (11-20 argyrophilic plaques); or severe (more than 21 argyrophilic plaques) (Table 1).

Immunohistochemistry

Consecutive sections were stained using the immunoenzyme technique to

examine the deposition of various C-terminal and N-terminal Aβ subtypes in each brain (Table 3). To inactivate endogenous peroxidase, deparaffinized sections were immersed in 1% hydrogen peroxide in methanol for 20 minutes and then washed with Tris-buffered saline (TBS). For Aβ antigen retrieval, the sections were immersed in 99% FA for 5 minutes. The sections were then incubated with primary antibodies listed in Table 3 at 4 °C overnight. Immunolabeled antigen was visualized using the Dako Envision+ System (Dako, Carpenteria, CA, USA). Shortly, the sections were incubated with the HRP Labeled Polymer at 37°C for 40 minutes, reacted with 0.05% 3'3-diaminobenzidine plus 0.03% hydrogen peroxide in tris-hydrochloric acid buffer, and then counterstained with hematoxylin. Negative controls were obtained by omitting the primary antibodies.

Indirect immunofluorescence double-staining

The immunofluorescence double-staining technique was also performed to determine the coexistence of the N-terminus and C-terminus varieties of Aβ peptide. The four combinations of primary antibodies listed in Table 3 were used; i.e., AβN1/AβC42, AβN1/AβC40, AβpN3/AβC42, and AβpN3/AβC40. After incubation with the primary antibodies at 4°C overnight, the sections were washed with TBS. As secondary antibodies, ALEXA488-conjugated goat anti-mouse IgG (Invitrogen, Eugene, OR, USA) and ALEXA594-conjugated goat anti-rabbit IgG (Molecular Probes, Eugene, OR, USA) were mixed in TBS, each at a dilution of 1:100. The sections were then incubated with the secondary antibody mixture at 37°C for one hour, mounted with

Vectashield (H-1500, Vector Laboratories, Burlingame, CA, USA), and examined under a Leica DMI 3000B fluorescence microscope (Leica Microsystems, Tokyo, Japan).

Evaluation of AβN1 and AβpN3 deposition in the canine brains

The immunoreactivity of AβN1 and AβpN3 in the brain parenchyma was examined throughout the whole circumference of the cortex under a microscope (×100) and was semiquantitatively scored as 0 (no staining), 1+ (few positively stained areas were detected), 2+ (positive staining was scattered less than half of the cortical circumference), 3+ (positive staining was scattered more than half of the cortical circumference), or 4+ (immunoreactive deposits were observed throughout the entire cortical circumference) (Table 1). Spearman's rank correlation coefficient (rs) with two-tailed *P*-value was performed to determine the significance of correlation between age and the mean AβN deposition score (Figure 1A).

3. Results

Parenchymal AβpN3 deposits in the canine brains

AβpN3 deposition in the cortical parenchyma was observed in the canine brains as early as 8 years of age and was observed in almost all dogs (15/18) over 13 years of age (Table 1). On the other hand, AβN1 was deposited as early as 7 years of age (Table 1). Both AβpN3 and AβN1 deposition increased significantly in an age-dependent manner (AβpN3 rs=0.999, $P<0.01$; AβN1 rs=0.589, $P<0.05$), although

the AβN1 deposition score showed a lower correlation coefficient, apparently due to the cessation of the increase in its levels in the second decade of life (Figure 1A). In fact, AβN1 was not detected in some of the very old dogs (Table 1, Nos. 35 and 42). Hence, the deposition of these two Aβ subtypes shifted from AβN1-dominant to AβpN3-dominant in the canine brains between the first decade and the second decade of life (Figure 1A). As the argyrophilic plaques developed, AβpN3 immunoreactivity was increased. The immunoreactivity of AβN1 did not exceed that of AβpN3 (Figure 1B). Even in the very old dogs, no SP developed when no AβpN3 was deposited (Table 1, Nos. 39 and 41). Furthermore, the dogs that displayed severe SP formation had a high AβpN3/AβN1 ratio (Figure 1B). In such dogs, AβpN3 was the main component of the SP (Figure 2A), and the centers of the SP were strongly immunopositive for AβpN3 (Figure 2B). However, the margins of the SP were negative for AβpN3 and AβN1 (Figures 2B and 2C).

Vascular AβpN3 deposition in the canine brains

Microvascular amyloid angiopathy (MVAA) was observed in the canine brains as early as 7 years of age, even in cases with no parenchymal deposition (Table 1). MVAA was distributed focally, frequently in the deep cortex and occasionally in the WM (Figure 3). The Aβ deposits in the vascullar wall consisted of both AβpN3 and AβN1 species, regardless of age (Figure 3A).

Aβ components of the SP observed in dogs and other animal species

As it has been previously described, AβpN3 was the predominant N-terminal Aβ species that composed the SPs of the AD patient (Figures 4 and 5). In the canine brains, the diffuse plaques contained C-terminal AβC42 but not AβC40 (Figure 5). Beside the dogs, SP also developed in the Japanese macaque, American black bear, and APP-transgenic mouse. No PAM-positive SP were detected in the cat or woodpecker, whereas Aβ deposits and Aβ angiopathy, respectively, were immunohistochemically confirmed in the two species. In the feline brain, weak diffuse Aβ42 deposition was observed in the deep cortex. However, these deposits were not recognized by either of the N-terminal antibodies used in this study. In the woodpecker brain, numerous AβpN3 and AβN1 positive MVAA were observed, similar to the results seen in dogs (Figure 3).

The SPs in the brains of the monkey and bear showed roughly equal immunoreactivity o the antibodies used in this study (Figure 5). The APP-transgenic mouse (B6SJL-Tg) was 14 weeks old, which corresponds to the initial phase of amyloid deposition in this mouse strain [The Jackson Laboratory, http://jaxmice.jax.org/strain/006554.html]. At this age, the mouse had not developed any AβpN3 deposits (Figure 5).

4. Discussion

Aβ protein is conserved among various animal species, and the amino acid sequence of canine full-length Aβ is identical to that of humans [Johnstone 1991; Selkoe 1987]. Aβ that have been truncated at the N-terminal position 3 is catalyzed by

glutaminyl cyclase, which produces abundant AβpN3 in the AD brain, but not in NA brain tissue [Schilling 2008; Schilling 2008]. Glutaminyl cyclase is also conserved among plants and animals and is widely distributed in the mammalian brain [Pohl 1991; Schilling 2008; Stephan 2009; Sykes 1999]. Therefore, as it has been recently demonstrated in monkeys [Hartig 2010], AβpN3 is presumably produced and deposited in the brain of many animals such as dogs, bears, woodpeckers and TG mice shown in this chapter.

Several questions are raised in consideration of common phenomena of brain aging among mammalian species. Is the formation of AβpN3-dominant SP specific to human AD? Furthermore, does AβpN3 production iduce AD pathogenesis (i.e. progressive neurodegeneration and neuronal loss) in non-human animals? In this chapter, the age-dependent deposition of AβpN3 was confirmed in canine brains. AβpN3 immunoreactivity was detected whenever argyrophilic plaques developed in dogs (Table 1). Also AβpN3 occupied the center of the SP (Figure 3). These findings may support the assertion that the production of AβpN3 enhances the aggregation of Aβ fibrils during the initial phase of SP formation in vivo [Schilling 2008; He 1999; Sanders 2009]. On the other hand, the margins of the SPs were negative for both AβpN3 and AβN1 (Figures 2B and 2C). This can be explained by the existence of other N-terminal-modified Aβ species (such as Aβp11-42 and Aβ17-42 [Portelius 2010; Tekirian 2001]) or by the relatively low sensitivity of the N-terminal antibodies compared to the C-terminal antibodies used in this study. The author concludes that the AβpN3 deposition is associated with SP formation in dogs.

However, since the dogs with severe AβpN3 deposition does not show NFTs and neuronal loss, the shift from AβN1-dominant to AβpN3-dominant deposition in the brain by itself is not likely to be the key event in AD onset; i.e., progression to marked neurodegeneration. Rather, as has been demonstrated in DS, AβpN3 production occurs in an age-dependent manner [Russo 1997]. This is also suggested by the absence of AβpN3 plaques in the young transgenic mouse. Since the only factor that is conclusively known to affect AD onset is aging, AβpN3 deposition may occur parallel to AD pathogenesis. However, it is evident that AβpN3 is specifically deposited in AD brains compared with age-matched control human brains [Schilling 2008]. The author assumes that AβpN3 is partially involved in AD pathogenesis; i.e., Aβ aggregation, although there may be other factors that make humans vulnerable to AD.

One of the current therapeutic strategies for AD is to suppress or dissolve fibrillar amyloid proteins using specific antibodies against Aβ [Citron 2004; Solomon 2004]. The N-terminal of the Aβ peptide is considered to be a significant target of such immunotherapy since the site is exposed to antibody binding even in its aggregated form [Bard 2003; Solomon 1997]. However, the immuno-dominant epitope within the Aβ peptide is likely to differ among mammalian species. Aβ-immunized mice and guinea pigs predominantly produce antibodies against the EFRH epitope, whereas rabbits and humans effectively produce antibodies against AβpN3 [Acero 2009; Britschgi 2009; Frenkel 2000]. It has been also reported that dogs immunized with full-length Aβ (Aβ1-42) produce antibodies specific to the N-terminal region [Head

2008]. In the report, the Aβ1-42 and Aβ1-40 levels in the frontal cortex were significantly decreased during a vaccination program (the dogs were 8.4 to 12.4 years old), although the recovery from their cognitive decline was very limited. The results of the present study indicate that dogs over the age of 10 are affected by AβpN3 deposition rather than deposition of the full-length Aβ peptide. Thus, it is possible that AβpN3, rather than AβN1, plays an important role in the Aβ-related neural and cognitive impairment in aged dogs [Bernedo 2009; Cummings 1996; Head 1998; Rofina 2006; Tapp 2003; Tapp 2003]. Indeed, recent studies have demonstrated the neurocytotoxicity of AβpN3 *in vitro* and *in vivo* [Russo 2002; Wirths 2009].

In this chapter, characteristic differences in Aβ deposition in the brain between each animal species were also examined. The aged dogs often developed MVAA composed of both AβpN3 and AβN1 in their WM (Figure 2). These lesions were distributed focally, suggesting the involvement of the vascular system in the development of these lesions. One possible explanation is a local drop in the perivascular drainage system [Weller1998]. Capillaries in the WM are at the distal extremities of this drainage system. In the feline brain, AβC42 deposits were detected in the deep cortex. However, these deposits were not recognized by any of the N-terminal antibodies used.

In conclusion, AβpN3 is deposited in the brains of many animal species, from birds to non-human primates, and in dogs this deposition is likely to be an age-dependent phenomenon. Although AβpN3 aggregation is inadequate for the onset of AD of the human type by itself, the impact of AβpN3 peptides on cognitive

deterioration in aged dogs should be determined to differentiate AD-related dementia from other kinds of cognitive decline, including mild cognitive impairment (MCI) [Vanderstichele 2005]. Further investigation on AβpN3 deposition in mammals in connection with age-related cognitive symptoms may elucidate the genuine pathology of AD.

5. Tables and Figures

Table 1. Breed, age, gender, severity of SP formation and Aβ N-terminal immunoreactivity scores of dogs

No.	Breed	Age (year)	Gender	SP(PAM)	Immunoreactivity score** AβpN3		AβN1	Focal MVAA AβpN3***
1	Beagle	1	ND*	-	0	=	0	-
2	Beagle	1	ND	-	0	=	0	-
3	Beagle	1	Female	-	0	=	0	-
4	Beagle	1	Female	-	0	=	0	-
5	Mixed breed	2	Male	-	0	=	0	-
6	Siberian Husky	3	Female	-	0	=	0	-
7	Beagle	3	Male	-	0	=	0	-
8	Shiba	5	ND	-	0	=	0	-
9	Jack Russell Terrier	5	Castrated male	-	0	=	0	-
10	Welsh Corgi	7	Female	-	0	=	0	-
11	Yorkshire Terrier	7	Female	-	0	<	1	+
12	Beagle	7	Male	-	0	=	0	-
13	Golden Retriever	7	Castrated male	-	0	=	0	-
14	Shih Tzu	8	Female	-	0	=	0	+
15	Yorkshire Terrier	8	Male	-	1	>	0	+
16	Labrador Retriever	8	Male	-	1	<	2	-
17	Unknown	9	ND	-	0	<	1	-
18	Golden Retriever	9	Spayed female	-	0	=	0	-
19	Whippet	9	Male	-	0	=	0	+
20	German Shepherd Dog	10	Male	-	0	<	1	-
21	Mixed breed	10	ND	-	0	<	1	-
22	Unknown	10	ND	-	1	<	2	-
23	Welsh Corgi	10	Female	mild	1	>	0	-
24	Shiba	11	ND	-	0	=	0	-
25	Shih Tzu	11	Female	-	0	=	0	-
26	Shetland Sheepdog	11	Male	-	1	>	0	-
27	Beagle	12	Female	-	0	=	0	-
28	Beagle	12	Female	-	0	=	0	+
29	Beagle	12	Male	-	0	=	0	-
30	Beagle	13	Male	moderate	1	>	0	+
31	Miniature Dachshund	13	Female	mild	1	>	0	+
32	Miniature Dachshund	13	Female	-	1	>	0	-
33	Chihuahua	13	Female	-	3	>	1	+
34	Yorkshire Terrier	14	ND	-	0	=	0	+
35	Mixed breed	14	Female	severe	3	>	0	+
36	Unknown	14	ND	moderate	4	=	4	+
37	Italian Greyhound	14	Castrated male	-	2	>	1	+
38	Pomeranian	15	Spayed female	-	3	>	2	+
39	Mixed breed	15	Female	-	0	<	1	+
40	Yorkshire Terrier	16	ND	moderate	3	=	3	+
41	Pomeranian	16	Female	-	0	<	1	+
42	Shih Tzu	16	Male	severe	3	>	0	+
43	Mixed breed	16	Male	mild	2	>	1	+
44	Maltese	18	ND	mild	3	>	1	+
45	Yorkshire Terrier	18	Male	-	1	=	1	+
46	Yorkshire Terrier	20	Castrated male	mild	2	>	1	+
47	Unknown	20	ND	severe	3	>	1	+

*Not determined; **Scoring of AβpN3 and AβN1 immunoreactivity 0: no staining, 1: little positive staining was detected, 2: positive staining was scattered in less than half of the cortical circumference, 3: positive staining was scattered throughout more than half of the cortical circumference, 4: immunoreactive deposits were observed throughout the entire cortical circumference; ***Focal MVAA: 5 or more capillaries were affected by AβpN3 deposition in a x400 power field.

Table 2. Age and gender of the animal species other than the dog used in the present study

Species	Age	Gender
Human: sporadic AD patient (*Homo sapiens*)	73y★	Female
APP-transgenic mouse: B6SJL-Tg hemizygote (*Mus musculus*)	14w★★	Male
Japanese macaque (*Macaca fuscata*)	>26y	ND★★★
American black bear (*Ursus americanus*)	20y	Female
Cat (*Felis catus*)	>18y	Female
Greater spotted woodpecker (*Dendrocopos major*)	>16y	Male

★Years. ★★Weeks. ★★★Not determined.

Table 3. Primary antibodies used in the present study

	Specificity	Clone	Dilution	Manufacturer
C-terminus	Aβ peptide ending at amino acid residue 42	Mouse monoclonal antibody (clone12F4)	1 : 1000	Millipore, Temecula, CA, USA
	Aβ peptide ending at amino acid residue 40	Mouse monoclonal antibody (clone11A5-B10)	1 : 1000	Millipore, Temecula, CA, USA
N-terminus	Aβ peptide starting at amino acid residue 1	Rabbit polyclonal antibody	1 : 100	IBL, Gunma, Japan
	Aβ peptide starting at amino acid residue 3 (pyroglutamate)	Rabbit polyclonal antibody	1 : 100	IBL, Gunma, Japan

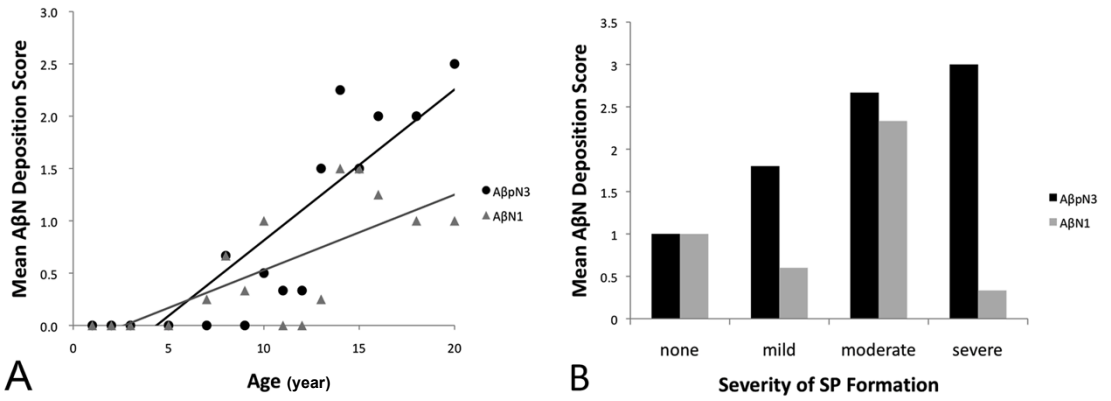

Figure 1. (A) Deposition of Aβ N-terminal species in different aged dogs. Both AβpN3 and AβN1 deposition significantly increased in an age-dependent manner (AβpN3 rs=0.999, $P<0.01$; AβN1 rs=0.589, $P<0.05$). The AβN1 deposition score showed a lower correlation coefficient than that of AβpN3, apparently due to the cessation of the increase in its levels in the second decade of life. (B) Comparison of AβpN3 and AβN1 deposition between groups displaying different degrees of SP formation. AβpN3 deposition increased with the progression of SP formation, whereas AβN1 deposition did not. Note that the severe SP formation group displayed a high AβpN3/AβN1 ratio.

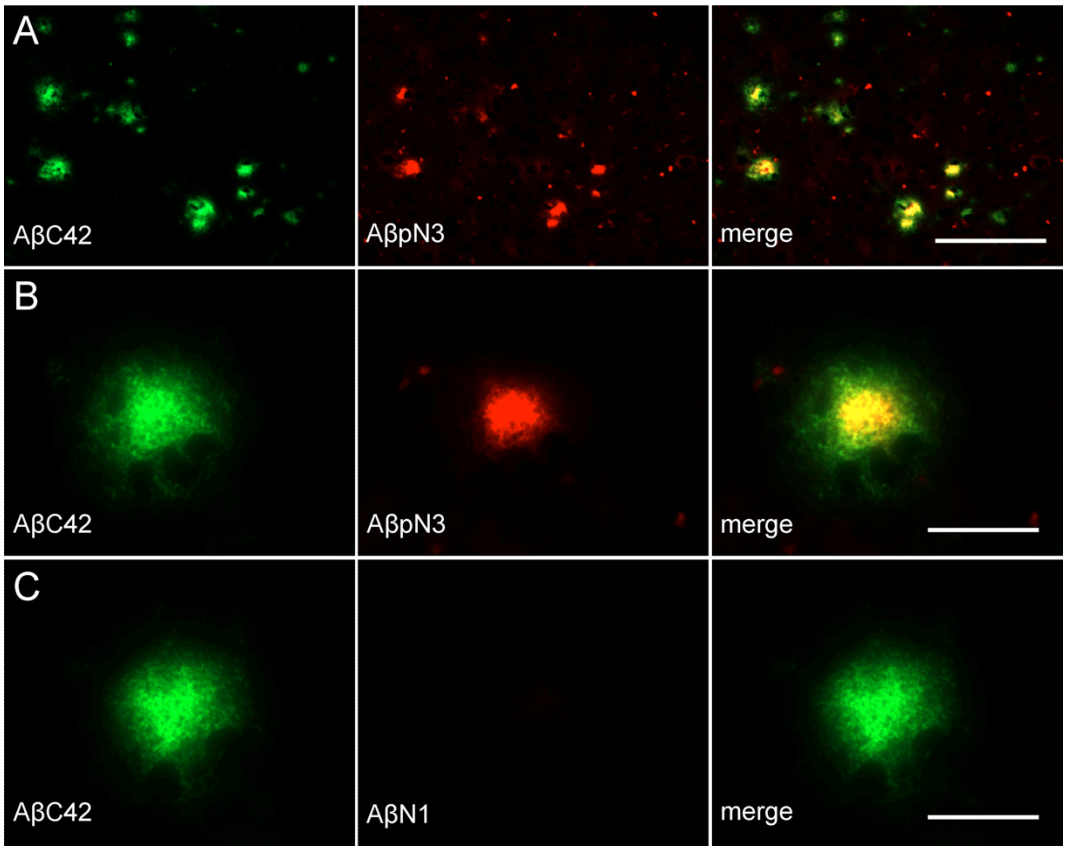

Figure 2. SPs in a dog brain (No. 47). Immunofluorescence double-staining for AβC42/AβpN3 (A and B) and AβC42/AβN1 (C). (A) AβpN3 was the main component of SP. (B and C) The center of the SP is strongly immunopositive for AβpN3. However, the margin of the SP is negative for AβpN3 and AβN1. b and c show the same SP in serial sections. Scale bars are 200 μm for A; 50 μm for B and C.

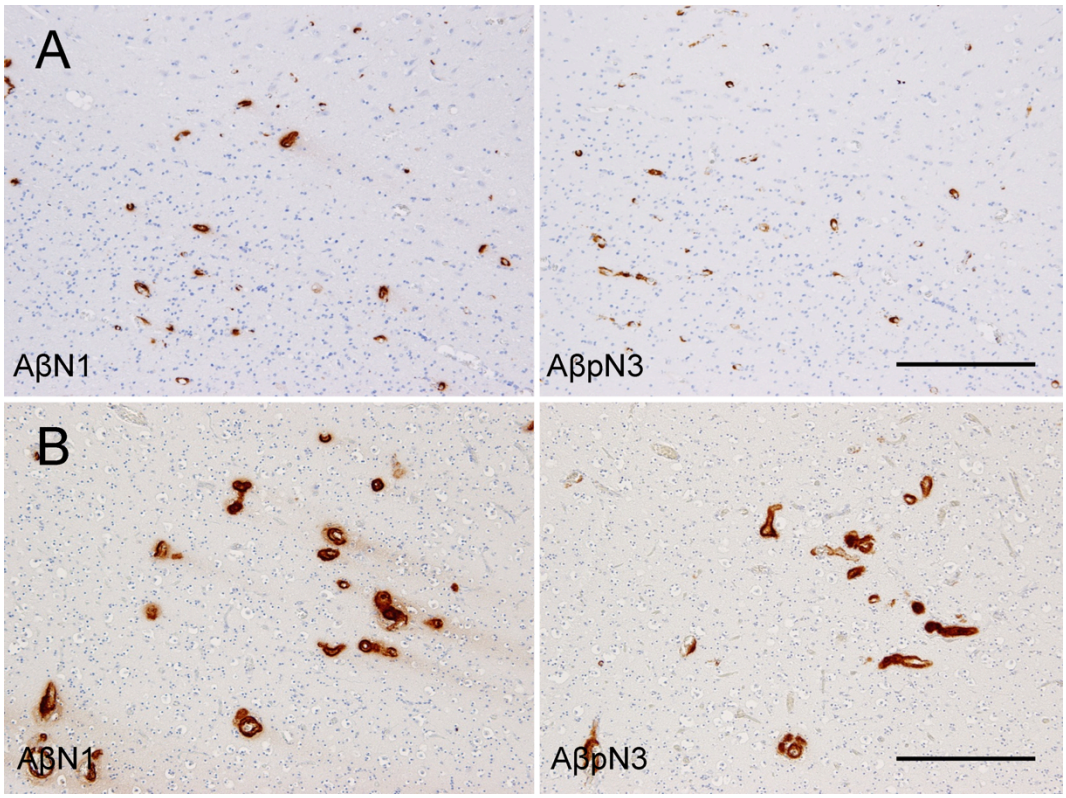

Figure 3. Microvascular Aβ deposits in a dog (A, No. 44) and a woodpecker (B). Both AβpN3 and AβN1 are deposited in the vascular walls. These lesions are distributed focally, mainly in the deep cortex and occasionally in the white matter. Scale bars are 200 μm.

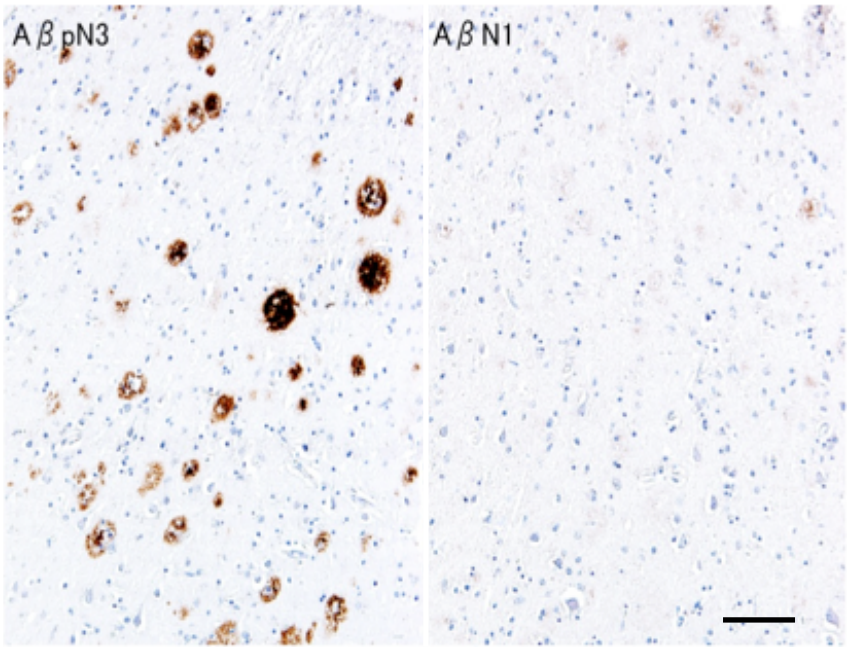

Figure 4. Aβ N-terminal subtypes in the cebral cortex of AD patient. SPs are mostly composed of AβpN3 while AβN1 deposition is subtle. Scale bar, 100μm.

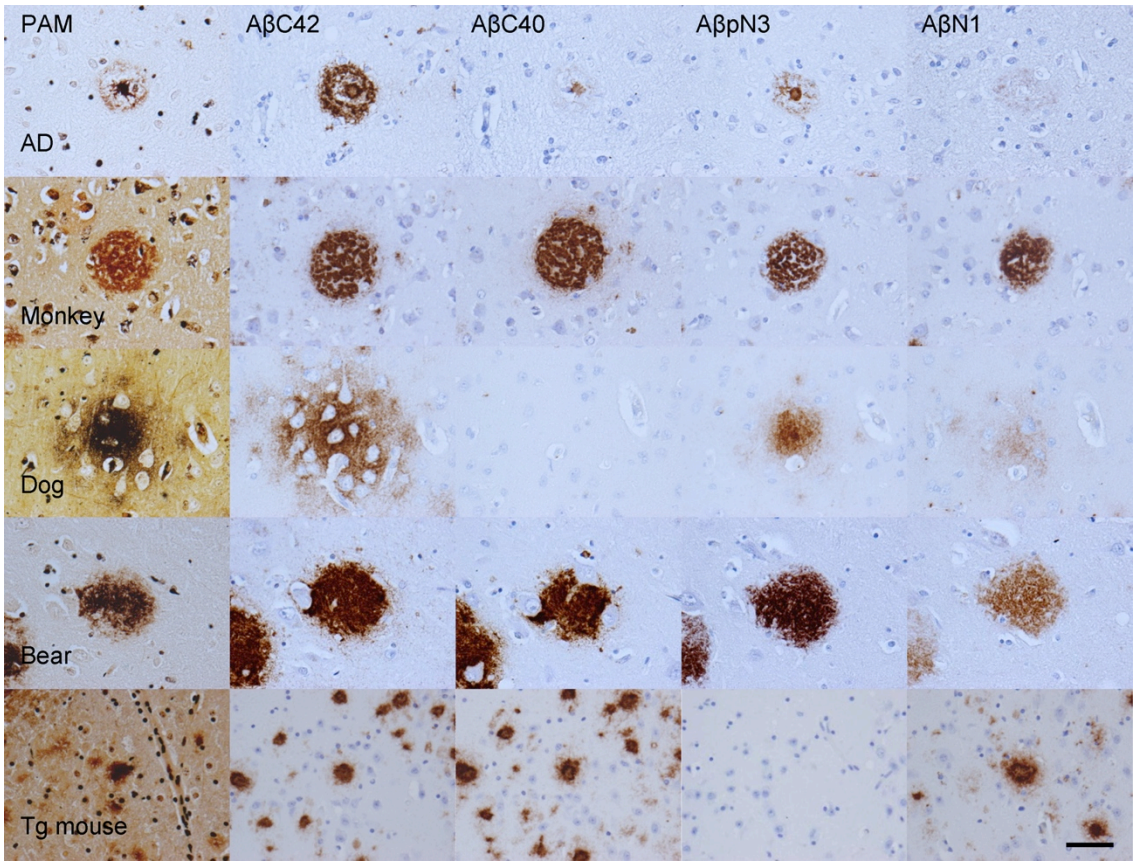

Figure 5. Serial sections of SPs in an AD patient, a macaque, a dog (No. 36), a bear, and a B6SJL-Tg mouse stained with PAM and immunostained for AβC42, AβC40, AβpN3 and AβN1. Scale bar, 40 μm.

6. Abstract

Senile plaques are characteristic histopathological manifestations of AD, but are also found in NA. Recent studies have demonstrated that Aβ proteins that have been truncated at the N-terminal position 3 are the predominant component of SPs in AD, but not in NA. The study in this chapter revealed that AβpN3 was deposited in an age-dependent manner in canine brains. Moreover, AβpN3 was the main component of the SPs that developed in very old dogs. The deposition of AβpN3 increased in accordance with the number of SPs, but that of N-terminally intact Aβ did not. In addition, AβpN3 was also deposited in the SPs of a Japanese macaque and an American black bear, but not in a feline brain. Focal microvascular cerebral amyloid angiopathy was also observed in the deep cortices and the white matter of the dogs and a woodpecker. Those were always composed of both AβpN3 and AβN1. In conclusion, though non-human animals do not develop full pathology of AD of the human type, AβpN3 is widely deposited in the brains of senescent vertebrates.

Chapter 2

Vascular Deposit Patterns of Aβ Subtypes in the Brains of Aged Squirrel Monkeys

1. Introduction

Aβ aggregates in the brain parenchyma and blood vessel walls with aging, and forms microscopic lesions termed SPs and cerebral amyloid angiopathy (CAA) [Hardy 2002; Revesz 2003]. In AD patients, excessive amounts of Aβ accumulate in the brain, with development of numerous SPs, and cause progressive cognitive deterioration due to neuronal impairment [Hardy 2002; LaFerla 1997]. AD is a major dementing disorder of humans, and CAA is known to aggravate the cognitive deficits of AD [Esiri 1999; Goedert 2006], making Aβ the principal factor in dementia in humans [Walsh 2004]. AD is becoming a social problem, due to the increasing number of patients with it and the lack of an effective cure for it.

An increase in production or decrease in clearance may cause accumulation of Aβ in the brain. However, it is known that excessive production of Aβ does not occur in more than 99% of AD patients, and decrease in Aβ clearance is considered the cause of the majority of AD cases [Farris 2007]. This common type of AD is termed late-onset AD (LOAD) or sporadic AD, because its clinical symptoms appear in the 60's or later, and there is no evidence of familial occurrence [Goedert 2006]. Therefore, examination of the degradation and clearance of Aβ is currently the central strategy in research on LOAD therapy. Recently, a major Aβ degrading protease, neprilysin (NEP), was identified [Iwata 2001; Iwata 2006; Shirotani 2001]. Research

with knockout mice has demonstrated that hypofunction of NEP not only promotes the development of SPs but also significantly increases the Aβ burden in blood vessels [Farris 2007] Moreover, NEP is reduced in AD brains, and is correlated with SP and CAA development [Miners 2006; Yasojima 2001], and has thus received attention as a target of AD therapy [Saido 2006].

In addition, the fact that more than 90% of AD patients develop CAA simultaneously suggests that a relationship exists between Aβ deposition in the blood vessels and decreased Aβ clearance from the brain [Attems 2008]. A decline of Aβ clearance via the transporters at the blood-brain barrier (BBB) or perivascular drainage of the brain interstitial fluid is considered the reason for manifestation of CAA [Weller 2008; Wilhelmus 1999].

Although Aβ deposits have been detected in brains of the dog [Czasch 2006; Shimada 1991; Uchida 1991; Uchida 1995], cat [Nakamura 1996], monkey [Nakamura 1995; Struble 1985; Walker 1990; Wisniewski 1973], bear [Cork 1988; Uchida 1995], wolverine [Roertgen 1996], camel [Nakamura 1995], and woodpecker [Nakayama 1999], it is generally believed that AD is a human-specific disease, since whether a correlation exists between such lesions and cognitive changes in animals is still controversial [Cummings 1996]. Hence, strains of transgenic mice have mainly been used as experimental models of AD and CAA [Gotz 2008; Herzig 2006], although these animals replicate only some aspects of the disease, and do not represent its systemic pathological features.

Squirrel monkeys are useful for AD and CAA research for several reasons: 1)

Aβ deposition occurs at an early age, e. g. in the teens, due to their relatively short lifespan; 2) they develop mature SPs comprised of a central core accompanied by degeneration of nearby axons, although the SPs are small compared to those in humans; 3) CAA is more prominent than SPs, in contrast to other primates such as the rhesus monkey [Walker 1990; Cork 1993; Walker 1987].

Researches on AD therapy are currently in progress worldwide, and monkeys are becoming an experimental animal model of integral importance to drug experimentation. The deposition patterns of two Aβ subtypes (Aβ40/Aβ42) and the distribution of the Aβ degrading enzyme NEP in the brains of aged squirrel monkeys are examined to obtain findings on this species as an experimental animal for studies of Aβ pathology.

2. Materials and Methods

Animals

Retrospective analysis was performed using paraffin-embedded brain tissues (fixed in 10% phosphate-buffered formalin) of 10 aged squirrel monkeys from the collection of the Laboratory of Pathology, Department of Veterinary Medicine, Azabu University. The monkeys were bred in different facilities in Japan, but necropsies were performed in our laboratory. The age (four of them unknown), genders, and pathological diagnoses of the monkeys are listed in Table. 1. None of the monkeys had a history of neurological abnormalities. All procedures in this study were in accordance with the guidelines approved by the Animal Research Committee of Azabu

University, and strictly adhere to Japanese law.

Histopathology

Transverse slices of the cerebrum and cerebellum were cut into 4-μm-thick sections. To evaluate SPs and CAA histochemically, deparaffinized sections were stained with PAM and Congo red, respectively. For PAM staining, sections were treated with 0.5% periodic acid for 15 minutes, washed in distilled water and then placed in methenamine silver solution in the dark at 60°C for 80 to 100 minutes. The methenamine silver solution consisted of 3% methenamine 40ml, 5% silver nitrate 2ml, and 5% borax 2ml.

Immunohistochemistry

The immunoenzyme technique was performed to examine deposition of two Aβ subtypes (Aβ40, Aβ42) and the distribution of the NEP expression in each brain. Tissue sections were mounted on glass slides coated with 3-aminopropyltriethoxysilane and deparaffinized in xylene. To deactivate endogenous peroxidase, the sections were immersed in 1% hydrogen peroxide in methanol for 20 minutes and washed with phosphate-buffered saline (PBS). For antigen retrieval for Aβ and NEP, sections were immersed in 99% formic acid (FA) for 10 minutes or autoclaved at 121°C for 10 minutes in citrate buffer (pH 6.0), respectively. After being washed with PBS, sections were treated with 5% skim milk at room temperature (RT) for 20 minutes to block nonspecific binding. Rabbit anti-Aβ1-42 polyclonal antibody (IBL, Gunma,

Japan), rabbit anti-Aβ1-40 polyclonal antibody (IBL, Gunma, Japan), and mouse anti-NEP monoclonal antibody (Novocastra, Newcastle, UK) were used as primary antibodies. All the antibodies were diluted to 1:100 with 1% bovine serum albumin containing PBS, mounted on slides, and incubated at 4°C overnight. After being washed in PBS, the sections were sequentially incubated with the peroxidase-conjugated secondary antibody Histofine-Simplestain MAX-PO (MULTI) (Nichirei, Tokyo, Japan) at RT for one hour. Immunolabeled antigen was visualized using 3'3-diaminobenzidine, and then counterstained with hematoxylin. Negative controls were obtained by omitting the primary antibodies. Aβ burden of each brain was evaluated by scoring the distribution of Aβ deposits and the severity of SP and CAA using sections stained for Aβ40 and Aβ42. The scoring criteria and results are listed in Table 1.

To clarify the patterns of deposition of the two Aβ subtypes in the blood vessel wall and parenchyma of the brain, indirect immunofluorescence double-staining technique was applied on a monkey brain with abundant Aβ deposition (No. 5). The same pretreatment with the immunoenzyme technique against Aβs was also performed. As primary antibodies, rabbit anti-Aβ1-42 polyclonal antibody (IBL) and mouse anti-Aβ35-40 monoclonal antibody (IBL, Gunma, Japan) were mixed in 1% bovine serum albumin containing PBS, each to a dilution of 1:100. After incubation with primary antibodies at RT for two hours, sections were washed with PBS. As secondary antibodies, ALEXA488-conjugated goat anti-rabbit IgG antibody (Invitrogen, Oregon, USA) and ALEXA568-conjugated goat anti-mouse IgG antibody (Invitrogen)

were mixed in 1% bovine serum albumin containing PBS, each to a dilution of 1:100. Sections were incubated with the secondary antibodies at RT for one hour, and examined under a fluorescence microscope.

3. Results

Aβ deposition in the brains of aged squirrel monkeys

The brains of 5 of 6 aged monkeys were positive for both subtypes of Aβ on immunohistochemistry, although the brains of monkeys under 11 years of age were negative for both (Table 1). Aβ deposits were observed predominantly in the parietal and temporal cortex in mild cases, but spread over the entire cortex and hippocampus in severe cases. SPs were observed predominantly in the third and fifth layers of the cerebral cortex (Figure 1). Deposition in the blood vessel walls was more pronounced than that in the parenchyma in all Aβ positive brains. In cases with high Aβ burden in the cerebrum, the meningeal vessels were also positive for Aβ in the cerebellum (Table 1). The Aβ in the cerebellum was comprised of both subtypes (Aβ40/Aβ42), without preponderance of either, although it was confined to the meningeal vessels and was not present in the cerebellum parenchyma. On a PAM stainined section, mature plaques with dystrophic neurites and diffuse plaques were observed in the cerebral cortex (Figures 2A and 2B). Some mature plaques could be observed on HE stained section (Figure 2C). Dense-core plaque-like structures were often found adjacent to capillaries (Figure 2D).

Distribution of NEP in squirrel monkey brains

Staining for NEP was positive in the caudate nucleus, putamen, globus pallidus, and substantia nigra, and weakly positive in the molecular layer of the dentate gyrus, exhibiting a diffuse fine-granular pattern (Figure 3). The cerebral cortex, hippocampus, and WM were negative for NEP immunoreactivity. NEP was thus not expressed where Aβ deposition occurs. However, neither differences in NEP and Aβ severity or age were found through immunohistochemical examination.

Patterns of deposition of Aβ subtypes in blood vessel walls

The patterns of deposition of the two Aβ subtypes in blood vessels were compared. Aβ40 was deposited predominantly in larger vessel walls such as arterioles in the meninges, whereas Aβ42 was deposited in capillary walls (Figure 4). To specify this pattern of selective deposition, immunofluorescence double-staining was performed for the two subtypes, and confirmed that the depositions of Aβ subtypes definitely differed between the arterioles and the capillaries that branch from the arterioles (Figures 5A and 5B). Furthermore, the dense-core plaques observed adjacent to the capillaries were strongly immunoreactive for Aβ42 (Figure 5C).

4. Discussion

Aβ deposition in brains of aged squirrel monkeys

Aβ is derived from amyloid precursor protein (APP), which is highly conserved among vertebrates [Collin 2004; Coulson 2000], and the cDNA sequence of

squirrel monkey APP is roughly identical to that in humans [Levy 1995]. APP is an integral membrane protein that is constitutively metabolized by α-secretase [Esch 1990; Sisodia 1990]. However, the plaques and vascular amyloid deposits of AD are principally composed of the 42 and 40 residue of Aβ proteins generated by sequential proteolysis of APP by β- and γ-secretase enzymes [Citron 1996; Vassar 1999; Walsh 2007]. The two subtypes of Aβ possess somewhat different biochemical properties that contribute to Aβ pathology. Aβ42 is more prone to fibril formation, and is initially deposited in association with SP formation [Iwatsubo 1994; Jarett 1993]. On the other hand, the comparatively soluble Aβ40 is physiologically present in the plasma and cerebrospinal fluid [Seubert 1992; Shoji 1992], and participates in SP maturation and vessel deposition [Herzig 2004].

In squirrel monkey brains, SPs were observed predominantly in the third and fifth layers of the cerebral cortex, but spread to the hippocampus in severe cases, similar to their localization in humans [Ogomori 1989]. As reported in dogs, transgenic mice, and AD patients [Ogomori 1989; Kumar-Singh 2005; Rofina 2003; Shimada 1992], dense-core plaques were often found adjacent to capillaries, indicating capillary-related SP formation in squirrel monkeys as well. The cores of these plaques were comprised of Aβ42 (Figure 5C), the subtype with more amyloidogenic character.

Distribution of NEP in squirrel monkey brains

NEP, also known as neutral endopeptidase, enkephalinase or CD10, is a type-II membrane metalloendopeptidase expressed in various tissues [Turner 1995;

Roques 1993]. In the brain, it is expressed on the synaptic membrane, and before it was recently established that NEP catabolizes Aβ peptides in the brain [Iwata 2000], it was known to degrade neuropeptides. The NEP distribution in the brain has been studied in humans [Akiyama 2001], pigs [Matsas 1986], dogs and cats [Takeuchi 2008], and mice [Fukami 2002], but not in non-human primates. Hence, this is the first study to demonstrate the NEP distribution in a non-human primate. In squirrel monkey brains, NEP was expressed in the caudate nucleus, putamen, globus pallidus, substantia nigra, and the molecular layer of the dentate gyrus (Figure 3). Although this distribution is generally consistent with that in humans and other animals, some differences in distribution exist among species in the dentate gyrus, hippocampus, and the cerebral cortex. NEP is not expressed in the dentate gyrus of dogs and cats [Takeuchi 2008], but is weakly expressed there in squirrel monkeys. In mice as well as humans, NEP is weakly expressed in the hippocampus and cerebral cortex, in addition to the dentate gyrus [Akiyama 2001; Fukami 2002]. However, NEP was not detected immunohistochemically in the hippocampus and cerebral cortex of squirrel monkeys (Figure 3). Although NEP immunoreactivity is known to decline in teh brains of AD patients, and exhibits a negative correlation with Aβ deposition [Wang 2005], in squirrel monkeys, as reported in dogs and cats, no differences in NEP immunoreactivity and either age or Aβ severity were found. Although quantitative analysis of NEP expression was not performed, the present immunohistochemical findings indicate that Aβ is deposited in the squirrel monkey brains in age-related fashion, in areas that constitutively lack NEP expression. These findings suggest that

Aβ aggregation is prevented by the constitutive expression of NEP. Nonhuman animals do not develop AD, and Aβ deposits in the animals are considered to be age-related rather than pathological. Therefore the decrease in NEP expression is not the direct cause of Aβ deposition in nonhuman animals. In fact, decreased NEP immunoreactivity is also not observed in the brains of humans without AD but with age-related Aβ deposits [Wang 2005].

Different distribution of Aβ40 and Aβ42 deposits in blood vessel walls

Brain-derived solutes of the interstitial fluid of the brain are partially drained via the perivascular pathway physiologically [Carare 2008]. Substantial evidence, including the abluminal deposition of Aβ in blood vessel walls, suggests that aggregation of soluble Aβ in the perivascular fluid participates in the pathogenesis of CAA [Weller 2008; Calhoun 1999; Preston 2003; Weller 1998]. Meningeal arterioles that penetrate vertically into the cortex collect the interstitial fluid of the perivascular drainage system, and are accompanied by the Virchow-Robin space. The present study demonstrated that Aβ40, the comparatively soluble subtype of Aβ, is selectively deposited in these types of vessels in squirrel monkeys, similarly to humans [Roher 1993]. It was previously found in an ultrastructural study that Aβ is deposited in the basal lamina of the blood vessels in squirrel monkey brains [Elfenbein 2007]. The author concludes that the pattern of selective deposition of soluble Aβ indicates perivascular drainage of Aβ in squirrel monkey brains. A pathological study of AD patients immunized against Aβ42, have demonstrated that the perivascular pathway

causes CAA in human brains [Boche 2008]. The present findings clearly shows that perivascular pathway participates in the development of CAA also in squirrel monkeys, which makes the squirrel monkey a suitable animal model for studying spontaneous Aβ pathology of the brain.

It is already known that, in squirrel monkey brains, dense-core plaques are often formed adjacent to the capillaries in the cerebral cortex [Walker 1990]. In this study, Aβ deposits in the capillary walls, as well as the dense-core plaques adjacent to them, were mainly composed of Aβ42 (Figure 5). These findings suggest that these dense-core plaques are associated with Aβ deposition in the capillaries. It has also been found in AD patients that Aβ42 tends to be deposited in the capillaries of the brain parenchyma, rather than the meningeal arterioles [Revesz 2003].

In addition to the perivascular clearance pathway mentioned above, certain transporters at the BBB are known to participate in Aβ clearance from the brain into the blood circulation [Weller 2008; Wilhelmus 2007]. The former pathway is mainly present at arterioles that are accompanied by the perivascular space, while the latter pathway is present at capillaries. Thus, these differences in patterns of deposition among types of vessels and Aβ subtypes suggest the presence of different mechanisms of clearance.

Unlike human cerebellum, Aβ deposits were not observed in the cerebellum of squirrel monkeys in previous studies [Elfenbein 2007; Bading 2002]. In the present study, however, vascular Aβ deposits were found in the cerebellar meninges in squirrel monkeys with severe Aβ burden in the cerebrum. This suggests that the Aβ in the

cerebellum originated in the cerebrum and was transferred from it via the perivascular drainage system to the cerebellar meninges, since there were no deposits in the cerebellar parenchyma or vessels elsewhere in the meninges.

Examination of the degradation and clearance of Aβ is currently the central strategy in LOAD therapy research. The immunohistochemical distribution of NEP in squirrel monkey brains is similar to that in human brains except for the absence of NEP in the cortex of squirrel monkey brains. The author concludes that in squirrel monkey brains the perivascular drainage system plays the main role in the clearance of Aβ deposition, which is somehow decreased in aged individuals. On the other hand, NEP does not contribute to the clearance of age-related Aβ deposition. Furthermore, the two subtypes of Aβ (Aβ40 and Aβ42) are likely to be exported through different vasculature-related clearance pathways. The contribution of the perivascular drainage system to the etiology of AD is currently being reviewed by researchers. Squirrel monkeys may be used for further study in the clearance mechanism of Aβ through the perivascular drainage system.

5. Tables and Figures

Table 1. Immunohistochemical scoring of Aβ severity.

Case	Age (years)	Gender	Distribution*	SP**	CAA***		Pathological Diagnoses
					Cerebrum	Cerebellum	
1	8	Female	−	−	−	−	Systemic hyperostosis
2	10	Male	−	−	−	−	Systemic hyperostosis
3	11	Female	−	−	−	−	Toxoplasmosis
4	11	Male	−	−	−	−	Asphyxia
5	15<	Female	++	+	++	+	Traumatic shock
6	18<	Female	++	++	++	+	Heat stroke
7	aged	Female	+	+	+	−	Subdural hemorrhage
8	aged	Female	++	+	+	+	Anesthetic death
9	aged	Female	+	+	+	−	Traumatic shock
10	aged	Female	−	−	−	−	Hemorrhagic death

*Distribution of Aβ deposits. −: negative. +: Aβ deposited mainly in the parietal and temporal cortex. ++: Aβ deposited diffusely throughout the entire cerebral cortex and hippocampus.
**Severity of SP. −: negative. +: mild. ++: severe.
***Severity of CAA. −: negative. +: mild. ++: severe.

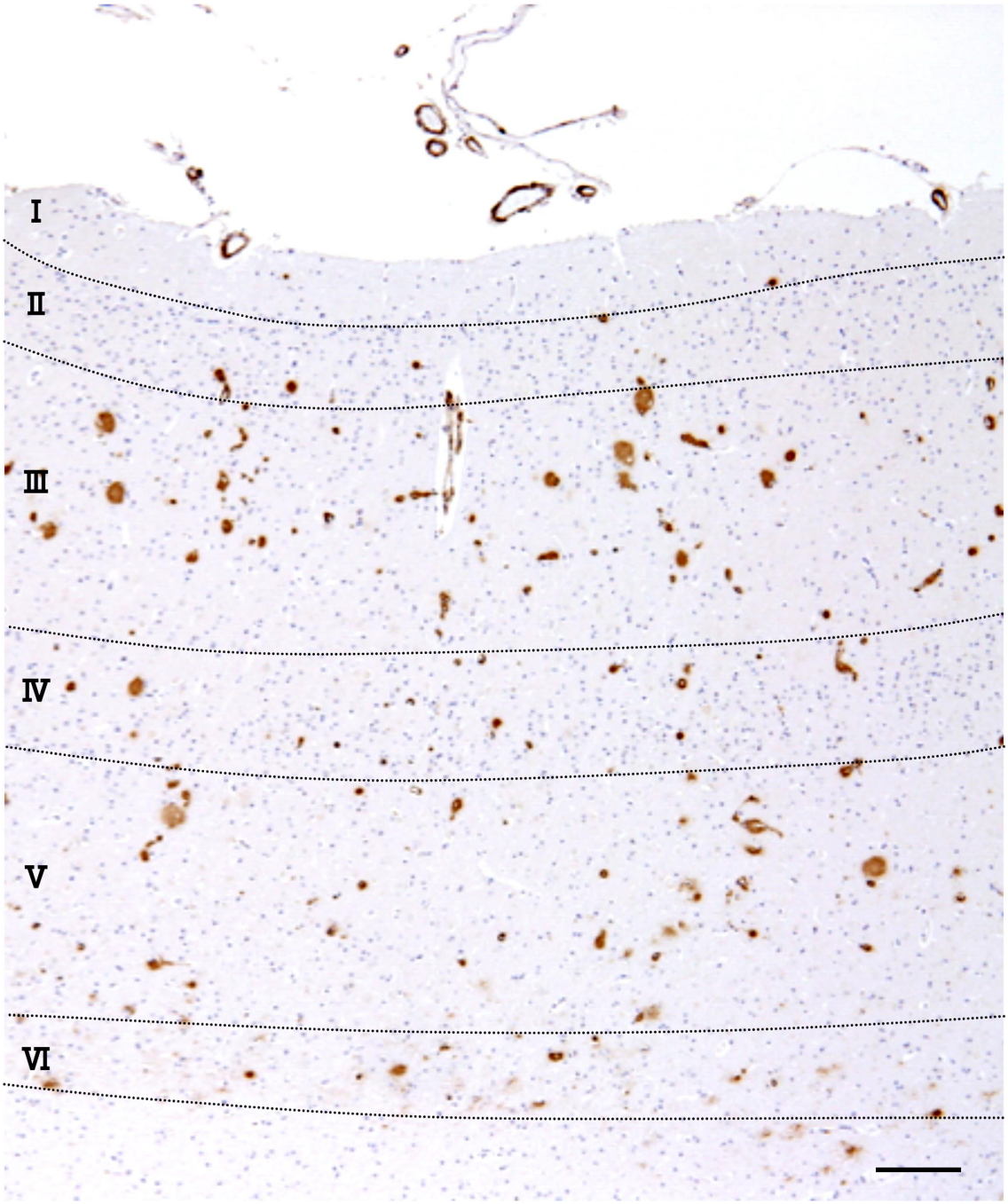

Figure 1. Immunohistochemistry for Aβ42. SPs are observed predominantly in the third and fifth layers of the cerebral cortex. Vessel walls in the meninges as well as the parenchyma are also positive for Aβ42 (bar = 100μm).

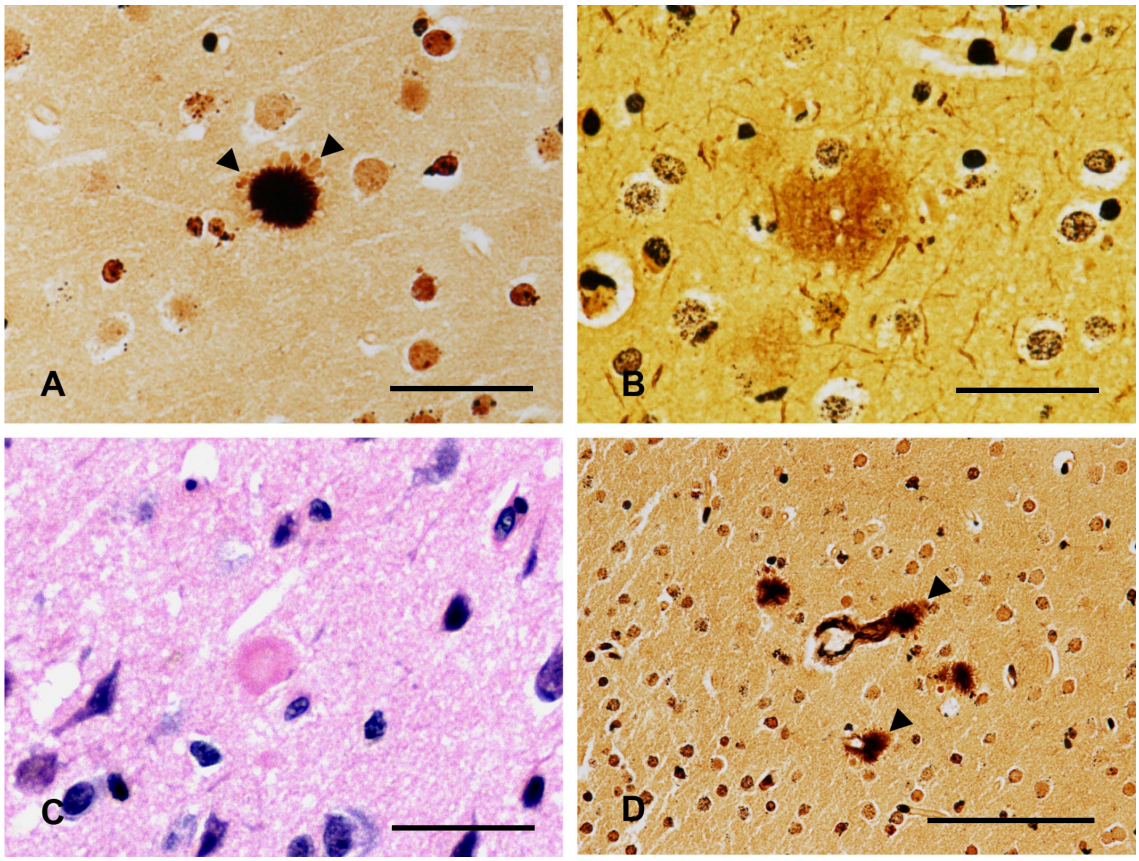

Figure 2. Senile plaques in the brains of squirrel monkeys. (A) Mature plaque with dystrophic neurites surrounding a central core (arrowheads). PAM staining (bar = 50μm). (B) Diffuse plaque without dystrophic neurites. PAM staining (bar = 50μm). (C) Mature plaque observed on a consecutive section. HE (bar = 50μm). (D) Dense-core plaque-like structures are observed adjacent to capillaries (arrowheads). PAM staining (bar = 100μm).

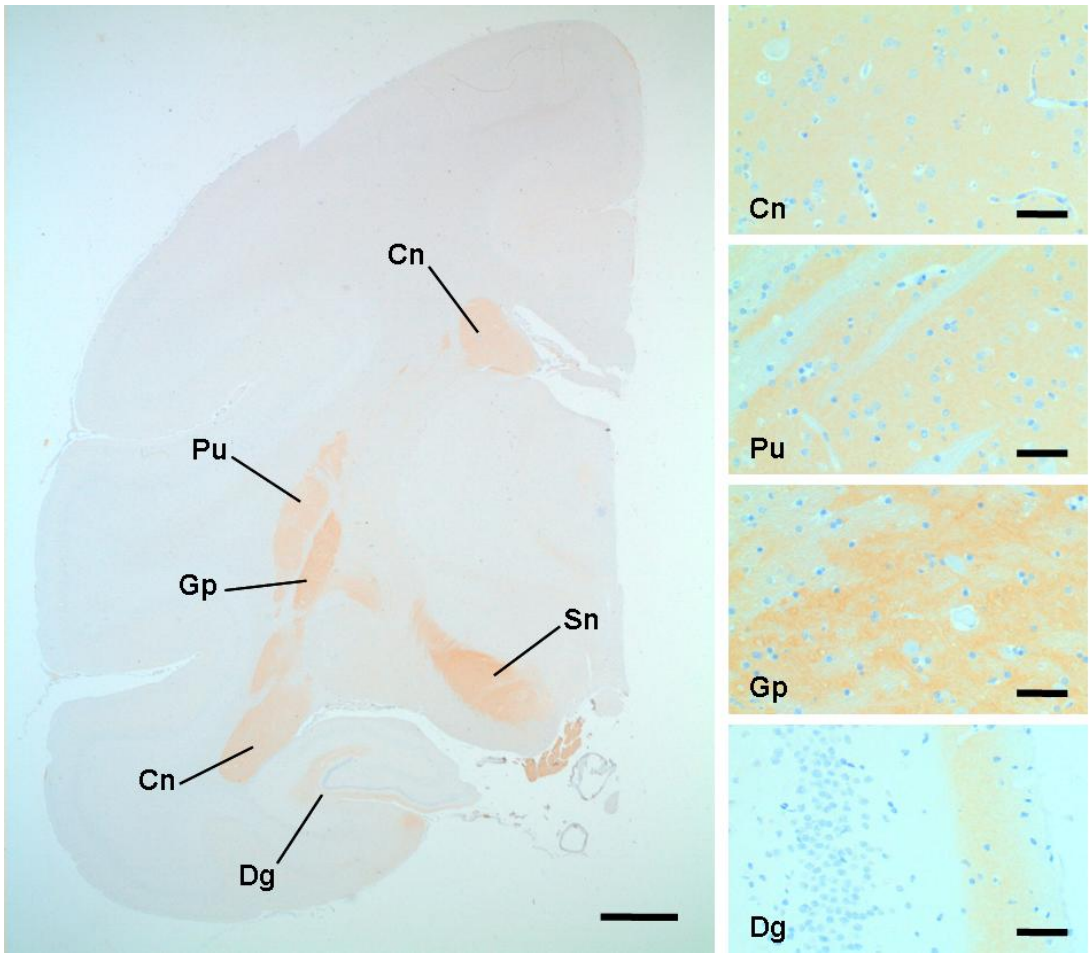

Figure 3. Transverse section of cerebrum. Case 10. Immunohistochemistry for NEP. Low-power field at left (bar = 2mm), and high-power field at right (bar = 50μm). Cn = caudate nucleus, Pu = putamen, Gp = globus pallidus, Dg = dentate gyrus, Sn = substantia nigra.

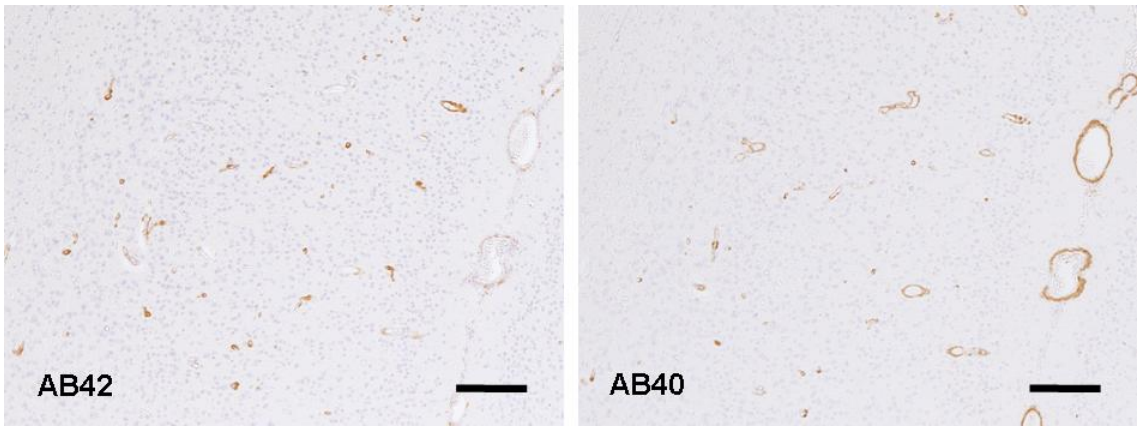

Figure 4. Serial sections stained for Aβ42 and Aβ40, respectively. Cerebral cortex of case 8. Aβ40 is deposited predominantly in larger vessel walls such as those of the arterioles in the meninges, whereas Aβ42 occupies capillary vessel walls (bar = 100μm).

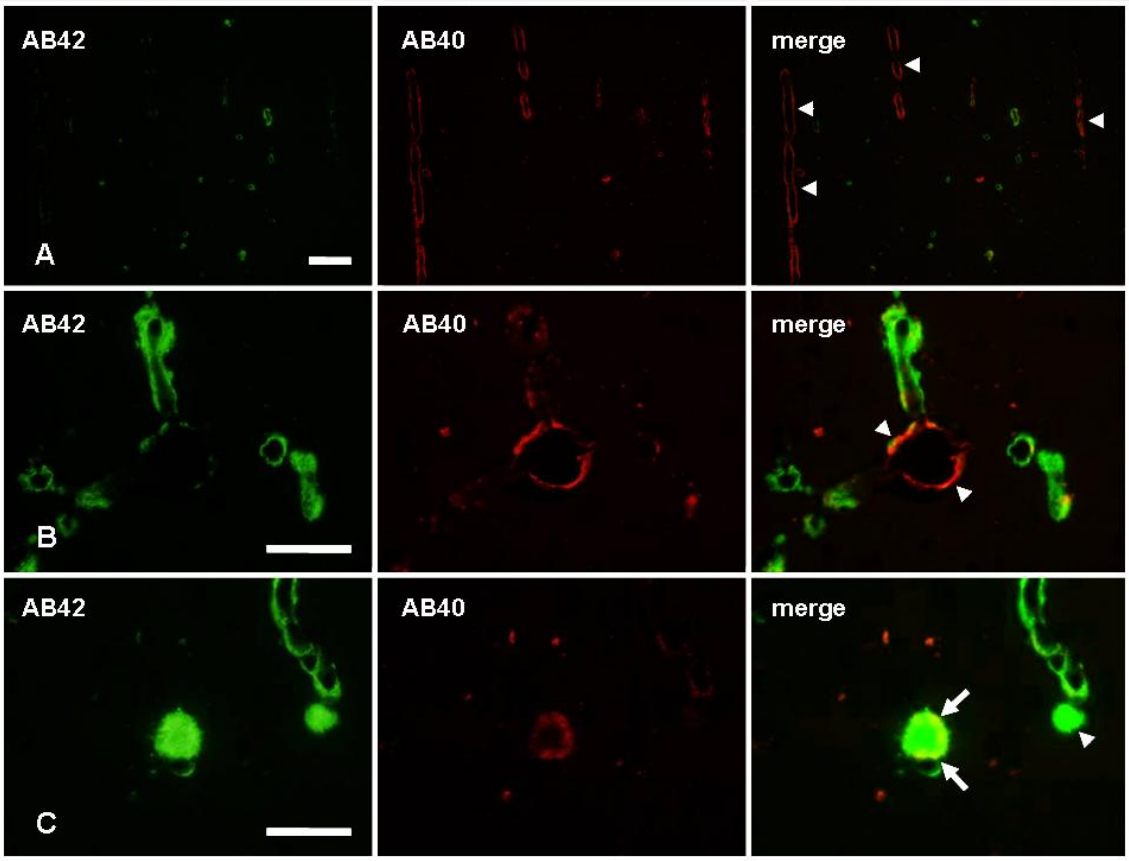

Figure 5. Immunofluorescence double-staining for Aβ42 (green) and Aβ40 (red). Cerebral cortex of case 5. (A) Low-power field (bar = 100μm). Aβ40 is deposited predominantly in the arterioles of the cerebral cortex that penetrate vertically from the meninges (arrowheads). (B) High-power field (bar = 50μm). Aβ42 is deposited predominantly in the capillaries that branch from the arterioles (arrowheads). (C) High-power field (bar = 50μm). The dense-core plaques observed adjacent to the capillaries are strongly immunoreactive for Aβ42 (arrowheads). Staining for Aβ40 is often positive at the margins of SPs, since it aggregated in addition to the Aβ42 core (arrows).

6. Abstract

Beta amyloid is deposited in the parenchyma and blood vessel walls of the aged brain, and forms lesions termed SPs and CAA. Since excessive Aβ is linked to cognitive deterioration in AD, the mechanisms of degradation and clearance of Aβ are now being researched for use in AD therapy. Deposition patterns of two Aβa subtypes (Aβ40 and Aβ42) and the distribution of the Aβ degrading enzyme NEP were studied in the brains of aged squirrel monkeys, a species known to develop CAA and SPs Aβ deposits were observed mainly in the cerebral cortex of five older monkeys, and were absent in monkeys under 12 years of age. NEP expression was observed in the caudate nucleus, putamen, globus pallidus, substantia nigra and the molecular layer of the dentate gyrus, and thus exhibited a distribution complementary to those of CAA and SPs in cerebral cortex and hippocampus. It is known that CAA is more prominent than SPs in squirrel monkey brains. In the present study, however, Aβ40 was deposited predominantly in the arterioles of the meninges and penetrates vertically into the cerebral cortex, whereas Aβ42 is deposited predominantly in the capillaries of the cerebral cortex. These distinct patterns of deposition of Aβ subtypes are likely related to the difference in biochemical character of these two subtypes.

Chapter 3

White matter myelin loss in the brains of aged dogs

1. Introduction

The degree of cerebral WM myelination is decreased in patients with VD, compared to that in normal aging controls (Ihara 2010). Also, the appearance of WM hyperintensity on magnetic resonance imaging (MRI) is a common manifestation of VD [Barber 1999; Ferrer 2010; Smith 2000]. Therefore, CAA is considered to be one of the major factors affecting WM myelin loss in the aged human brain [Roher 2003]. Although CAA is a manifestation of VD and AD, it is often observed in normal aging brains. MRI WM intensity increases even in cognitively normal senescent people. It has also been reported that the cortical myelin content is reduced in an age-dependent manner in cognitively normal human brains [Lintl 1983]. Since MRI WM hyperintensity is related to the onset and progression of dementia [Staekenborg 2009], it is necessary to assess the histological WM myelin density in subjects of various ages in order to confirm the occurrence of age-dependent myelin loss in the WM.

MRI WM-hyperintensity has been reported in the brains of aged dogs as well as humans [Kimotsuki 2005; Tapp 2006]. Also, dogs are known as an adequate animal model of CAA [Walker 1997]. The cerebral cortex and hippocamupus, which are severely affected by AD, have been extensively studied in aged dogs, although age-related changes in the canine cerebral WM are yet to be studied, particularly with regard to their relevance to the WM alterations that occur in elderly humans [Head

2011; Rofina 2006]. In Chapter 1, the author found the occurrence of CAA of the capillaries in the cerebral WM of aged dogs. In humans, the apolipoprotein E (Apo E) 4 genotype is associated with Aβ deposition in the WM vasculature [Trembath 2007], and Apo E4- Aβ complexes are deposited in the vascular walls of the perivascular drainage system [Attems 2011; Thal 2002]. Interestingly, dogs are homozygous for the Apo E4 allele (Sarasa 2010; Zicker 2008).

This study revealed age-dependent myelin loss in the canine brain, which was correlated with perivascular accumulation of ceroid-lipofuscin (CL)-laden phagocytes. It has been demonstrated in short-term experiments using mice that the cerebral perivascular space is a drainage route for soluble substances, while phagocytes can become stuck and accumulate within the perivascular space [Carare 2008]. However, no spontaneous lesions have been definitively linked to this putative drainage route. The novel insights that are presented in this paper will aid the elucidation of the alterations that occur in aging mammal brains.

2. Materials and Methods

Canine brains

Fifty-one canine brains were obtained through routine necropsies performed at the Departments of Veterinary Pathology the University of Tokyo and Kagoshima University. The ages of the dogs ranged from 1 to 20 years old. The dogs were euthanized or died spontaneously from various disorders, but individuals with major neurological symptoms or major brain lesions, such as neoplasia or inflammatory

diseases that had been confirmed grossly or microscopically using HE-stained sections were excluded from the study. Various breeds were included, although most of the dogs were small breed dogs, except for 4 large breed dogs (two Golden Retrievers, one Labrador Retriever, and one German Shepherd Dog, all of which died in the range of 7 to 10 years old). Age-related behavioral deficits were not assessed in the dogs. After they had died, their brains were fixed in 10% phosphate-buffered formalin, coronally sliced, and then conventionally embedded in paraffin blocks. The frontal lobe, where the vascular contribution to WM integrity is most severe in people with MCI and AD [Uh 2010] and also where Aβ is initially deposited in dogs [Yoshino 1996], was selected as the region of interest.

Histopathology

The paraffin-embedded tissues were cut into 4-μm-thick serial sections. Deparaffinized sections were then stained with HE for general pathological evaluation, and luxol fast blue (LFB) for assessing WM myelin density. Periodic acid Schiff (PAS) and Ziehl's carbol fuchsin stains were also done for the characterization of oxidized lipid pigments [Prophet 1992]. Berlin blue (BB) staining was performed to detect microhemorrhage in the cerebrum. Microhemorrhage of each dog brain was scored as: 0, no BB-positive staining; 1, few BB-positive macrophages; 2, aggregates of BB-positive macrophages; 3, small hematoma surrounded by BB-positive macrophages. Non-stained sections were also used for the detection of CL auto-fluorescence.

For immunohistochemistry, the antibodies listed in Table 1 were used as

primary antibodies Immunolabeled antigen was visualized using the Dako Envision+ System (Dako, Carpenteria, CA, USA). Shortly, the sections were incubated with HRP-labeled polymer at 37°C for 40 minutes, reacted with 0.05% 3'3-diaminobenzidine plus 0.03% hydrogen peroxide in tris-hydrochloric acid buffer, and then counterstained with hematoxylin. Negative controls were obtained by omitting the primary antibodies. The immunofluorescence double-staining technique was also performed to determine the perivascular coexistence of Aβ peptide and Apo E. After being incubated with the primary antibodies at 4°C overnight, the sections were washed with TBS. As secondary antibodies, Alexa488-conjugated goat anti-mouse IgG (Invitrogen, Carlsbad, CA, USA) and Alexa594-conjugated goat anti-rabbit IgG (Invitrogen) were mixed with TBS, at a dilution of 1:100. The sections were incubated with the secondary antibodies at 37°C for one hour, mounted with Vectashield (H-1500, Vector Laboratories, Burlingame, CA, USA), and examined under a Leica DMI 3000B fluorescence microscope (Leica Microsystems, Tokyo, Japan).

Confocal microscopy

To analyze the localization of perivascular CL-laden phagocytes and the vascular structure, 200-μm-thick sections were examined under a confocal microscope. Briefly, 10% phosphate-buffered formalin-fixed canine frontal lobes were embedded in 3% agarose and then sliced into 200 μm sections using a Microslicer DTK-1000 vibratome (DSK, Kyoto, Japan). Floating sections were then washed with 0.3% Triton X-100 (Sigma-Aldrich, St. Louis, MO, USA) and PBS and incubated in 10μg/ml

Proteinase K (Wako Pure Chemical, Osaka, Japan) at 37°C for one hour for antigen retrieval. After treating the sections with 5% skimmed milk to block nonspecific antigens, they were immersed in anti-collagen IV primary antibody at 4°C for two nights. As the secondary antibody, Alexa488-conjugated goat anti-rabbit IgG (Invitrogen) was applied at a dilution of 1:1000 overnight. Finally, the sections were mounted with Vectashield (Vector Laboratories). Three-dimensional images were reconstructed from 100 Z stack images (approximate optical thickness: 1μm) acquired with an Olympus FV10i-DOC laser scanning confocal microscope (Olympus, Tokyo, Japan). Using this method, the vascular structure could be visualized for CL particles using an aqueous staining procedure.

Semi-quantitative analyses of WM lesions

The myelin density of the WM was assessed using the method described by Yamamoto *et al.* with some minor modifications [Ihara 2010; Yamamoto 2009]. Briefly, 6 μm-thick paraffin sections were stained with LFB alone, and then TIFF images were captured with a Nikon COOLSCAN IV ED camera (Nikon Imaging, Tokyo, Japan). After the WM had been outlined using the wand tool, the area (mm^2) and the gray value [0 (white) to 255 (black)] of each pixel were measured using the Image J software (MBF Image J for microscopy, http://www.macbiophotonics.ca/imagej/index.htm). The mean WM gray value was calculated by dividing the total gray value by the number of pixels within the WM.

The number of total Aβ-laden vessels per square millimeter (CAA/mm^2) was

calculated by adding the number of vessels containing Aβx-40 and Aβx-42 deposits and dividing it by the WM area (mm^2) obtained above.

The degree of perivascular CL accumulation was assessed with PAS-stained sections Ten large vessels in the WM were examined and scored as 0 (no CL accumulation), 1 (less than a quarter of the vessel was surrounded by CL), 2 (less than half of the vessel was surrounded by CL), 3 (less than three quarters of the vessel were surrounded by CL), or 4 (more than three quarters of the vessel were surrounded by CL). The scores for the ten vessels were added up to give the total score (maximum score: 40).

Anti-Olig2 antibody was used as a marker of oligodendrocytes (Table 1), which was recently demonstrated in dogs (Millan et al., 2010). For each individual, high-magnification (x400) digital images were captured in 10 randomly selected areas within the WM, using a Nikon DXM1200F digital camera and the ACT-1 software (Nikon Instruments, Tokyo, Japan). The numbers of Olig2-positive nuclei and total nuclei were counted manually, and the percentage of Olig2-positive cells was calculated.

Spearman's rank correlation coefficient with two-tailed *P*-values was performed to determine the significance of the correlations between the mean WM gray value, age, CAA/mm^2, perivascular CL accumulation score, percentage of Olig2-positive cells, and the total number of cells within the WM, respectively. All of the dog brains were analyzed (n=51), except for 5 samples that showed no immunoreactivity with anti-Olig2 antibody, possibly due to a postmortem change

(Table 2).

3. Results

Significant correlations were confirmed between the age of the dogs and either the decrease in WM myelin density, the increase in the number of Aβ-laden vessels, the degree of perivascular CL accumulation, and the total number of cells within the WM (P<0.001, n=51) (Table 2 and Figure 2). The percentage of Olig2-positive cells did not show any significant correlation with the age of the dogs (r=-0.283, P<0.1, n=46) (Table 2). As shown in Figure 1, the LFB-stained myelin density was decreased throughout the WM, and no locational relationships with the vascular lesions described below were confirmed. There was no correlation between the percentage of Olig2-positive cells and myelin breakdown (r=0.193, P<1, n=46), whereas the total number of cells within the WM was negatively correlated with myelin breakdown (r=-0.439, P<0.001, n=51) (Table 2). Since the total number of the WM cells increased with aging, the faint staining for LFB in the aged dogs was not likely to have been due to the thickness of the sections.

In aged dogs, abundant pigment-laden phagocytes were observed within the perivascular spaces of the WM (Figure 3a). These pigments were positive for PAS, LFB, and Ziehl's carbol fuchsin (Figures. 3b and c) and also displayed auto-fluorescence. These staining patterns are consistent with those of CL. Such phagocytes were located between astrocyte foot processes that were positive for GFAP and the type IV collagen-positive basal lamina of the vessels. Myelin basic protein

(MBP)-positive granules were often detected in these phagocytes (Figure. 3d). A significant negative correlation was confirmed between WM myelin density and the degree of perivascular CL accumulation (r=-0.664, P<0.001, n=51) (Table 2 and Figure 2). Dogs of over 10 years of age consistently displayed some degree of perivascular CL accumulation in the WM. In addition, ubiquitin-positive granules were scattered throughout the WM of the aged dogs but not in young dogs (Figures 4a and b).

Although perivascular CL accumulation was mainly and frequently observed in the WM, it was also detected in the perivascular spaces of the cerebral cortex to a lesser extent (Figure 5a). Interestingly, these phagocytes seemed to be located at the bifurcations of the vascular branches (Figure 5b). Furthermore, abundant CL particles were seen in the meninges (Figure 5c).

In the canine brain WM, focal Aβx-42 and Aβx-40 deposits were observed in the vessel walls, but not in the parenchyma. Interestingly, most of the vascular Aβ deposits in the WM were located in the capillary walls and rarely in arteriole walls (Figure 4c and d). However, all the dogs with WM Aβ deposition had cortical Aβ deposition. Cortical Aβ deposits of aged dogs were observed in the parenchyma, vessels and most severely in the meningeal arterioles, as it has been previously described [Borras 1999; Uchida 1991; Uchida 1992; Yoshino 1996]. Aβx-42 and Aβx-40 were deposited in a similar pattern, although the number of Aβx-40-laden vessels was slightly less. In addition, a significant correlation was detected between the number of total Aβ-laden vessels per square millimeter and WM myelin density (r=-0.647, P<0.001, n=51) (Table 2 and Figure 2). The immunofluorescent

double-staining technique revealed the colocalization of Aβx-42 and Apo E protein in some capillary walls (Figures 6a and b).

No microhemorrhage was observed in the younger dogs (5-9 years old). In aged dogs (10-14 years old and 15-20 years old), microhemorrhages were occasionally observed in the cerebral cortices in relation with meningeal arterioles, but not in the WM (Figure 7).

4. Discussion

In the present study, age-dependent WM myelin loss was histologically confirmed in aged canine brains (Table 2 and Figure 2). Since the percentage of Olig2-positive cells did not decrease along with myelin density (Table 2 and Figure 2), it is likely that the demyelination observed in the aged dogs was due to the breakdown of the myelin sheath membrane rather than a decrease in the number of oligodendrocytes. On the other hand, the total number of cells within the WM increased during the demyelination process, indicating the reactive proliferation of glial cells.

Several mechanisms have been proposed for the pathogenesis of WM demyelination in elderly humans. In patients with VD, myelin density is more severely reduced than in other dementing disorders and age-matched-controls [Ihara 2010]. Another factor involved in WM demyelination is oxidative stress, which is a common aging phenomenon among humans and dogs [Head 2002; Head 2009; Head 2008; Opii 2008]. Interestingly, feeding dogs with antioxidants improves age-related

cognitive dysfunction, possibly by reducing free radicals in the brain [Cotman 2002; Skoumalova 2003]. Aβ is related to both VD and oxidative stress, and is known to elicit myelin damage [Thal 2007; Varadarajan 2000; Xu 2001].

In humans, CAA is morphologically categorized into two types according to whether Aβ is deposited in the capillary walls, in addition to larger vessels [Attems 2010; Thal 2002]. The Apo E4 genotype is associated with CAA in the WM [Trembath 2007] and is known to induce blood flow disturbance [Thal 2009]. Also, the Apo E4 genotype is related to the age-dependent loss of WM integrity in humans [Ryan 2011]. The present study revealed the colocalization of Apo E and Aβ in the capillary walls of the aged canine brain. It should be noted that dogs are homozygous for the Apo E4 allele [Sarasa 2010; Zicker 2008]. Apo E4-Aβ complexes aggregate within the basement membranes of capillaries, leading to the development of CAA [Attems 2011; Rolyan 2011]. The high occurrence of WM capillary CAA in dogs is likely to be a trait of this species, since WM CAA is very limited in humans. The present study suggests that, at least in dogs, capillary CAA may be one of the factors that impair WM integrity [Brown 2000; Iwamoto 1997].

The degree of perivascular CL accumulation was correlated with age and also with the decrease in myelin density (Table 2). The significance of the correlation and the distribution of the lesions (i.e., WM) indicate that these CL may have been derived from oxidized myelin lipids. The abundance of ubiquitin-positive granules in the WM of the aged dogs suggests the ubiquitination of such WM debris (Figure 4a). Myelin debris is also seen in the perivascular spaces of the brains of patients with multiple

sclerosis (MS), which is a progressive demyelinating human disorder [Kooi 2009]. In the brain, solutes are physiologically drained through the vascular basement membrane, although phagocytes in the brain accumulate around blood vessels [Carare 2008; Weller 2009]. The CL particles in the meninges have drained through the perivascular drainage system and been phagocytosed by indigenous histiocytes in the meninges [Ide 2011].

In elderly humans, WM lesions are associated with gait disturbance and urinary incontinence [Bennett 1992], which are equivalent to the symptoms seen in aged dogs [Colle 2000; Kiatipattanasakul 1996]. In the report by Tapp *et al.*, a significant decrease in frontal lobe volume, including the periventricular WM, was demonstrated in aged dogs with cognitive impairments [Tapp 2004]. Myelin breakdown disrupts neuronal conduction velocity and impacts on brain functions that are deteriorated in aged humans [Bartzokis 2004]. Therefore, decreased WM myelination might be associated with an age-related cognitive decline in dogs. Though it cannot be established from the present study, it should be noted that breed predilection to age-related changes of the dog brain have been documented [Pugliese 2010].

CAA is one of the major causes of microhemorrhage in humans [Thal 2012]. It is also known that dogs develop microhemorrhage in relation with CAA [Uchida 1990], however the prevalence and severity of microhemorrhage in dogs have not been studied. In the present study, microhemorrhages were observed in the cerebral cortices of dogs over 10 years old (Figure 7). As it has been documented in humans and dogs with CAA, microhemorrhages were observed in relation to meningeal arterioles but not

in the cerebral WM. These lesions may also account for cognitive decline in aged dogs as well as in humans.

Abundant studies on the AD-related lesions in dogs have been performed, which suggested that the full spectrum of AD pathology does not occur in this species [Head 2011]. The present study revealed that cerebral demyelination occurs in an age-dependent manner in aged dogs, as well as in humans [Lintl 1983]. Here, the author propose that WM myelin breakdown should be taken into consideration as one of the major factors associated with cognitive decline in aged dogs. Since the etiological discrimination of normal aging, VD and AD remains difficult also in humans [Fotuhi 2009; Grinberg 2010; Iadecola 2010], dogs, though do not develop AD, could be useful for chronological studies of age-related WM changes.

5. Tables and Figures

Table 1. Primary antibodies used in the present study.

Specificity	Type	Dilution	Antigen retrieval	Manufacturer
Aβ x-42	Mouse monoclonal (clone12F4)	1:1000	Formic acid	Millipore, Temecula, CA, USA
Aβ x-40	Mouse monoclonal (clone11A5-B10)	1:1000	Formic acid	Millipore, Temecula, CA, USA
Apo E	Rabbit polyclonal	1:100	Autoclave	IBL, Gunma, Japan
Olig2	Rabbit polyclonal	1:200	Autoclave	Millipore, Temecula, CA, USA
Collagen IV	Rabbit polyclonal	1:1000	Proteinase K	Abcam, Tokyo, Japan
GFAP	Rabbit polyclonal	1:400		Dako, Carpenteria, CA, USA
MBP	Rabbit polyclonal	1:1000	Autoclave	Dako, Carpenteria, CA, USA
Ubiquitin	Rabbit polyclonal	1:100		Dako, Carpenteria, CA, USA

Apo E, apolipoprotein E; GFAP, glial fibrillary acidic protein; MBP, myelin basic protein.

Table 2. Statistical correlation analyses of age, mean WM gray value, CAA per mm square, perivascular CL accumulation, the total number of cells, and the percentage of olig2-positive cells using Spearman's rank correlation coefficient and two-tailed *P*-values.

	Age	WM gray value	CAA / mm^2	Perivascular CL accumulation	Total number of cells	Percentage of Olig2+ cells
Age	*r*=1.000 n=51					
WM gray value	*r*=-0.567 *P*<0.001	*r*=1.000 n=51				
CAA / mm^2	*r*=0.741 *P*<0.001	*r*=-0.647 *P*<0.001	*r*=1.00 n=51			
Perivascular CL accumulation	*r*=0.871 *P*<0.001	*r*=-0.664 *P*<0.001	*r*=0.762 *P*<0.001	*r*=1.00 n=51		
Total number of cells	*r*=0.568 *P*<0.001	*r*=-0.439 *P*<0.01	*r*=0.590 *P*<0.001	*r*=0.533 *P*<0.001	*r*=1.00 n=51	
Percentage of Olig2+ cells	*r*=-0.283 *P*<0.1	*r*=0.193 *P*<1	*r*=-0.337 *P*<0.05	*r*=-0.211 *P*<1	*r*=-0.355 *P*<0.05	*r*=1.00 n=46

WM, white matter; CAA, cerebral amyloid angiopathy; CL, ceroid-lipofuscin.

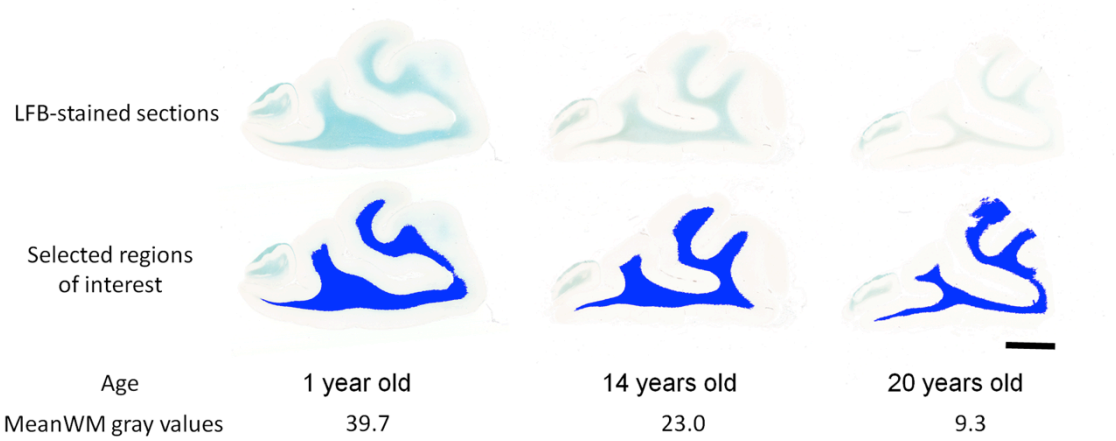

Figure 1. Representative sections of luxol fast blue (LFB)-stained canine frontal lobes from different aged dogs (top row). In the second row, the regions of interest (WM: white matter) are depicted in blue. The amount of LFB-stained myelin was decreased throughout the WM in an age-dependent manner. Bar = 50 mm.

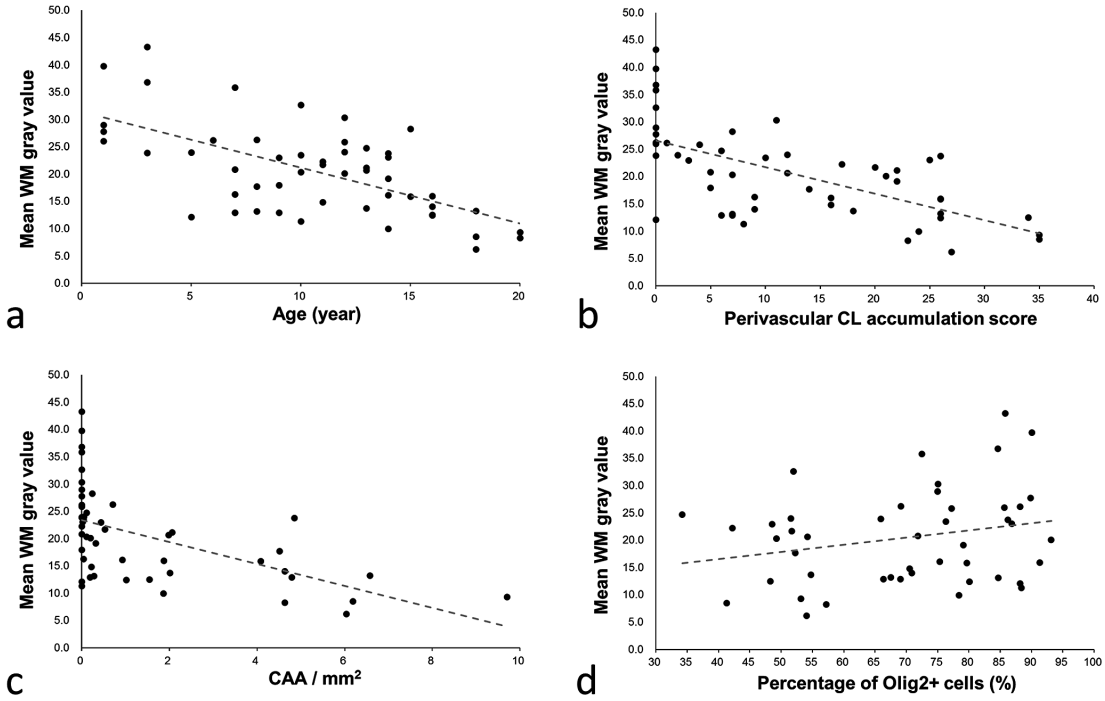

Figure 2. Scatter plots of mean white matter (WM) myelin density and either age (a), perivascular CL accumulation (b), cerebral amyloid angiopathy (CAA) per square millimeter (c), or percentage of Olig2-positive cells (d).

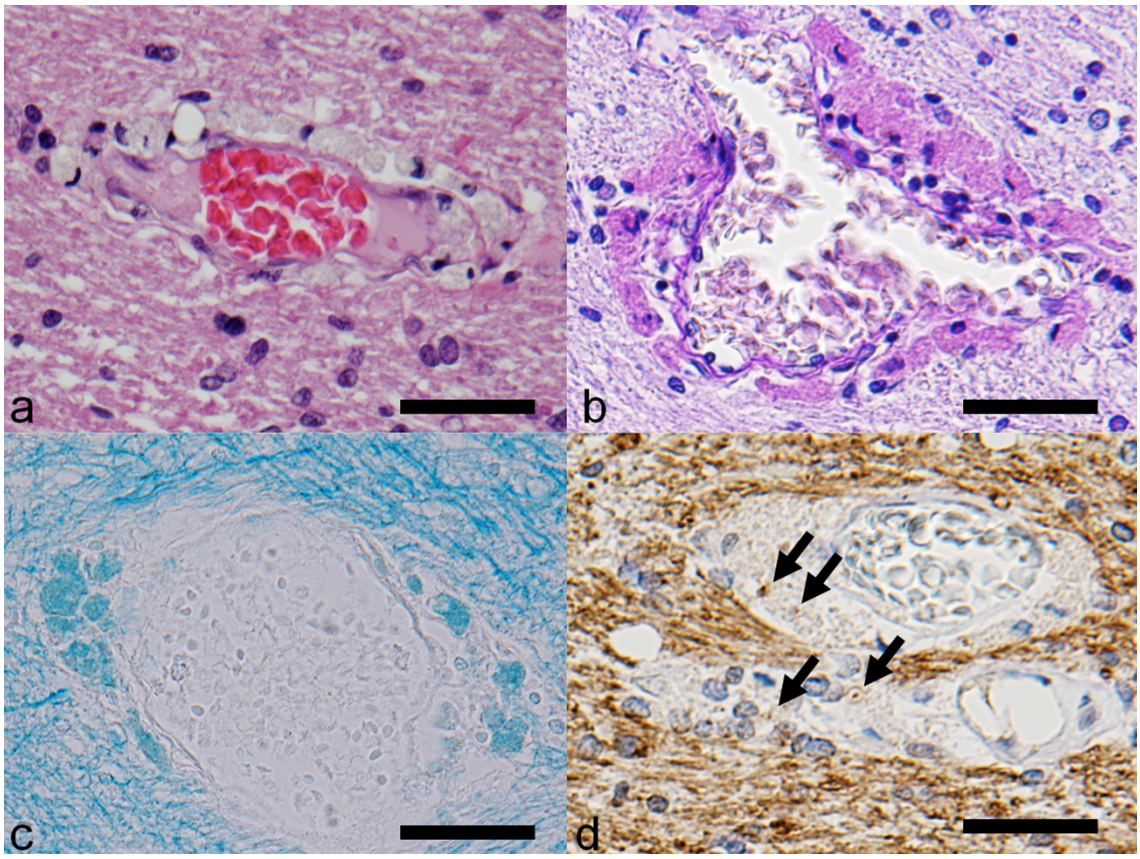

Figure 3. Perivascular ceroid-lipofuscin (CL) accumulation in the cerebral white matter (WM) of an 18-year-old dog. Bar = 50 μm. (a) Phagocytes with yellowish-brown pigments accumulated in the perivascular space. HE stain. (b) Pigment staining for periodic acid Schiff (PAS). (c) Pigment staining for luxol fast blue (LFB). (d) MBP-positive granules were observed in some of the phagocytic vacuoles (arrows). Stained with anti-MBP antibody.

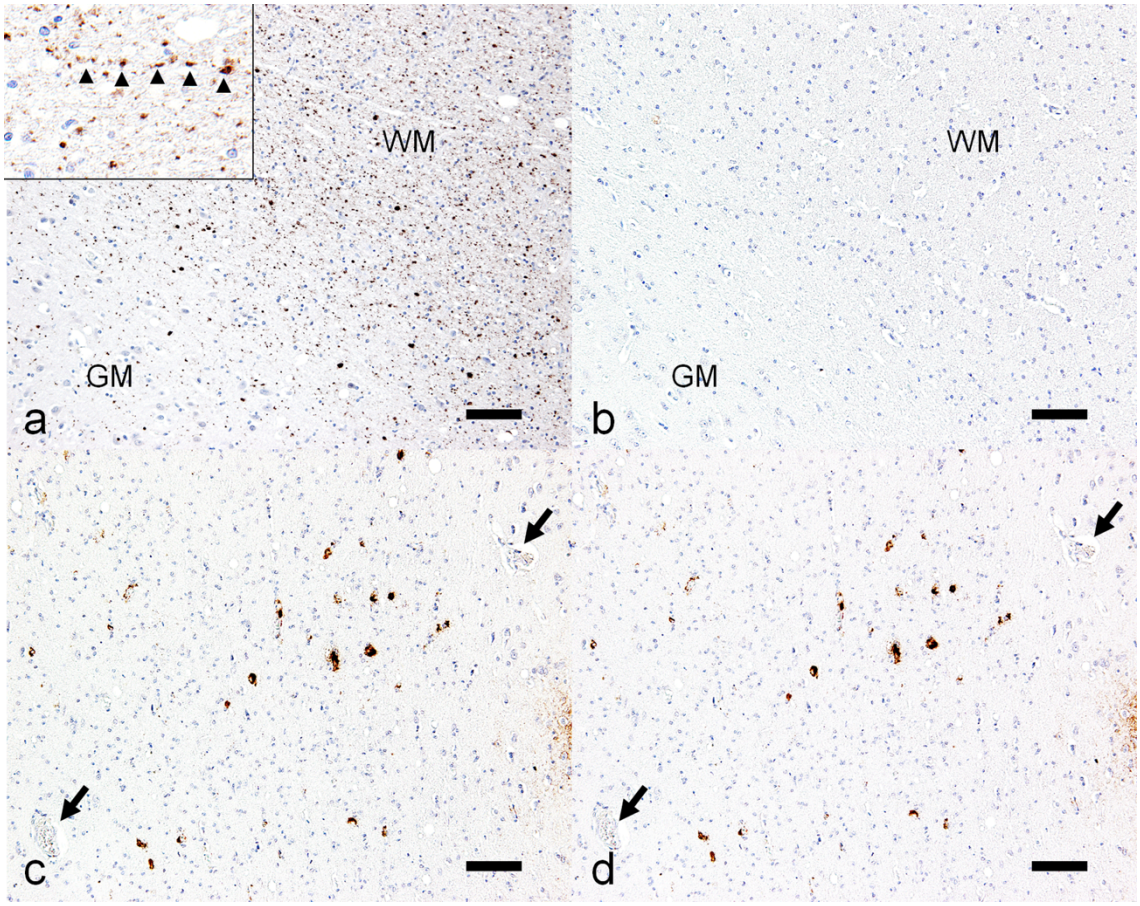

Figure 4. Immunohistochemistry for ubiquitin (a and b), Aβ42 (c) and Aβ40 (d). (a) Abundant ubiquitin-positive granules are scattered selectively in the white matter (WM) and less in the gray matter (GM) of an aged dog with myelin loss (16-year-old, mean WM gray value = 12.5). These granules are often distributed in a linear pattern (inset, arrowheads), indicating the involvement of myelinated nerve fibers. (b) No ubiquitin-positive granules are observed in the brain of a young dog (1-year-old, mean WM gray value = 39.7). (c and d) Aβ42 and Aβ40 are deposited in the WM capillaries in a similar pattern. Note that Aβ is not deposited in the arterioles (arrows), which perivascular spaces are dilated. Bars = 100 μm.

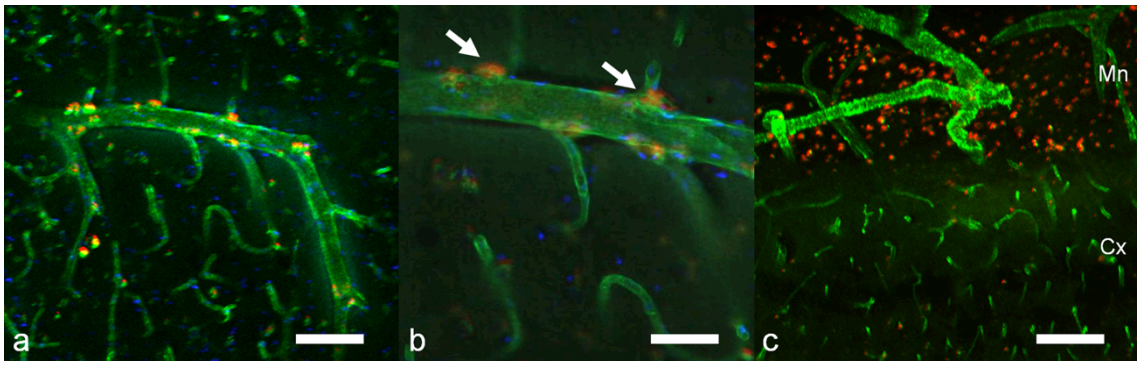

Figure 5. Confocal microscopic images of the blood vessels of the cortex (a and b) and meninges (c) of a 14-year-old dog. Thick sections (200μm) stained for collagen type IV (green). (a) A few phagocytes containing autofluorescent particles (orange) were observed adjacent to the basement membrane of a blood vessel. Bar = 100 μm. (b) The phagocytes were located at the bifurcations of the vascular branches (arrows). Bar = 30 μm. (c) Abundant autofluorescent particles accumulated in the meninges (Mn) compared to the number in the cortex (Cx). Mn: meninges, Cx: cortex. Bar = 100 μm.

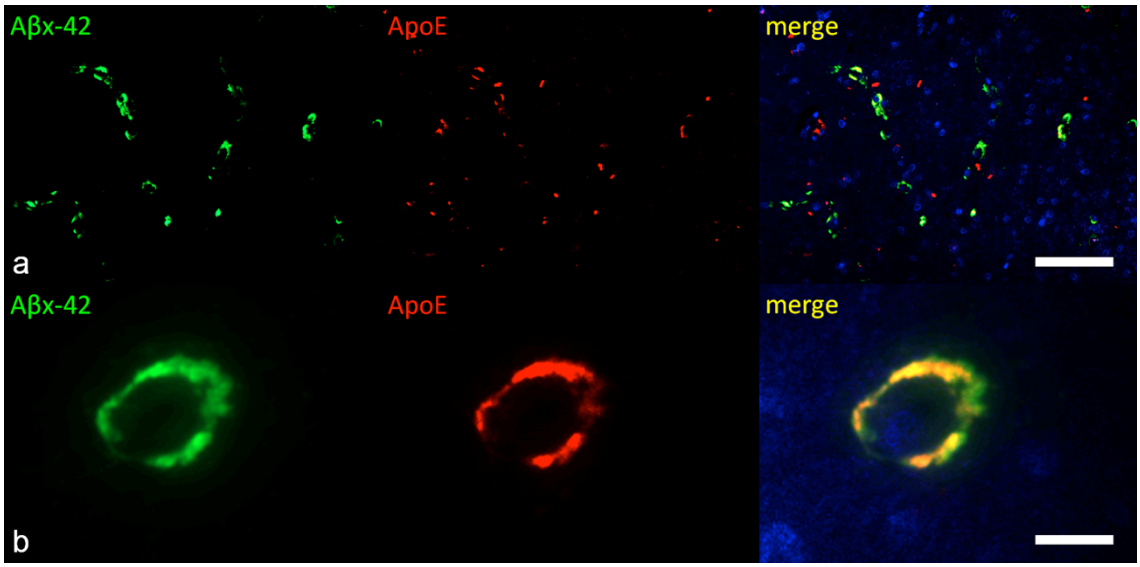

Figure 6. Immunofluorescent double-staining for Aβx-42 (green) and Apo E (red) in a 16-year-old dog. (a) Aβx-42 was deposited focally in the capillary walls of the WM. Bar = 100 μm. (b) ApoE protein colocalized with Aβx-42. Bar = 20 μm.

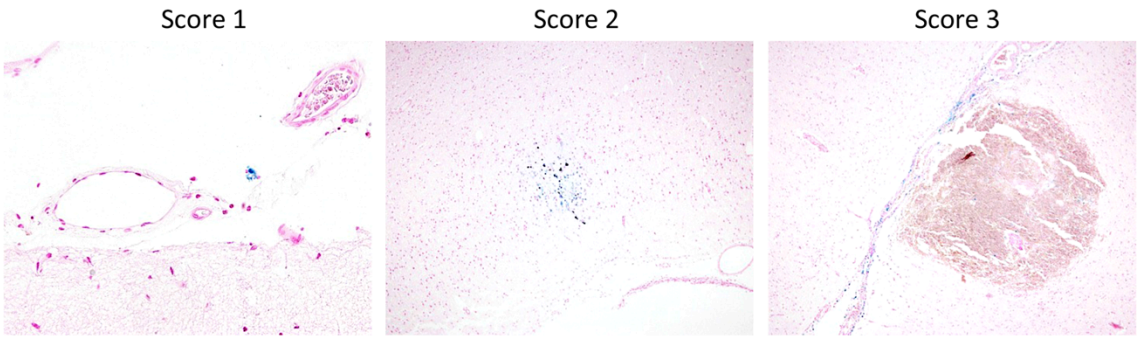

Microhemorrhage Score	5-9 years old (n=12)	10-14 years old (n=20)	15-20 years old (n=10)
0	100%	85%	70%
1	0%	5%	20%
2	0%	10%	0%
3	0%	0%	10%

Figure 7. Prevalence and severity of microhemorrhage in dog brains assessed by BB staining. Microhemorrhage of each dog brain was scored as: 0, no BB-positive staining; 1, few BB-positive macrophages; 2, aggregates of BB-positive macrophages; 3, small hematoma surrounded by BB-positive macrophages. No microhemorrhage was observed in the younger dogs (5 to 9 years old). In aged dogs (10 to 14 years old and 15 to 20 years old), microhemorrhages were occasionally observed in the cerebral cortices.

6. Abstract

The significance of cerebral WM demyelination in the cognitive decline of elderly humans is disputed. Cognitive decline also occurs in aged dogs, although the age-related changes that occur in the canine cerebral WM are yet to be studied, particularly with regard to their relevance to the WM alterations of elderly humans. The present study revealed an age-dependent myelin loss in the frontal lobe WM of canine brains. The accumulation of ceroid-lipofuscin-laden phagocytes was also observed in the perivascular spaces of the WM and was correlated with the decrease in myelination. Also, MBP was detected in some of the vacuoles of these phagocytes. In the WM of the canine brain, Aβ was deposited focally in capillary walls, and colocalized with Apo E. The dog is homozygous for Apo E4, which genotype is related to capillary CAA in humans. These findings indicate that WM demyelination occurs in aged dogs as well as in aged humans, hence WM alterations may account for age-related behavioral changes of the dog. In conclusion, dogs are useful for chronological studies of age-related WM changes.

Chapter 4

Aged domestic cats naturally develop neurofibrillary tangles and neuronal loss associated with Aβ oligomers

1. Introduction

The SPs and NFTs are the two histopathological hallmarks of AD. They appear as extracellular and intracellular argyrophilic aggregates that are mainly composed of Aβ protein and hyperphosphorylated tau, respectively. Studies on post mortem human brains have shown that these two lesions are developed age-dependently and are related to the onset and progression of AD [Braak 1991; Thal 2002]. Although the detailed relationship between Aβ plaques and NFTs in the pathogenesis of AD remains controversial [Selkoe 2011; Ittner 2011], there is emerging evidence that supports recent idea that neocortical NFTs would be induced by pathological Aβ species (Aβ oligomers) [Jack 2013]. Furthermore, it has been demonstrated that neuronal loss and clinical symptoms of AD are more closely related to NFTs than SPs [Gomez-Isla 1997; Bennett 2004].

Post mortem examination of aged animal brains have shown that SPs also develop in many non-human mammalian species, including the monkey, dog, bear, camel, horse and seal [Chambers 2011; Nakamura 1998; Kimura 1997; Gearing 1997; Chambers 2010; Uchida 1990; Uchida 1992; Uchida 1995; Tekirian 1996; Nakamura 1995; Capucchio 2010; Takahashi 2014]. According to previous reports and the protein database, these animals possess the same Aβ amino acid sequence as human

(Table 2) [Johnstone 1991; Selkoe 1987; Gotz 2008; Podlisny 1991]. Interestingly, either NFT or progressive hippocampal neurodegeneration, both of which are observed in human AD, does not occur in these animals [Selkoe 1987; Oikawa 2010; Brakk 1994]. On the other hand, Aβ proteins of rodents (mice and rats) are three amino acid-different in its N-terminal region compared with human type Aβ (Table 2) [Yamada 1987], and these animals do not naturally develop SPs [Podlsny 1991]. Moreover, NFTs are not either formed in these animals. Even in transgenic (Tg) mice that bear the mutated *APP* or *PSEN* (presenilin) gene causing familial AD and accordingly exhibit excessive Aβ deposition in the brain, NFT formation does not occur[Duyckaerts 2008].

The *Felinae* subfamily, which includes the leopard cat (*Prionailurus bengalensis*), the cheetah (*Acinonyx jubatus*), and the domestic cat (*Felis catus*), shows an Aβ amino acid sequence different from human and rodents with one substitution compared with human Aβ (Table 2). The author found abundant NFTs as well as Aβ deposits (not SPs but small granular aggregates) in the brains of aged leopard cats and cheetahs [Serizawa 2012]. Since leopard cats and cheetahs are endangered wild animals, the domestic cat, which diverged from a common ancestor with the leopard cat and cheetah approximately 6.2 million years ago [Johnson 2006], is easier to study. This study shows that aged domestic cats spontaneously develop abundant NFTs without argyrophilic SP formation but with intracellular Aβ and soluble Aβ oligomers, leading to severe hippocampal degeneration similar to AD brains. Our findings

indicate that domestic cat could be an excellent animal model that naturally develops AD pathologies, especially Aβ oligomers, NFTs and neuronal loss.

2. Materials and Methods

Brain samples

Cat brain tissues of various ages were examined, including fetal to aged tissues (see Table 2). All the adult cat brains were obtained through routine necropsies performed at the Department of Veterinary Pathology, the University of Tokyo or at referral animal clinics. The fetus brain samples were purchased from a laboratory animal supplier (Nisseiken Co. Ltd., Tokyo, Japan). The hemisphere of the brain was fixed in 10% phosphate-buffered formalin, and the other hemisphere was coronally sectioned and then frozen at -80°C until use.

Histology

Formalin fixed paraffin-embedded tissues were cut into 4-μm-thick serial sections. The deparaffinized sections were then stained by the Gallyas-Braak method as well as with HE and PAM. Digital images were obtained using an Olympus BX 50 microscope (Olympus, Tokyo, Japan) equipped with a Nikon DS-Ri1 digital camera (Nikon, Tokyo, Japan).

Immunohistochemistry

Consecutive sections were stained using the immunoenzyme technique.

Sections were deparaffinized and rehydrated and antigen retrieval was done by heat or by FA (for Aβ). In order to inactivate endogenous peroxidase, the sections were immersed in 1% hydrogen peroxide in methanol for 20 minutes and then in 5% skimmed milk in TBS. The following primary antibodies were used: mouse anti-hyperphosphorylated-tau Ser202/Thr205 (clone AT8, 1:100, Thermo Scientific, Rockford, IL), mouse anti-hyperphosphorylated-tau Ser212/Thr214 (clone AT100, 1:100, Thermo Scientific), mouse anti-3-repeat-tau RD3 (clone 8E6/C11, 1:100, Millipore, Temecula, CA), mouse anti-4-repeat-tau RD4 (clone 1E1/A6, 1:100, Millipore), rabbit anti-pan-tau (1:100, Sigma, St Louis, MO), mouse anti-Aβ42 (clone 12F4, 1:1000, Millipore), rabbit anti-Aβ42 (1:1000, IBL, Gunma, Japan), anti-NeuN (clone A60, 1:100, Millipore). After incubation with each primary antibody at 4°C overnight, immunolabeled antigens were visualized using the Dako Envision+ System (Dako, Carpinteria, CA). In brief, the sections were incubated with HRP-labeled polymer at 37°C for 40 minutes, reacted with 0.05% 3′3-diaminobenzidine plus 0.03% hydrogen peroxide in Tris-hydrochloric acid buffer, and then counterstained with hematoxylin. Negative controls were obtained by omitting the primary antibodies. Neuronal loss in the pyramidal cell layer of the hippocampal CA1 region was evaluated by counting NeuN-positive cells displayed in Figure 4a. Comparisons of the means among the three groups were performed with one-way ANOVA followed by Tukey's HSD test using the SPSS software (IBM, Tokyo, Japan). Differences with a *P* value of <0.001 were considered significant.

Double-labelling immunofluorescence

After incubation with each of the primary antibodies at 4°C overnight, the sections were washed with TBS. The sections were then incubated with corresponding secondary antibodies at 37°C for one hour, mounted with Vectashield (H-1500, Vector Laboratories, Burlingame, CA), and examined under a Leica DMI 3000B fluorescence microscope (Leica Microsystems, Tokyo, Japan) or a Carl Zeiss LSM700 Confocal Laser Scanning Microscopy (Carl Zeiss, Tokyo, Japan). Primary antibodies used were as follows: mouse anti-hyperphosphorylated-tau Ser202/Thr205 (clone AT8, 1:100, Thermo Scientific), rabbit anti-MAP2 (1:1000, Millipore), rabbit anti-GFAP (1:400, Dako), rabbit anti-Olig2 (1:200, Millipore), mouse anti-RAB9 (1:100, LSBio, Seattle, WA) and rabbit anti-Aβ42 (1:100, IBL). Secondary antibodies used were as follows: ALEXA594-conjugated goat anti-mouse IgG (1:100, Invitrogen, Eugene, OR), ALEXA488-conjugated goat anti-rabbit IgG (1:100, Life Technologies, Eugene, OR), ALEXA594-conjugated goat anti-rabbit IgG (1:100, Life Technologies) and ALEXA488-conjugated goat anti-mouse IgG (1:100, Invitrogen).

Protein extraction

For tau extraction, hippocampus and parietal cortex tissues were homogenized in 4 volumes of TBS containing a protease inhibitor cocktail (cOmplete Mini, Roche, Mannheim, Germany) and a phosphatase inhibitor cocktail (PhosSTOP, Roche) and fractioned by three-step ultracentrifugation including TBS, sarkocyl (sodium N-dodecanoylsarcosinate) and guanidine hydrochloride (GuHCl) extraction, essentially

as described previously [Goedert 1992]. In brief, the homogenates were centrifuged at 125,000 × G at 4°C for 1 hour, and the supernatants were harvested as TBS-soluble fractions. The precipitates were dissolved by sonication in 4 volumes of 1% sarkosyl TBS containing the protease inhibitor cocktail and the phosphatase inhibitor cocktail and then the solutions were incubated at RT for 1 hour. After centrifugation at 125,000 × G at RT for 15 minutes, the supernatants were removed. The sarkosyl-insoluble precipitates were then dissolved by sonication in 2 volumes of 4 mol/L GuHCl and incubated at RT for 1 hour. After a second centrifugation at 125,000 × G at RT for 15 minutes, the supernatants were harvested and the solvent (GuHCl) was exchanged with TBS containing the protease inhibitor cocktail and the phosphatase inhibitor cocktail using Amicon Ultra 10K filter devices (Millipore). For Aβ extraction, hippocampus and parietal cortex tissues were homogenized in 4 volumes of TBS containing the protease inhibitor cocktail and fractioned by a three-step ultracentrifugation including TBS, SDS and FA extraction [Tomiyama 2010]. In brief, the homogenates were centrifuged at 100,000 × G at 4°C for 1 hour, and the supernatants were harvested as the TBS fractions. The precipitates were dissolved with the Teflon/glass homogenizer (8 strokes) in 4 volumes of 2% SDS/TBS containing the protease inhibitor cocktail, centrifuged at 100,000 × G at RT for 1 hour, and the supernatants were harvested as SDS fractions. The precipitates were finally dissolved with the Teflon/glass homogenizer (8 strokes) in 70% FA in water. After being centrifuged at 100,000 × G at RT for 1 hour, the supernatants were harvested as FA fractions. The TBS and SDS fractions were diluted 10- and 20-fold, respectively, in

TBS containing the protease inhibitor cocktail, and the FA fractions were neutralized by 1:10 dilution into 1M Tris solution, pH 11. The protein concentrations of the resultant solutions were determined by the BCA protein assay (Thermo Scientific).

Western blotting

For tau analysis, extracts of hippocampus were incubated with alkaline phosphatese mix (500mM Tris-Hcl pH9.0, 500mM $MgCl_{22}$, 0.1M DTT (Invitrogen)) at 37°C overnight for dephosphorylation. Subsequently, aliquots (5 μg of protein) were electrophoresed on 4-12% Bolt Bis-Tris gel (Life Technologies), and transferred on to 0.45 μm PVDF membranes (Millipore). Nonspecific binding was blocked with 5% skimmed milk in TBS containing Tween 20 (TBS-T, 20 mM Tris-HCl buffer, pH 7.0, containing 50 mM NaCl and 0.1% Tween 20) for 30 min. The following primary antibodies were used: mouse anti-tau (clone TAU-5, 1:1000, Life Technologies), RD3 (clone 8E6/C11, 1:1000, Millipore), mouse anti-4-repeat-tau RD4 (clone 1E1/A6, 1:1000, Millipore). Alkaline phosphatase-conjugated anti-mouse IgG was then applied The blotting signals were visualized with NBT/BCIP and imaged with a Image Quant LAS 4000 mini bio-molecular imager (GE Healthcare Bio-Sciences AB, Uppsala, Sweden). For Aβ analysis, aliquots (50 μg of protein) of the TBS and SDS fractions were electrophoresed on 4-12% Nupage Bis-Tris 4–12% polyacrylamide gels (Life Technologies), and transferred on to 0.45 μm PVDF membranes (Millipore). Nonspecific binding was blocked with 5% skimmed milk in TBS containing Tween 20 (TBS-T, 20 mM Tris-HCl buffer, pH 7.0, containing 50 mM NaCl and 0.1% Tween 20)

for 30 min. Anti-Aβ antibody (clone 6E10, 1:3000, Covance, Emeryville, CA) was used as the primary antibody. Horseradish peroxidase-conjugated secondary antibody (1:5000, Dako) was then applied. The blotting signals were visualized with the chemiluminescence ECL Select Western Blotting Detection Kit (GE Healthcare Bio-Sciences AB, Uppsala, Sweden) and imaged with a Image Quant LAS 4000 mini bio-molecular imager (GE Healthcare Bio-Sciences AB).

Dot blot

For dot blot immunoanalysis, aliquots (50 μg of protein) of the TBS, SDS and FA fractions were dotted onto 0.45 μm PVDF membranes (Millipore) in a dot-blot apparatus (Bio-Rad). The blots were probed with a polyclonal antibody A11 specific for amyloid oligomers (1:1000, Biosource, Camarillo, CA), followed by alkaline phosphatase–conjugated goat anti-rabbit antibody (1:5000, Thermo Scientific), and visualized with the BCIP (5-bromo-4-chloro-3'-indolylphosphatase p-toluidine salt) /NBT (nitro-blue tetrazolium chloride) (BCIP/NBT) detection system (Wako Chemicals, Osaka, Japan).

ELISA

To quantify the amount of Aβ oligomers in the extracts from cat brains, BAN50 single-antibody sandwich (SAS)-ELISA that is specific for high-molecular-weight (HMW) Aβ oligomers (10-20 mers)[37] was used in duplicate. The buffers and assay procedures were similar to those described previously [Fukumoto

2010; Kasai 2012]. As a standard for inter-plate calibration, synthetic 'multiple antigenic' peptide (MAP) containing 16 copies of the monoclonal antibody were used, BAN50, epitope linked to a branching lysine core. The SuperSignal ELISA Femto Maximum Sensitivity Substrate (Thermo Scientific) and a luminometer (SpectraMaxL; Molecular Devices, Osaka, Japan) were used for signal detection.

3. Results

Spatial and temporal expression of tau isoforms in the cat brain

In the feline fetal and neonatal (2-week-old) brains, 3-repeat tau was intensely expressed throughout the cerebrum, though 4-repeat tau was not detected in the fetal brains (Figures 1a and 2a). The hippocampal pyramidal cells begin to express 4-repeat tau in the developing brain of the 2-week-old cat (Figure 2a). In the adult cat brains (3- to 22-year-old), both 3-repeat and 4-repeat tau isoforms are expressed. Age-dependent shift from the dominance of 3-repeat tau to both 3-repeat and 4-repeat tau expression was also confirmed by Western blotting of a TBS-soluble fraction obtained from the cerebrum (Figure 1b). In the fetal brains, AT8-positive hyperphosphorylated tau was detected in the surface of the developing cerebrum (Figures 1a and 2b).

In some of the aged cats (over 14-years-old) with cerebral Aβ deposits, aggregates of hyperphosphorylated tau were observed in their brains (Figure 1a, Table 1). In mild cases, few AT8-positive cells were observed in the entorhinal cortex (Figure 3a), and in more severe cases it spread to the hippocampus and cerebral cortices

(Figure 1a, Table 1). Note that the cerebrum is atrophied in the aged cat compared to that of the young cat (Figure 1a). Also, few AT8-positive cells were observed in the locus ceruleus (Figure 3b). AT8- and AT100-positive hyperphosphorylated tau proteins were detected from the sarcosyl-insoluble guanidine HCl-soluble fraction of hippocampus in aged cats with NFTs (Figure 1c). Note that in cats with abundant hyperphosphorylated tau deposition (case No. 12 and 22), the smear band pattern resolved into clear bands consisting of both 3-repeat and 4-repeat tau isoforms after dephosphorylation treatment (Figure 1c).

NFTs and neuronal loss naturally emerged with aging in the cat brains

Gallyas-Braak staining-positive NFTs (Figure 4a) and ghost tangles were found in the hippocampus and entorhinal cortex of the cat brains corresponding to the distribution of hyperphosphorylated tau detected by immunohistochemistry. NFTs were observed intracellularly occupying the neuronal soma and neurites, and ghost tangles were observed extracellularly where the neuron had died out. On consecutive sections, NFTs were stained positively for hyperphosphorylated tau (AT8 and AT100) and ubiquitin (Figure 4b). Regarding the affected cell types, hyperphosphorylated tau aggregates were detected mainly in MAP2-positive neurons and also in some Olig2-positive oligodendrocytes, but not in GFAP-positive astrocytes (Figure 4c). Argyrophilic aggregates in the oligodendrocytes were also observed on Gallyas-Braak stained sections (Figure 4a, arrowhead). No inclusions were observed in astrocytes either by immunohistochemistry or Gallyas-Braak staining (Figure 4c). The absence

of astrocytic tau inclusions such as astrocytic plaques or tuft-shaped astrocytes indicates that the hyperphosphorylated tau aggregates in the feline brains differ from those of 4-repeat tauopathy (i.e. CBD; PSP) [Ikeda 1998].

Aged cats develop intra- and extra-cellular Aβ aggregates without forming argyrophilic SPs

It was reported that cats only develop diffuse plaques, which are not visualized by silver staining and can only be detected by immunohistochemical methods [Nakayama 2001]. In the present study, Aβ deposits were found in the brains of cats older than 8 years of age that proceed the development of tau pathologies (Table 1). Parenchymal Aβ deposits were detected on FA-pretreated sections as small granular aggregates in the neuropil throughout the cerebral cortex but rarely in the hippocampus (Figures 5a and 6a). However, on heat-pretreated sections, intracellular Aβ aggregates were observed predominantly in the pyramidal cells of the hippocampal CA1 to CA3 region but rarely in the cerebral cortex (Figure 5a). These intracellular Aβ colocalized with Rab9 by confocal laser scanning microscopy, indicating that some of these Aβ peptides are located in the late-endosomes (Figure 5a). Such intracellular Aβ was not detected in younger cats without parenchymal Aβ deposits on FA-pretreated sections.

Many of the higher mammalian animals develop argyrophilic SPs with central core composed of an N-terminally truncated Aβ species, AβpN3 [Chambers 2011; Takahashi 2014; Frost 2013]. It is also known that AβpN3 is markedly increased in SPs of AD compared to normal aging [Schilling 2008]. Interestingly, Aβ deposits in

the cat brains were not immunohistochemically detected with Aβ N-terminal antibodies, either anti-AβpN3 or anti-AβN1 (Figure 5a), because of low affinity of feline Aβs to these antibodies against human Aβ due to the different amino acid residue at the 7th position between human and feline Aβs (Table 2) [Chambers 2012; Brinkmalm 2012; Mattsson2012].

Oligomeric Aβs were detected in the SDS fraction of hippocampal tissues of the aged cat brains by dot blot analysis using an antibody A11 specific to amyloid oligomers (Figure 5b). FA fraction showed no positive reaction with dot blot analysis using A11 antibody (Figure 5b), indicating that biochemical nature to FA-treatment of Aβ oligomer was identical to intracellular Aβ aggregates observed in immunohistochemical analysis. By Western blotting analysis using anti-pan Aβ antibody, two distinct bands were detected from the SDS-extracts of aged cat brains, at approximately 24 kDa and 54 kDa, representing Aβ hexamers and dodecamers, respectively (Figure 5c). The presence of Aβ oligomers was also confirmed by enzyme-linked immunosorbent assay (ELISA) specific for high-molecular weight Aβ oligomers (Figure 6b) [Fukumoto 2010].

Neuronal loss in the hippocampus of the cats affected with NFTs

Aggressive neuronal loss in the hippocampus and cerebral cortex is critical for the manifestation of dementia in AD. Although hippocampal degeneration is considered to be an early event in AD [Hamoel 2008], it has not been detected in non-human species together with Aβ and tau pathology. The author assessed whether

hippocampal neurons were degenerated in cats with NFTs. The number of NeuN-positive cells in the hippocampal CA1 region were compared between 3 groups: young cats with no Aβ deposits and no NFTs (Aβ–/NFT–, n=3, mean age 3.7-year-old), aged cats with Aβ deposits but no NFTs (Aβ＋/NFT–, n=3, mean age 18.0-year-old) and aged cats with Aβ deposits and NFTs (Aβ＋/NFT＋, n=3, mean age 17.6-year-old) in the hippocampus. In the Aβ＋/NFT– group, NeuN-positive cells were slightly but not significantly decreased compared to the Aβ–/NFT– young cats (Figure 7a, b), whereas in the Aβ＋/NFT＋ cats the NeuN-positive cells were significantly decreased compared to other two groups (Figure 7a, b). Degenerated neurons were observed on HE sections (Figure 7c, black arrows). Inclusions composed of hyperphosphorylated tau (AT8 and AT100-positive on consecutive sections) were observed in neurons in the CA1 region (Figure 7c, inset, green arrowheads). These results show that pyramidal neurons in the CA1 region, where NFTs were detected, are strikingly damaged in the brains of aged cats.

4. Discussion

This study demonstrated that domestic cats develop not only Aβ deposits but also NFTs and neuronal loss in their brains with aging. The distribution of the changes (hippocampus and entorhinal cortex), affected cells (neurons and occasionally oligodendrocytes) and tau isoforms (3-repeat and 4-repeat tau) of NFTs were consistent with those of AD in human. It is noteworthy that hyperphosphorylated tau was not detected in the brains of adult cat without cerebral Aβ deposits, and that temporal order

in the emergence of cortical Aβ deposition and severe hippocampal NFTs was the same as that in AD brains (Table 1). In the brains of cats with severe NFTs, the number of hypocampal pyramidal cells was significantly decreased. Thus, aged cats naturally recapitulate human AD pathology, characterized by the following two distinctive features unlike other nonhuman animal species: 1) Formation of NFTs similar to those of AD brains, and 2) induction of NFTs and neuronal loss in a shorter time compared to human AD brains.

The expression patterns of 3-repeat and 4-repeat tau isoforms differ among animal species and age [Gotz 2008; Couchiem 1985; Goedert 1990]. Both in humans and mice, only the 3-repeat isoform of tau is expressed in their fetal brains. In the adult brains, both 3-repeat and 4-repeat isoforms are expressed equally in humans, while only the 4-repeat isoform is expressed in mice [McMillan 2008]. It is well known that NFTs have not been recapitulated in the brains of Tg mice that express mutant *APP* and mutant *presenilin-1* linked to familial AD [Duyckaerts 2008]. However, recent studies have shown that NFTs are formed in Tg mice expressing wild-type human tau composed of 3- and 4-repeat tau isoforms with or without co-expressing *APP* gene with AD-related mutation [Umeda 2014; Andorfer 2003]. In the present study, only the 3-repeat tau was expressed in the fetal brains of cats, whereas both 3-repeat and 4-repeat tau isoforms were expressed in the adult brains. Moreover, NFTs in the cat brains are composed of the both tau isoforms, similar to those in AD brains (Figures 1c, 1d and 2b). Thus, the expression of both 3-repeat and 4-repeat tau isoforms seems to be a critical factor for NFT formation.

Higher mammalian species such as the monkeys harbor tau proteins highly analogous to that of human (Table 3). In addition, these animals express both 3-repeat and 4-repeat isoforms in adult age [Holzer 2004]. However, in these animals, NFTs have been seldom observed [Selkoe 1987; Gotz 2008], except for very advanced aged animals such as baboon (30 years old) [Schulz 2000], cynomolgus monkey (36 years old) [Oikawa 2010] and bison (24 years old) [Hartig 2001]. Furthermore, neuronal cell shedding resulting from severe hyperphosphorylated tau accumulation has not been detected in nonhuman animals including those above mentioned. In contrast, cat tau is less analogous to human tau than monkey and dog tau, and is also different from mouse tau (Table 3). Nevertheless, NFTs and the accompanying neurodegeneration appeared in the examined cat brains as early as 14 years of age (Table 1), which are exceptional and unique to cats among various mammalian species. This suggests that the formation of NFTs does not simply depend on amino acid sequence of tau protein or expression pattern of tau isoforms.

NFTs and neuronal loss were induced in a shorter time in cat brains compared to human AD brains. Because the distribution and tau isoforms of NFTs in cat brains were consistent with those of AD as mentioned above, there must be some factors that cause earlier tauopathy and neurodegeneration in cats other than the properties of tau protein. Although the detailed pathological cascade of AD is yet to be elucidated, accumulating evidence leads to the current hypothesis that emphasizes the interactive role of Aβ and tau in the pathogenesis of AD [Ittner 2011; Benilova 2012]. Recent idea on the development of AD pathology is that NFTs are induced by pathological Aβ

species (Aβ oligomers) that accelerate the antecedent tau deposition in the limbic system and spread to the neocortex [Jack 2013]. Interestingly, Aβ deposits found in the cat brains were morphologically different from those of other mammalian (non-felid) species [Nakayama 2001]. In the cats, there were small Aβ aggregates diffusely distributed in the neuropil on FA-pretreated sections (Figure 5a), but cored plaques were not observed even in cats with heavy NFT burden. Besides, unlike other mammalian species, Aβ deposition in the vascular wall (amyloid angiopathy) was absent in the cat brains. The peculiar small granular Aβ aggregates in the neuropil without cored plaque formation are also observed in the brain of other felids, namely the cheetah and leopard cat that also develop NFTs [Chapter 4; Serizawa 2012]. The amino acid sequence of Aβ peptide in those felids and human are different only at the 7th amino acid residue (felid, glutamic acid; human, aspartic acid, Table 2) [Chapter 4; Serizawa 2012; Brinkmalm 2012; Mattsson2012]. Meanwhile, many higher mammalian species, namely the monkey, dog, bear, camel and horse, harbor Aβ proteins of which amino acid sequence are identical to that of human, and have been reported to spontaneously develop cored plaques. [Chapters 1 and 2; Uchida 1992; Uchida 1995; Tekirian 1996; Johnstone 1991; Selkoe 1987; Frost 2013; Cummings 1993]. From these findings together with the present results, it is likely that in the cat brains Aβ species of different aggregation properties from those of other mammalians is related to the earlier emergence of NFTs and nurodegeneration compared to human and other animals.

Next, as reported in human brains [Ohyagi 2007; D'Andrea 2003], intraneuronal Aβ aggregates were detected in the hippocampal pyramidal cells of the cat brains by using heat-pretreatment, which is optimized for the detection of intracellular Aβ, of histopathological specimens, but not by using FA-pretreatment (Figure 5a). The FA-vulnerable intracellular Aβ aggregates were stained with Aβ42 C-terminus antibody that does not bind with intramembrane full-length APP or β-secretase-cleaved APP [D'Andrea 2003]. Besides, Aβ aggregates colocalized with Rab9 (Figure 5a), indicating that these FA-vulnerable Aβ aggregates are partially locating in late endosomes [LaFerla 2007; Meli 2014; Takahashi 2002]. In the cat brains, FA-vulnerable Aβ aggregates predominantly detected in the pyramidal cells of the hippocampus where severe NFT burden and neurodegeneration existed. In other words, NFTs in the cat brains developed mainly in the hippocampus where Aβ deposition was predominantly observed as intracellular FA-vulnerable aggregates without substantial extracellular granular aggregates. From these results, the intracellular FA-vulnerable Aβ aggregates should therefore be closely related to the formation of NFTs. Furthermore, no significant neuronal loss was observed in cat brains without NFTs even though intracellular Aβ aggregates existed (Figures 7a and 4b). This indicates the importance of NFTs in the development of hippocampal neurodegeneration in aged cats (Figure 7), similar to human AD brains in which neuronal loss and clinical symptoms are more closely related to the NFT formation than to the Aβ burden [Gomez-Isla 1997; Bennett 2004]. This study demonstrated that the aged cats are frequently involved in NFT formation and neuronal loss together with

intraneuronal FA-vulnerable Aβ aggregates, but without typical SPs, in the hippocampus.

Identifying the molecular characters of the intraneuronal FA-vulnerable Aβ aggregates is an important issue. Abundant Aβ oligomers were detected from SDS-soluble fractions of the hippocampi of the aged cats with dot blot analysis using A11 antibody specific to Aβ oligomers (Figure 5b), which preferentially recognizes prefibrillar Aβ oligomers larger than dimers and trimmers [Kayed 2010]. Higher levels of Aβ oligomers were detected in the hippocampus than in the cortex (Figure 5b). Aβ oligomers were also detected by Western blotting using anti-Aβ antibody and thereby determined that they consist of hexamers and dodecamers based on electropheretic mobility (Figure 5c). There have been some previous reports suggesting that Aβ dodecamer is the most neurotoxic Aβ species detected in AD brains [Lesne 2006; Lesne 2013]. There are two known mutations of Aβ N-terminus that cause familial AD in human: the English mutation (H6R) and the Tottori mutation (D7N). Both of these mutations result in increased Aβ oligomers with higher cytotoxicity [Ono 2010; Chen 2012]. Furthermore, it has been shown that racemization of the 7th Asp residue affects Aβ aggregation property to inhibit its fibril formation [Tomiyama 1994]. These suggest that the substitution of the 7th amino acid in human Aβ, as seen in cats, may tend to enhance Aβ oligomerization. Our results showed a close topographical relation of soluble Aβ oligomers, intraneuronal FA-vulnerable Aβ aggregates, NFTs and neuronal loss in the hippocampus of the cat brains. Feline-type Aβ has a lower capability to form insoluble amyloid fibrils and does

not develop SPs, but it may intracellularly induce hyperphosphorylation and conformational changes of tau proteins. Previous studies have also shown that intraneuronal Aβ42 labeling inversely correlates with the progression of SP development in 2xTg ($APP_{SWE/London}$ and mutant $PS1_{M146L}$) and 3xTg (APP_{SWE}, tau_{P301L} and $PS1_{M146V}$ knock-in) mice [Langui 2004; Oddo 2006], suggesting that intraneuronal Aβs may be soluble Aβ species that is in equilibrium with insoluble extraneuronal fibrillar Aβ aggregates.

To date, in order to elucidate fundamental questions regarding the relationship between SPs (Aβ), NFTs (tau) and neuronal death in the pathogenesis of AD, enormous studies have been carried out using Tg mice harboring mutations in *APP* gene, *PSEN* genes, *MAPT* (tau) gene and even all of these 3 genes (3xTg) [Duyckaerts 2008; Frank 2008; Oddo 2003]. However, it has been argued that the pathological sequences observed in those mice are different from those in human AD brain since differences may be attributed to alterations in the expression levels and/or aggregation properties of APP and tau [Saito 2014]. Nontransgenic animals, such as nonhuman primates and nonprimate mammalian species, are also available for studying the relationship of pathological events in AD brains. Unlike Tg mice, the expression of Aβ and tau are within physiological ranges in nontransgenic animals, and the natural spatiotemporal profiles of Aβ and tau pathologies should accordingly be presented in the brains of these animals. However, NFTs have been reported in only few animal species, for example baboon, bison and cynomolgus monkey [Oikawa 2010; Schultz 2000; Hartig 2001], in very old age. Besides, obvious neurodegeneration was not observed in these animals.

The domestic cat is an ideal animal model to investigate "Aβ oligomer hypothesis" in AD pathogenesis, because they naturally express abundant soluble Aβ oligomers, and develop subsequent AD pathologies including Aβ deposition, NFTs and marked neuronal loss in the hippocampus of the aged brains. Thus, the author concludes that domestic cats recapitulate spatiotemporal profiles of the AD pathologies.

5. Tables and Figures

Table 1. Age, sex and immunohistochemical results for A β 42 and hyperphosphorylated tua in cats.

No.	Age	Sex	Aβ42	HP-tau
1	fetus (50 days)	F	−	+*
2	fetus (50 days)	M	−	+*
3	2-week-old	F	−	−
4	2-week-old	F	−	−
5	3-year-old	M	−	−
6	3-year-old	M	−	−
7	4-year-old	F	−	−
8	4-year-old	F	−	−
9	5-year-old	F	−	−
10	8-year-old	F	+	−
11	14-year-old	F	−	−
12	14-year-old	M	+	++
13	15-year-old	F	+	+
14	15-year-old	M	+	−
15	15-year-old	ND	+	−
16	16-year-old	F	+	−
17	16-year-old	M	+	−
18	17-year-old	F	+	−
19	17-year-old	F	+	+
20	17-year-old	ND	+	+
21	18-year-old	F	+	+
22	19-year-old	F	+	++
23	20-year-old	F	+	+
24	20-year-old	ND	+	++
25	22-year-old	M	+	+

HP-tau, hyperphosphorylated tau confirmed by AT8 and AT100 antibodies; F, female; M; male, ND, no data; -, negative, +, positive; ++, HP-tau was observed throughout the hippocampus; *, AT8-positive in the surface of the cerebrum.

Table 2. Aβ protein amino acid sequence of different species.

	Species [species, sequence ID]	Amino acid sequence
Human-type Aβ	Human [*Homo sapiens*, NP_000475.1]	1 D A E F R H D S G Y E V H H Q K L V F F A E D V G S N K G A I I G L M V G G V V I A 42
	Chimpanzee [*Pan troglodytes*, NP_001013036.1]	1 D A E F R H D S G Y E V H H Q K L V F F A E D V G S N K G A I I G L M V G G V V I A 42
	Cynomolgus monkey [*Macaca fascicularis*, XP_005548940.1]	1 D A E F R H D S G Y E V H H Q K L V F F A E D V G S N K G A I I G L M V G G V V I A 42
	Dog [*Canis familiaris*, NP_001006601.2]	1 D A E F R H D S G Y E V H H Q K L V F F A E D V G S N K G A I I G L M V G G V V I A 42
	Polar bear [*Ursus maritimus*, XP_008699989.1]	1 D A E F R H D S G Y E V H H Q K L V F F A E D V G S N K G A I I G L M V G G V V I A 42
	Camel [*Camelus bactrianus*, XP_010954929.1]	1 D A E F R H D S G Y E V H H Q K L V F F A E D V G S N K G A I I G L M V G G V V I A 42
	Horse [*Equus caballus*, XP_003364220.1]	1 D A E F R H D S G Y E V H H Q K L V F F A E D V G S N K G A I I G L M V G G V V I A 42
Felid-type Aβ	Cat [*Felis catus*, XP_006936005.1]	1 D A E F R H E S G Y E V H H Q K L V F F A E D V G S N K G A I I G L M V G G V V I A 42
Rodent-type Aβ	Mouse [*Mus musculus*, NP_001185752.1]	1 D A E F G H D S G F E V R H Q K L V F F A E D V G S N K G A I I G L M V G G V V I A 42
	Rat [*Rattus norvegicus*, NP_062161.1]	1 D A E F G H D S G F E V R H Q K L V F F A E D V G S N K G A I I G L M V G G V V I A 42

Table 3.Tau protein amino acid sequence of different species.

Species [species, sequence ID]	Amino acid sequence		
Human [*Homo sapiens*, NP_005901.2]	1 MAEPRQEFEVMEDHAGTYGLGDRKD---QGGYTMHQDQEGDTDAGLKESPLQTPTEDGSEEPGSETSDAKSTPTAEDVTAPLVDEGAPGKQAAAQPHTEI 97		
Chimpanzee [*Pan troglodytes*, XP_009430187.1]	1 MAEPRQEFEVMEDHAGTYGLGDRKD---QGGYTMHQDQEGDTDAGLKESPLQTPTEDGSEEPGSETSDAKSTPTAEDVTAPLVDEGAPGKQAAAQPHTEI 97		
Cat [*Felis catus*, XP_003997079.1]	1 MAEPRQDFTVMDDHAGTYGTGERKDLPSQGSYTLMQDHEGDVDQGLKESPLQTPADDGSEEPGSETSDAKSTPTAEDATAPLVDEGAPGEQAAAQPHTEI 100		
Dog [*Canis lupus familiaris*, XP_005624235.1]	1 MAEPRQEFDVMEDHAGTYGLGDRKD---QEGYTMLQDQEGDTDAGLKESPLQTPAEDGSEELGSETSDAKSTPTAEDVTAPLVDERAPGEQAAAQPHMEI 97		
Mouse [*Mus musculus*, NP_001033698.1]	1 MADPRQEFDTMEDHAG--------------DYTLLQDQEGDMDHGLKESPPQPPADDGAEEPGSETSDAKSTPTAEDVTAPLVDERAPDKQAAAQPHTEI 86		
	98 PEGTTAEEAGIGDTPSLEDEAAGHVTQARMVSKSKDGTGSDDKKAKGADGK--TKIATPRGAAPPGQKGQANATRIPAKTPPAPKTPPSSGEPPKSGDRS 195		
	98 PEGTTAEEAGIGDTPSLEDEAAGHVTQARMVSKSKDGTGSDDKKAKGADGK--TKIATPRGAAPPGQKGQANATRIPAKTPPAPKTPPSSGEPPKSGDRS 195		
	101 PEGTTAEEAGIGDTPNLEDQAAGHVTQARMVSKGRDGTGADDKKAKGADGKAGTKIATPRGAAPPGQKGQANATRIPAKTTPSPKTPPGTGDSGKSGDRS 200		
	98 PEGTTAEEAGIGDTPSLEDEAAGHVTQARMVSKSKDGTGSDDKKAKGADGK--TKIATPRGAAPPGQKGQANATRIPAKTPPAPKTPPSSGEPPKSGDRS 195		
	87 PEGITAEEAGIGDTPNQEDQAAGHVTQARVASKD--RTGNDEKKAKGADGKTGAKIATPRGAASPAQKGTSNATRIPAKTTPSPKTPPGSGEPPKSGERS 184		
	MBD1 MBD2		
	196 GYSSPGSPGTPGSRSRTPSLPTPPTREPKKVAVVRTPPKSPSSAKSRLQTAPVPMPDLKNVKSKIGSTENLKHQPGGGKVQIINKKLDLSNVQSKCGSKD 295		
	196 GYSSPGSPGTPGSRSRTPSLPTPPTREPKKVAVVRTPPKSPSSAKSRLQTAPVPMPDLKNVKSKIGSTENLKHQPGGGKVQIINKKLDLSNVQSKCGSKD 295		
	201 GYSSPGSPGTPGSRSRTPSLPTPPTREPKKVAVVRTPPKSPSSAKSRLQTAPVPMPDLKNVRSKIGSTENLKHQPGGGKVQIINKKLDLSNVQSKCGSKD 300		
	196 GYSSPGSPGTPGSRSRTPSLPTPPAREPKKVAVVRTPPKSPSSAKSRLQTAPVPMPDLKNVKSKIGSTENLKHQPGGGKVQIINKKLDLSNVQSKCGSKD 295		
	185 GYSSPGSPGTPGSRSRTPSLPTPPTREPKKVAVVRTPPKSPSASKSRLQTAPVPMPDLKNVRSKIGSTENLKHQPGGGKVQIINKKLDLSNVQSKCGSKD 284		
	MBD2 MBD3 MBD4		
	296 NIKHVPGGGSVQIVYKPVDLSKVTSKCGSLGNIHHKPGGGQVEVKSEKLDFKDRVQSKIGSLDNITHVPGGGNKKIETHKLTFRENAKAKTDHGAEIVYK 395		
	296 NIKHVPGGGSVQIVYKPVDLSKVTSKCGSLGNIHHKPGGGQVEVKSEKLDFKDRVQSKIGSLDNITHVPGGGNKKIETHKLTFRENAKAKTDHGAEIVYK		
	301 NIKHVPGGGSVQIVYKPVDLSKVTSKCGSLGNIHHKPGGGQVEVKSEKLDFKDRVQSKIGSLDNITHVPGGGNKKIETHKLTFRENAKAKTDHGAEIVYK		
	296 NIKHVPGGGSVQIVYKPVDLSKVTSKCGSLGNIHHKPGGGQVEVKSEKLDFKDRVQSKIGSLDNITHVPGGGNKKIETHKLTFRENAKAKTDHGAEIVYK		
	285 NIKHVPGGGSVQIVYKPVDLSKVTSKCGSLGNIHHKPGGGQVEVKSEKLDFKDRVQSKIGSLDNITHVPGGGNKKIETHKLTFRENAKAKTDHGAEIVYK 385		
	396 SPVVSGDTSPRHLSNVSSTGSIDMVDSPQLATLADEVSASLAKQGL 441	homology to human tau	100%
	396 SPVVSGDTSPRHLSNVSSTGSIDMVDSPQLATLADEVSASLAKQGL 441		100%
	401 SPVVSGDTSPRHLSNVSSTGSIDMVDSPQLATLADEVSASLAKQGL 446		93%
	396 SPVVSGDTSPRHLSNVSSTGSIDMVDSPQLATLADEVSASLAKQGL 441		92%
	385 SPVVSGDTSPRHLSNVSSTGSIDMVDSPQLATLADEVSASLAKQGL 430		89%

MBD: microtubule binding domain.

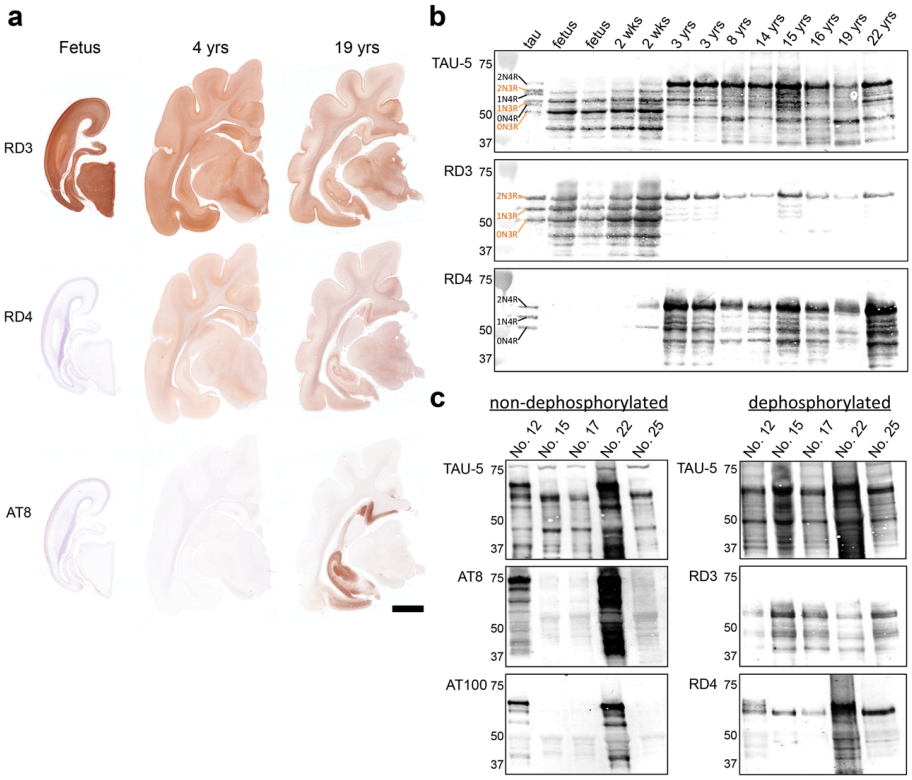

Figure 1. Expression pattern of tau isoforms and their phosphorylation status in cat brains. (a) Immunohistochemistry for 3-repeat tau (RD3), 4-repeat tau (RD4) and hyperphosphorylated tau (HP-tau, AT8) in the developing cat (Fetus, case No. 1), adult cat (4 years, No. 7) and aged cat (19-year-old, case No. 22) brains. Only the 3-repeat tau isoform is expressed in the fetal cat brain, while both 3-repeat and 4-repeat tau isoforms are expressed in the developed cat brains. Abundant AT8-positive HP-tau aggregates are observed in the hippocampus and entorhinal cortex of the aged cat brain. The surface of the developing cerebrum is weakly positive for AT8 HP-tau. Bar = 5mm. (b) Western blotting of TBS-soluble fraction treated with alkaline phosphatase (AP), obtained from the hippocampus of various ages. In the fetus brain, only the 3-repeat tau isoforms are expressed. In the adult cat brains, all six isoforms are detected using anti-tau antibody (tau5) and also RD3 and RD4 antibodies. (c) Western blotting of sarcosyl-insoluble guanidine HCl-soluble fraction without AP-treatment and with AP-treatment, obtained from the hippocampus of various ages. In cat hippocampi that were immunohistochemically positive for HP-tau (No.12 and 22), AT8- and AT100-positive tau proteins are detected. In these cats, the smear-like band pattern resolve into clear bands consisting of both 3-repeat and 4-repeat tau isoforms after dephosphorylation treatment.

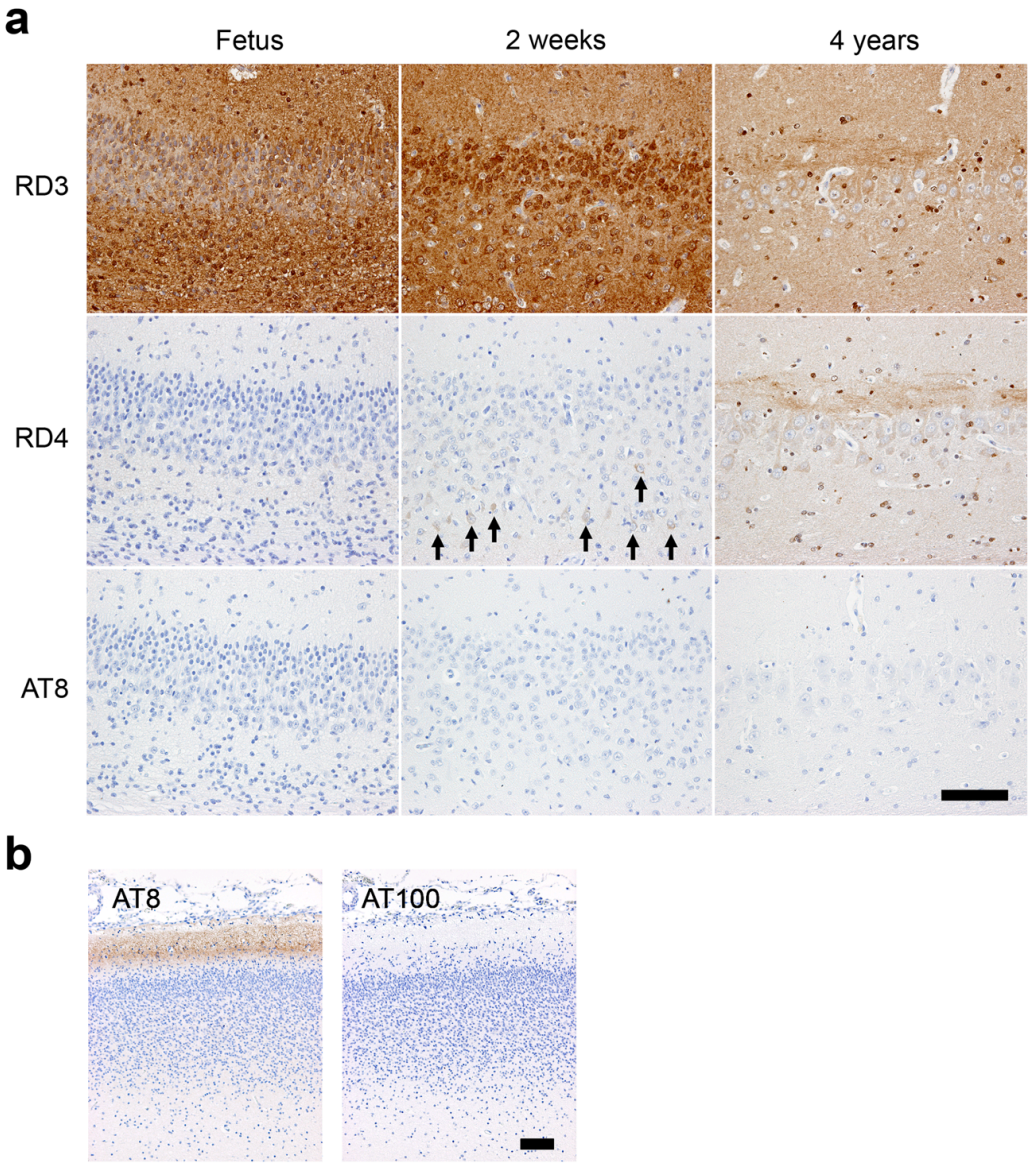

Figure 2. Expression of tau isoforms in the developing cat brains. (a) Immunohistochemistry for 3-repeat tau (RD3), 4-repeat tau (RD4) and hyperphosphorylated tau (AT8). Hippocampus CA1 region of fetus (case No. 1), 2-week-old (case No. 3) and 4-year-old (case No. 7) cat. Only the 3-repeat tau isoform is expressed in the fetal hippocampus. The hippocampal pyramidal cells begin to express 4-repeat tau in the 2-week-old cat. Both 3-repeat and 4-repeat tau isoforms are expressed in the hippocampus of adult cat brain. Bar = 50μm. (b) Immunohistochemistry for hyperphosphorelated tau (AT8 and AT100). Cerebral cortex of fetus cat. The surface layer of the fetal cerebral cortex is positive for AT8 and negative for AT100. Bar = 100μm.

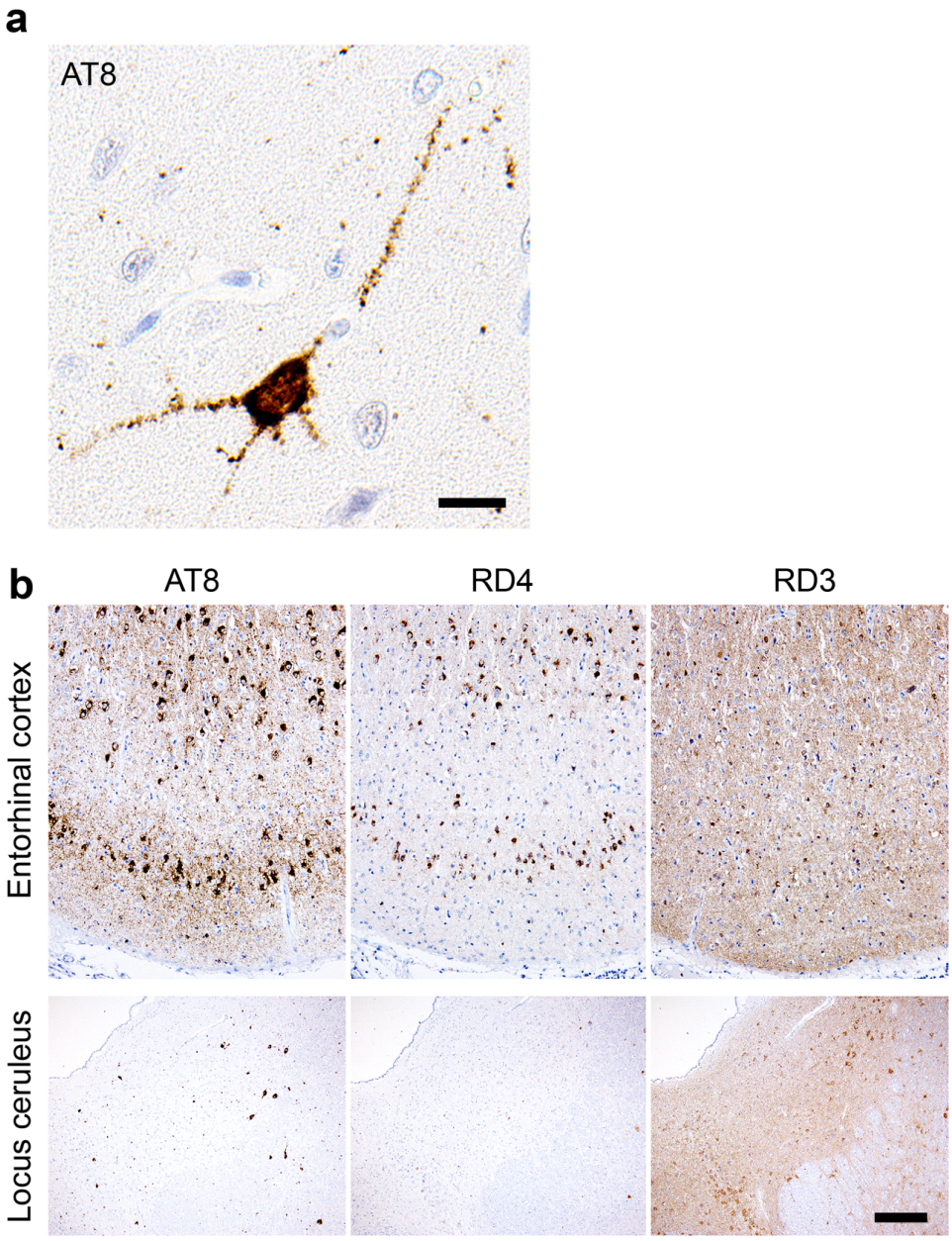

Figure 4. Hyperphosphorylated tau accumulation in the entorhinal cortex and locus ceruleus of cat brains. (a) Immunohistochemistry for hyperphosphorylated tau (AT8). Entorhinal cortex of a cat with mild hyperphosphorylated tau accumulation (15-year-old, case No. 13). The neuronal soma and dendrites are positively stained for hyperphosphorylated tau. (b) Immunohistochemistry for hyperphosphorylated tau (AT8), 3-repeat tau (RD3) and 4-repeat tau (RD4). Entorhinal cortex and locus ceruleus of a cat with severe hyperphosphorylated tau accumulation (14-year-old, case No. 12). AT-8 positive accumulates are also positively stained for 3-repeat tau and 4-repeat tau on consecutive sections.

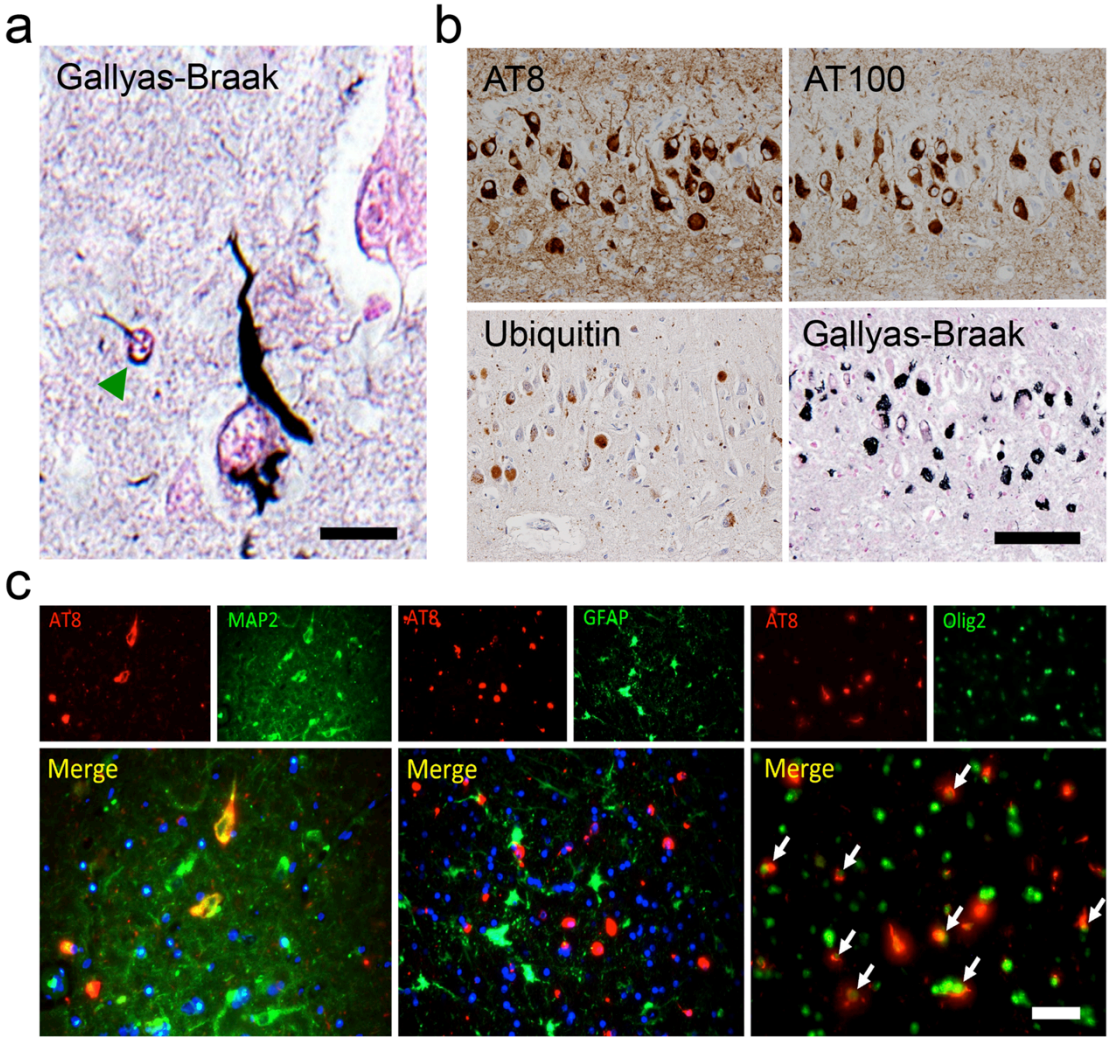

Figure 4. Aged cats develop NFTs. (a) Gallyas-Braak-positive argyrophilic aggregates are observed mainly in the neuronal soma, neurites and also in some oligodendroglial cells (green arrowhead) in the entorhinal cortex of an aged cat brain. Bar = 20μm. (b) Consecutive sections show AT8-, AT100- and ubiquitin-immunopositivity of NFTs. Bar = 100μm. (c) AT8-positive (red) hyperphosphorylated tau is observed in MAP2-positive (green) neurons (left) and Olig2-positive (green) oligodendrocytes (right), but not in GFAP-positive (green) astrocytes (middle). Bar = 50μm.

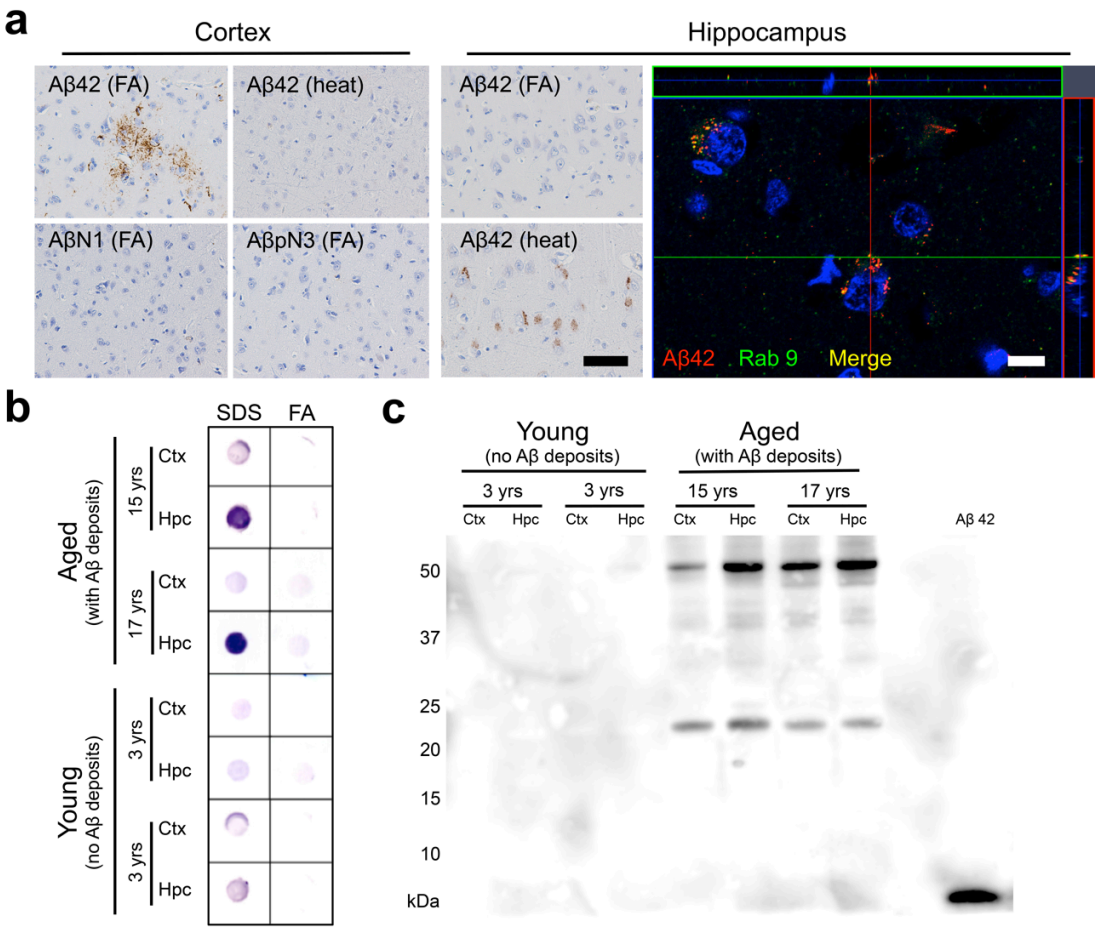

Figure 5. Aβ deposits in cat brains. (a) Aβ42 aggregates are detected in the parenchyma of the cerebral cortex with anti-Aβ42 antibody (12F4) on formic acid (FA)-pretreated sections but not on heat-pretreated sections. These aggregates are not detected with antibodies against the N-terminus of human Aβ (AβN1 and AβpN3). These extracellular Aβ aggregates were scarcely detected in the hippocampus. On the contrary, heat-pretreatment revealed intra-cellular Aβ42 aggregates in the pyramidal cells of the hippocampus but not in the cortex. Some of the intra-cellular Aβ42 aggregates colocalized with Rab9-positive vesicles. Black bar = 50μm, white bar = 10μm. (b) Dotblot analysis of SDS fraction and FA fraction of the cortex (Ctx) and hippocampus (Hpc) of young cats without Aβ deposits and aged cats with Aβ deposits. Aβ oligomers were detected with A11 antibody, predominantly in the SDS fraction from the hippocampus of aged cats. (c) Western blotting analysis of the SDS fraction. Two distinct bands were detected with anti-Aβ antibody 6E10 in the brains of aged cats: approximately 24 kDa and 54 kDa, indicating Aβ hexamers and dodecamers respectively. Ctx, cortex; Hpc, hippocampus.

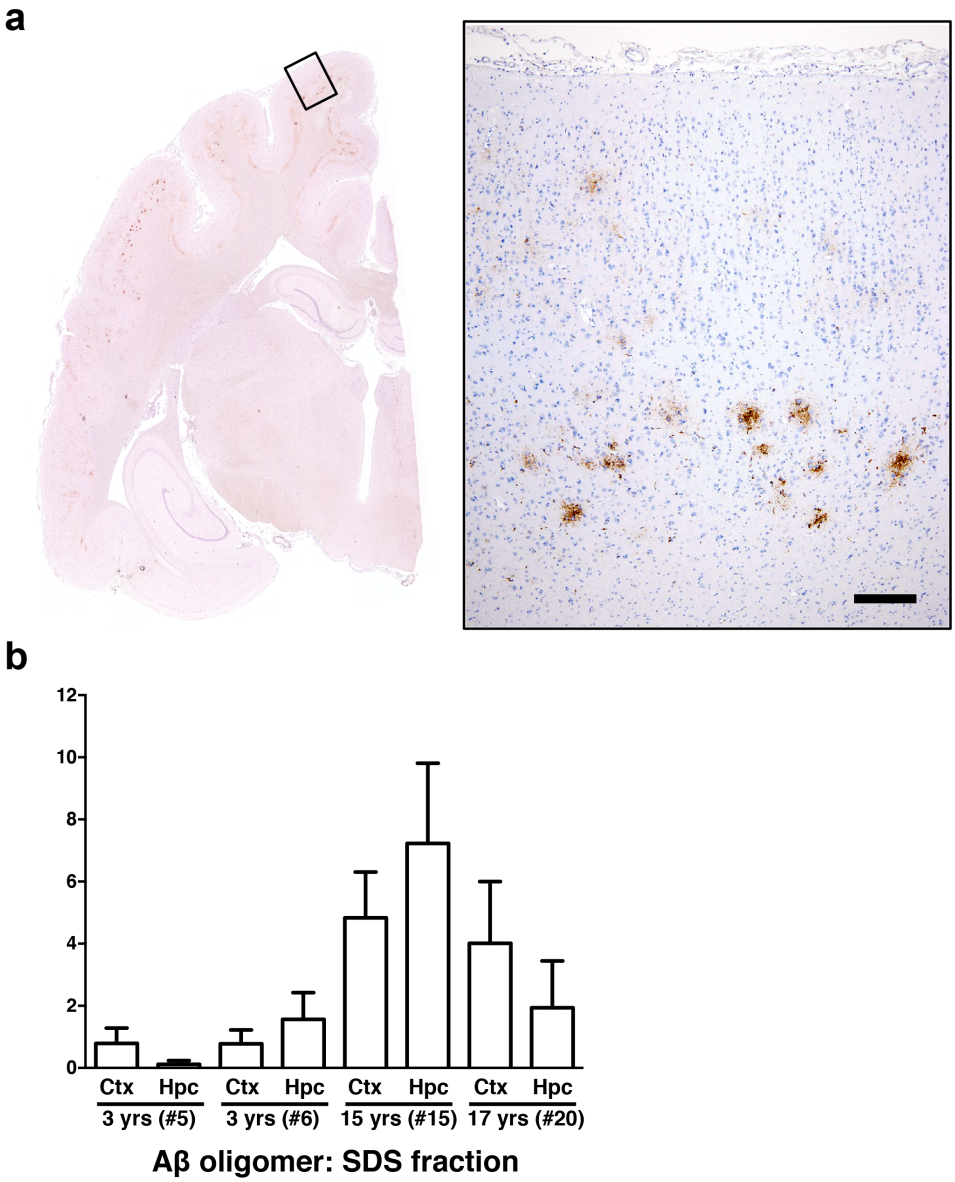

Figure 6. Aβ deposition in cat brains. (a) Immunohistochemistry for Aβ 42 with FA pretreatment. Cerebrum of 17-year-old cat (case No. 20). Aβ42 aggregates are observed in the cerebral cortex but not in the hippocampus by immunohistochemistry with FA pretreatment. Higher magnification of the parietal lobe (right). Bar = 100μm. (b) ELISA for high-molecular weight Aβ oligomers. Larger amounts of Aβ oligomers in the brains of aged cats (15-year-old, case No. 15; 17-year-old, case No.20) compared to brains of young cats (3-year-old, case No. 5; 3-year-old, case No. 6). Ctx, cortex; Hpc, hippocampus.

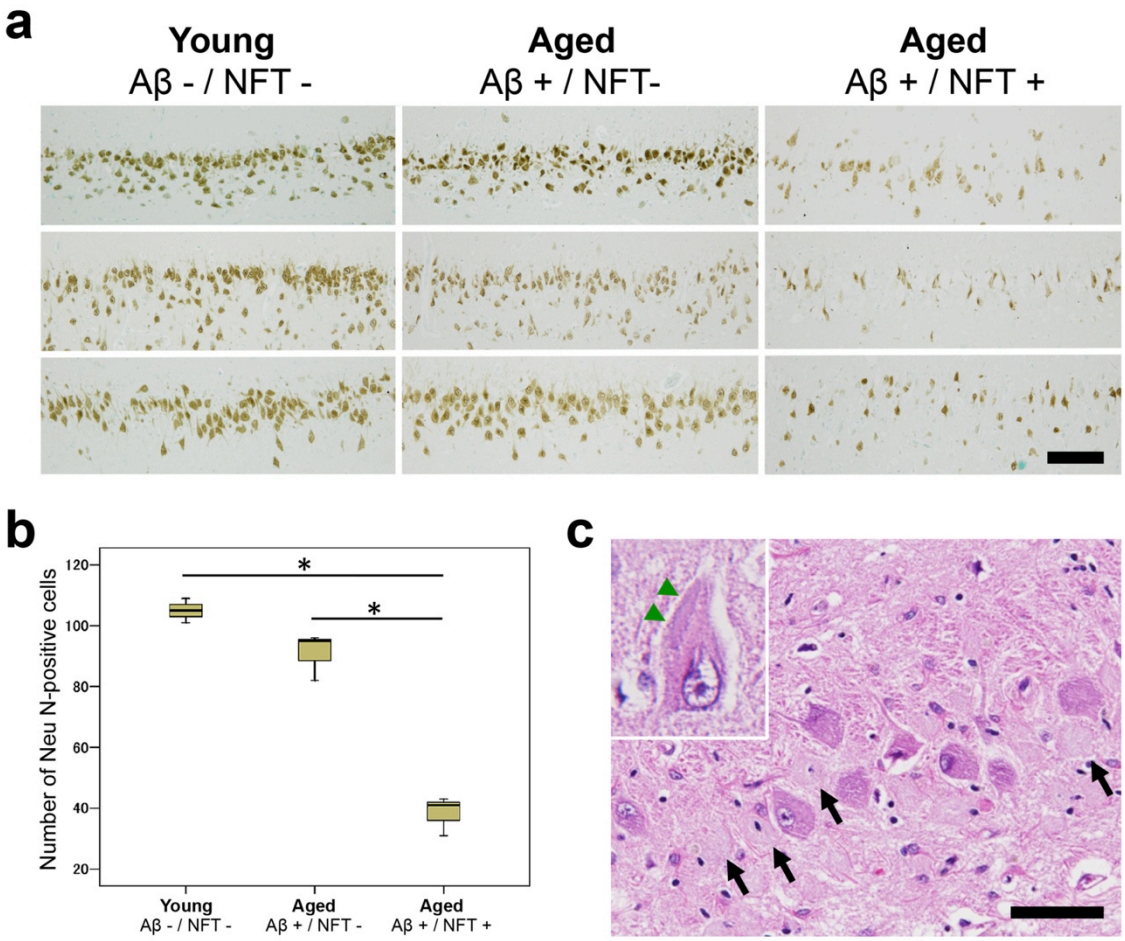

Figure 7. Hippocampal neuronal loss in cat brains with NFTs. (a) Immunohistochemistry for NeuN. Bar = 100μm. (b) The number of NeuN-positive pyramidal cells is significantly decreased in aged cats with Aβ deposits and NFTs (Aβ＋/NFT＋, n=3, mean age 17.6-year-old) compared to young cats (Aβ–/NFT–, n=3, mean age 3.7-year-old) and aged cats with Aβ deposits but no NFTs in hippocampus (Aβ＋/NFT–, n=3, mean age 18-year-old). *: P<0.001. (c) Gghost-cells (arrows) are observed on HE section. In some of the cells, inclusions (composed of hyperphosphorylated tau, confirmed on consecutive slides) were observed (inset, arrowheads). Bar = 50μm.

6. Abstract

Although many animal species develop senile plaques composed of Aβ protein identical to human, non-human mammals seldom develop NFTs and subsequent neurodegeneration, both of which are directly related to the development of dementia in human AD. This chapter shows that the NFT formation together with a significant neuronal loss naturally emerged in the hippocampus of aged domestic cats. The spatial distribution, affected cells and constituting tau isoforms of NFTs in the aged cat brains were identical to those of patients with AD. Interestingly, cats possess the Aβ amino acid sequence different from that of the human-type Aβ, and cats did not have mature argyrophilic amyloid plaques, but instead small intraneuronal Aβ aggregates in the form of oligomers vulnerable to FA were detected in the hippocampal pyramidal cells together with NFTs. Biochemical analysis detected abundant soluble Aβ oligomers (hexamers and dodecamers) in the hippocampus of the cats. The present results from the cat brain together with findings in other animal species that form argyrophilic plaques (chapters 1 to 4) indicate the importance of Aβ oligomers rather than senile plaques for the formation of NFTs and subsequent hippocampal neurodegeneration. The author propose that domestic cat is an excellent animal model that naturally develops AD pathologies, especially Aβ oligomers, NFTs and neuronal loss.

Chapter 5

Neurofibrillary tangles and beta amyloid deposition in the brains of wild Tsushima leopard cats

1. Introduction

NFT, one of the diagnostic lesions of AD, are rarely found in non-human animal brains. Although the etiology of AD is yet to be elucidated, the "amyloid hypothesis" is widely accepted to explain its pathogenesis [Hardy 2006]. According to this hypothesis, the age-dependent accumulation of Aβ peptides in the brain induces a subsequent cascade that culminates in NFT formation. Argyrophilic aggregates of Aβ peptide are called SPs, which are another diagnostic lesion of AD.

The AD-related alterations that occur in the aged brains of animals such as monkeys and dogs have been well studied [Chambers 2010; Miyawaki 2001; Nakamura 1998; Nakayama 2001; Uchida 1992]. However, although these animals frequently form SPs with aging, they rarely develop NFT [Braidy 2012; Mutsuga 2012; Sarasa 2009]. Even in the few reported animal cases of NFT, no pathological examinations were performed to exclude other diseases that could have caused the NFT to develop [Rosen 2008; Serizawa 2012]. Therefore, it has been a major interest whether AD is a human-specific disease [Ferrer 2012; Nakayama 2004].

The occurrence of NFT in the brains of captive cheetahs (*Acinonyx jubatus*) has been previously reported [Serizawa 2012]. The cheetah and the Tsushima leopard cats (*Prionailurus bengalensis euptilurus*) belong to the same subfamily (Felidae), two

closely related lineages that diverged approximately 6.7 million years ago [Johnson 2006]. The NFT of the leopard cats were Pathologically consistent with that of human AD and were also accompanied by diffuse granular Aβ42 deposits. Interestingly, unlike other animals such as monkeys and dogs [Chambers 2011], aged cheetahs and leopard cats do not develop argyrophilic SPs though they develop diffuse Aβ deposits in their brains. In the present study, analysis of the leopard cat APP gene revealed a substitution of a base, which altered the N-terminal amino acid sequence of the Aβ protein. Interestingly, many higher mammals that develop argyrophilic plaques, including dogs and monkeys, possess the same Aβ amino acid sequence as humans [Johnstone 1991; Selkoe 1987; Götz 2008]. The present study provides biological insights into the pathogenesis of AD.

2. Materials and Methods

Animal brains

Most of the animals used in this study were wild animals that had lived exclusively on Tsushima Island, Nagasaki Prefecture, Japan. The Tsushima leopard cat is a subspecies of the leopard cat (*Prionailurus bengalensis*) [Masuda 1995]. The leopard cat was designated as a national endangered species in 1994 and ever since has been the focus of a conservation program funded by the Japanese government [http://kyushu.env.go.jp/twcc/multilang/english/pamph.htm].

A retrospective study was performed using paraffin-embedded tissues from 14 individual brains (Table 1). The brains were obtained from routine necropsies

performed at the Laboratory of Veterinary Histopathology, Kagoshima University; Laboratory of Veterinary Pathology, Yamaguchi University; the Tsushima Wildlife Center of the Ministry of Environment of Japan; or the Department of Veterinary Pathology, the University of Tokyo. Most of these animals were killed in road accidents. No animal was killed for the purposes of this study. Unfortunately, the precise ages of the animals were not determined except for two individuals (Case No. 1: 3-day-old and Case No. 2: 3-year-old) that died at a reproduction facility (Table 1). Case No. 13 and 14 had been kept in captivity at the conservation facility for 10 and 15 years, respectively (Table 1).

Histopathology

All brains were fixed in 10% phosphate-buffered formalin, coronally sliced, and then conventionally embedded in paraffin. The paraffin-embedded tissues were cut into 4-μm-thick serial sections. The deparaffinized sections were then stained with HE, periodic acid-methenamine silver (PAM), and the Gallyas-Braak method.

Immunohistochemistry

Consecutive sections were stained using the immunoenzyme technique. In order to inactivate endogenous peroxidase, the deparaffinized sections were immersed in 1% hydrogen peroxide in methanol at RT for 20 minutes and then washed with TBS. The primary antibodies that were used in this study are listed in Table 2. After incubation with the primary antibody at 4 °C overnight, immunolabeled antigens were

visualized using the Dako Envision+ System (Dako, Carpinteria, CA, USA). In brief, the sections were incubated with HRP-labeled polymer at 37°C for 40 minutes, reacted with 0.05% 3'3-diaminobenzidine plus 0.03% hydrogen peroxide in Tris-hydrochloric acid buffer, and then counterstained with hematoxylin. Negative controls were obtained by omitting the primary antibodies.

Indirect double immunofluorescence staining

The double immunofluorescence staining technique was also performed to determine which cell types contained hyperphosphorylated tau. Anti-MAP2, GFAP, and Olig2 antibodies were used as markers of neuronal cells, astrocytes, and oligodendrocytes, respectively. In addition, the coexistence of hyperphosphorylated tau with glycogen synthase kinase 3-β (GSK 3-β), phosphorylated GSK 3-β (Ser9), and ubiquitin was also analyzed.

After incubation with the primary antibodies at 4°C overnight, the sections were washed with TBS. As secondary antibodies, ALEXA594-conjugated goat anti-mouse IgG (Invitrogen, OR, USA) and ALEXA488-conjugated goat anti-rabbit IgG (Molecular Probes, OR, USA) were mixed with TBS (dilution: 1:100 for both antibodies). The sections were incubated with the secondary antibody mixture at 37°C for one hour, mounted with Vectashield (H-1500, Vector Laboratories, Burlingame, CA, USA), and examined under a Leica DMI 3000B fluorescence microscope (Leica Microsystems, Tokyo, Japan).

Electron microscopic analysis

The formalin-fixed paraffin-embedded brain tissue from Case No. 13 was deparaffinized, cut into 1-mm cubes, fixed in 2.5% glutaraldehyde 0.1M phosphate buffer (pH 7.4), and then post-fixed in 1% osmium tetroxide 0.1 M cacodylate buffer (pH 7.2). The tissues were dehydrated in a graded series of ethanols, treated with QY-1 (Nisshin EM, Tokyo, Japan), and embedded in an epoxy resin (Quetol 651, Nisshin EM). Ultrathin sections from selected areas were stained with uranyl acetate and lead citrate and examined with a Hitachi H-7500 transmission electron microscope (Hitachi High-Technologies, Tokyo, Japan).

Scoring

The distributions of Aβ42 and hyperphosphorylated tau were assessed using the following scoring methods. Aβ42 deposition, −: none, +: diffuse Aβ42 deposition in the cerebral cortex, ++: diffuse Aβ42 deposition in the cerebral cortex and hippocampus, and +++: additional distinct plaque-like deposition; hyperphosphorylated tau, −: none, +: a few AT8-positive cells were found in the parahippocampal gyrus, ++: AT8-positive cells were found in the parahippocampal gyrus and hippocampal CA1 region, and +++: in addition to the parahippocampal gyrus and hippocampal CA1 region, AT8-positive cells were also found in the ectosylvian gyrus and hippocampal CA3 region.

APP transcript sequence analysis

Total RNA was extracted from the formalin-fixed paraffin-embedded brain tissues of three leopard cats (Case No. 7, 8 and 14 were selected as they displayed the least postmortem changes) using the RNeasy FFPE kit (Qiagen, Tokyo, Japan). Subsequently, 10 ng of RNA were reverse-transcribed and amplified using the OneStep RT-PCR kit (Qiagen, Tokyo, Japan) For cDNA amplification, a pair of primers was designed covering exons 11-12 (forward primer 5'-AGATCCGGTCCCAGGTTATG-3') and exons 16-17 (reverse primer 5'-GTCGACCTCCACGACACC-3') of the domestic cat (*Felis catus*) APP gene (ENSFCAG00000001556). The PCR products were electrophoresed on 2% agarose gel and then purified using the QIAquick Gel Extraction kit (Qiagen). Direct DNA sequencing was accomplished using the BigDye Terminator v3.1 Cycle Sequencing Kit (Applied Biosystems, CA, USA) on the 3730xl DNA Analyzer (Applied Biosystems).

3. Results

By immunohistochemical examinations, 6 brains were found to be positive for Aβ42, and 5 brains were positive for hyperphosphorylated tau (Table 1). All of the brains that possessed hyperphosphorylated tau also displayed Aβ42 deposits, but the reverse was not true. The hyperphosphorylated tau-positive cells first appeared in the parahippocampal gyrus, and they subsequently spread through regions CA1 to CA3 of the hippocampus and into the ectosylvian gyrus (temporal lobe) in the more severely affected cases (Figure 1A). On the other hand, Aβ42 was initially diffusely deposited in the parietal and temporal cortices and subsequently spread to the hippocampal region.

In some cases, Aβ42 was deposited in a speckled pattern (Figure 1B); however, these deposits were very diffuse, and none of the deposits in these cases were stained with PAM staining. Also, Aβ42 was not deposited in the vascular walls.

In general, Aβ42 was granularly deposited in the neuropil of the pyramidal cell layer (Figure 2A). Interestingly, these deposits were immunolabeled with neither anti-AβN1 antibody nor anti-AβpN3 antibody on sequential sections (Figures 2B and 2C). In addition to Aβ peptides, aggregates of hyperphosphorylated tau were observed in the neurites and perikarya (Figure 2D). These aggregates displayed intense staining for both the 3 repeat (3R) and 4 repeat (4R) tau isoforms (Figures 2E and 2F). Colocalization of tau recognized by anti-pan tau antibody and anti-hyperphosphorylated tau antibody, anti-3R-tau antibody and anti-4R-tau antibody, also Aβ recognized by anti-pan Aβ antibody and anti-Aβ42 antibody were confirmed (Figure 3). With Gallyas-Braak staining, argyrophilic NFT and neuropil threads were abundantly observed in the areas containing hyperphosphorylated tau-positive cells (Figure 4). Ultrastructurally, some neuronal somata and neurites had been filled with bundles of filaments (Figure 5A). These filaments formed paired structures with diameters of 10-20 nm. Most of the filaments were straight (Figure 5B), but some displayed helical structure (Figure 5C).

Double immunofluorescence staining examinations revealed that aggregates of hyperphosphorylated tau had developed not only in neuronal cells but also in some oligodendrocytes (Figure 6A and 6C). There were no astrocytic plaques (Figure 6B), which was also confirmed by the Gallyas-Braak method. In addition, the

unphosphorylated form of GSK-3β, which is the major kinase involved in tau phosphorylation, colocalized with hyperphosphorylated tau in neuronal somata, whereas staining for phosphorylated-GSK-3β was negative in these cells (Figures 7A and 7B). The hyperphosphorylated tau-positive cells were markedly positive also for ubiquitin, which was distributed in a granular pattern (Figure 7C). The aggregation of hyperphosphorylated tau was confirmed with AT100 antibody (Figure 7D), which detects different phosphorylation sites from AT8 antibody (AT8: Ser202/Thr205 and AT100: Ser212/Thr214).

Both 3R-tau and 4R-tau were expressed in the brains of adult individuals regardless of the presence or absence of NFT formation (Figure 8B and 8C). However, only the 3R-tau protein was expressed in the brain of a neonatal (3-days-old) leopard cat (Figure 8A).

Sequence analysis of the APP transcripts obtained from 3 leopard cats (Case No. 7, 8, and 14) revealed that their Aβ domains had identical sequences (Figure 9). Alignment with the human APP sequence (ENSG00000142192) showed 8 nucleic acid substitutions in the Aβ domain, one of which resulted in the substitution of the 7th amino acid residue (Asp in humans, Glu in leopard cats) of the Aβ peptide (Figure 8).

4. Discussion

Many animal species develop Aβ deposits, especially higher mammals (e.g., monkeys, dogs, bears, camels, and horses) [Nakamura 1998; Capucchio 2010; Nakamura 1995; Uchida 1990; Uchida 1995]. Most of these animals develop

argyrophilic plaques, and some even develop mature plaques with amyloid cores. In contrast, felids seldom develop argyrophilic SPs, but granular aggregates of Aβ peptide are often observed in aged domestic cats and cheetahs [Mutsuga 2012; Serizawa 2012; Gunn-Moore 2007; Nakamura 1996]. In the felid phylogenetic tree, the leopard cat lineage is located in between the cheetah lineage and the domestic cat lineage [Johnson 2006]. These three species are the most recent to have diverged among the 8 lineages of living felids. The findings obtained in this study further confirm the distinctive pattern of Aβ deposition that occurs in the brains of felids (Figure 2A). In addition, we found that the N-terminal epitope of the leopard cat Aβ peptide differs from that found in humans and other animals that develop argyrophilic plaques (Figure 2B, 2C, Figure 8) [Chambers 2010; Johnstone 1991; Selkoe 1987; Piccini 2005]. It has recently been established that the N-terminal subtype of Aβ peptides affects their aggregability, and hence, plaque formation [Schilling 2006; Schilling 2008]. The alternative N-terminal epitope of the leopard cat might be responsible for the low aggregability of its Aβ peptides, which do not seem to produce argyrophilic plaques or vascular deposits.

Most interestingly, nearly all of the individuals that displayed Aβ deposition also possessed NFT (Table 1, Figure 4). Considering that non-human animals rarely develop NFT, a high incidence of NFT is likely to be a trait of this species. In order to determine whether these NFTs correspond to the NFTs found in AD, the author investigated their histopathological characteristics. Since the distribution of hyperphosphorylated tau-positive cells in leopard cats was quite similar to that observed in human AD patients, the author developed a scoring system based on the Braak

staging method (Table 1) [Braak 1991]. Although only a limited number of cases were available for study, subjective assessments suggested that the spread of tau hyperphosphorylation in leopard cats corresponds to the progression of AD [Jucker 2011].

Human diseases that involve the development of intracellular aggregates of tau protein, such as Pick's disease (PiD), corticobasal degeneration (CBD), progressive supranuclear palsy (PSP), argyrophilic grain disease (AGD), and AD, are termed tauopathies. In CBD and PSP, tau often aggregates in astrocytic processes, forming lesions called astrocytic plaques and tufted astrocytes [Hasegawa 2006; Ikeda 1998]. PiD and AGD produce distinctive tau inclusions in neuronal cell bodies, which are known as Pick bodies and argyrophilic grains, respectively. In the brains of leopard cats, hyperphosphorylated tau aggregates in neuronal cells and some oligodendrocytes, but not in astrocytes (Figure 6). Oligodendrocytic tau inclusions are most prominently found in PSP and CBD, and to a lesser degree, in AD brains [Nishimura 1995]. In sections of the leopard cat brains that had been stained with the Gallyas-Braak method, NFT and neuropil threads were observed (Figure 4), whereas no Pick bodies or argyrophilic grains were found. Ultrastructurally, the NFT were composed of paired filaments with diameters of 10-20 nm (Figure 5B, 4C), which is consistent with the properties of NFT in AD brains [Tolnay 1999]. However, most of the filaments exhibited a straight laminar structure, rather than the helical structure that is often seen in AD brains [Arima 2006].

Tau protein is associated with microtubules and promotes their

polymerization and stabilization. Exon 10 of the tau gene encodes the second of four microtubule-binding repeat domains; therefore, the alternative splicing of exon 10 results in tau isoforms with either three (3R-tau) or four (4R-tau) microtubule-binding sites. Although the pathomechanism is yet to be elucidated, the dominant tau isoform in inclusions varies among diseases [de Silva 2003; Liu 2008. PiD develops coiled filaments composed of 3R-tau alone [Delacourte 1996; Delacourte 1998], whereas in CBD, PSP, and AGD the filamentous aggregates are composed of 4R-tau alone [Buée 1999; Togo 2002]. In the brains of the leopard cats, both 3R-tau and 4R-tau aggregated in neuronal cells (Figure 2E, 2F, 3B, 3C) [de Silva 2003; Jakes 1991; Yoshida 2006]. In addition, only the 3R-tau isoform was expressed in the brain of the neonatal leopard cat (Figure 8A). In human brains, tau expression shifts from the 3R-tau isoform alone to both the 3R-tau and 4R-tau isoforms between post-natal day 15 and 35 [Couchie 1985; Goedert 1989; Goedert 1990]. Therefore, the age-related expression pattern of tau isoforms and the components of the tau inclusions found in the leopard cat brains correspond to those of human aging.

GSK-3β is the major enzyme involved in tau phosphorylation, which culminates in NFT formation [Hooper 2008]. Phosphorylated-GSK 3-β (Ser9) is the inactive form of the enzyme, whereas the active form of GSK-3β (unphosphorylated) colocalizes with NFT (Figure 7A) [Leroy 2007; Yamaguchi 1996]. In the amyloid cascade hypothesis of AD, GSK 3-β links Aβ deposition and tau hyperphosphorylation in the pathological sequence [Takashima 1998].

As mentioned above, animals that develop argyrophilic SPs, such as monkeys

and dogs, are known to display the same Aβ peptide amino acid sequence as humans. On the other hand, Aβ deposition has never been demonstrated in non-transgenic wild-type rodents, such as rats and mice. Rodent Aβ displays three amino acid differences in its N-terminal region compared with human Aβ, which are presumed to account for the absence of amyloid deposits in wild-type rodents [Jucker 2011]. As it was also the case in the leopard cat, the different amino acid residues are intensively located in the N-terminal region of the Aβ protein [Götz 2008]. The findings of the present study indicate that the leopard cat Aβ peptide has an intermediate aggregative nature between those of human Aβ and rodent Aβ (Table 3). There is increasing evidence to suggest that weakly aggregative forms of Aβ are more important for neurodegeneration than classical argyrophilic plaques consisting of a mass of aggregated Aβ protein [Caughey 2003; Kawarabayashi 2004; Kayed 2003; Ma 2009; Nussbaum 2012; Tomiyama 2010]. However, wild-type rodents with non-aggregative Aβ do not develop NFT. In a study using PS1×APP transgenic mice, the age-dependent accumulation of small Aβ aggregates were found to be related to decreased GSK-3β phosphorylation, which resulted in tau phosphorylation [Jimenez 2011]. Since AD-type NFTs have never been observed in the brains of monkeys or dogs with SPs, it is generally considered that such non-human animals die before NFTs develop [Nakayama 2004]. The leopard cats that were examined in this study are only found on Tsushima Island, Japan. This subspecies has been geographically isolated on this island for approximately 0.1 million years, and a 2005 survey estimated that only 80-110 Tsushima leopard cats remain. The lack of genetic diversity in this subspecies

should be taken into consideration as a potential factor in the peculiar AD pathology seen in these animals.

5. Tables and Figures

Table 1. Immunohistochemical scoring for Aβ42 and hyperphosphorylated tau (AT8).

Case No.	Sex	Age	Aβ42	AT8
1	M[a]	3-day-old	—	—
2	F[b]	3-year-old	—	—
3	F	Adult[c]	—	—
4	M	Adult	—	—
5	M	Adult	—	—
6	F	Adult	—	—
7	M	Adult	—	—
8	F	Adult	—	—
9	F	Adult	++	—
10	F	Adult	+	+
11	M	Adult	++	+
12	F	Adult	+++	++
13	F	captive for 10 years	+++	+++
14	M	captive for 15 years	+++	+++

Scoring of Aβ42 deposition, +: diffuse Aβ42 deposits in the cerebral cortex, ++: diffuse Aβ42 deposits in the cerebral cortex and hippocampus, +++: additional distinct plaque-like deposits. Scoring of hyperphosphorylated tau, +: few AT8-positive cells in the parahippocampal gyrus, ++: AT8-positive cells in parahippocampal gyrus and hippocampal CA1 region, +++: AT8-positive cells extend to ectosylvian gyrus and hippocampal CA3 region. [a] male, [b] female, [c] age unknown.

Table 2. Primary antibodies used in the present study.

Specificity	Clone	Dilution	Antigen retrieval	Manufacturer
Aβ x-42	Mouse mono (12F4)	1:1000	Formic acid	Millipore, Temecula, CA, USA
Aβ N1	Rabbit poly	1:100	Formic acid	IBL, Gunma, Japan
Aβ pN3	Rabbit poly	1:100	Formic acid	IBL, Gunma, Japan
Aβ (pan Aβ)	Rabbit poly	1:100	Formic acid	Chemicon, Temecula, CA, USA
Hyperphosphorylated tau (Ser202/Thr205)	Mouse mono (AT8)	1:100	Autoclaving	Thermo Scientific, Rockford, IL, USA
Hyperphosphorylated tau (Ser212/Thr214)	Mouse mono (AT100)	1:100	Autoclaving	Thermo Scientific, Rockford, IL, USA
Three-repeat tau (RD3)	Mouse mono (8E6/C11)	1:100	Autoclaving	Millipore, Temecula, CA, USA
Four-repeat tau (RD4)	Mouse mono (1E1/A6)	1:100	Autoclaving	Millipore, Temecula, CA, USA
Tau (pan tau)	Rabbit poly	1:100	Autoclaving	Sigma, St Louis, MO, USA
MAP2	Rabbit poly	1:1000	Autoclaving	Millipore, Temecula, CA, USA
GFAP	Rabbit poly	1:400	Autoclaving	Dako, Carpinteria, CA, USA
Olig2	Rabbit poly	1:200	Autoclaving	Millipore, Temecula, CA, USA
GSK-3β	Rabbit poly	1:100	Autoclaving	Cell Signaling, Danvers, MA, USA
Phospho-GSK-3β(Ser9)	Rabbit poly	1:100	Autoclaving	Cell Signaling, Danvers, MA, USA
Ubiquitin	Rabbit poly	1:200	Autoclaving	Dako, Carpinteria, CA, USA

PHF-tau, paired helical filament tau; MAP2, microtubule-associated protein; GFAP, glial fibrillary acidic protein; Olig2, oligodendrocyte transcription factor 2; GSK-3β, glycogen synthase kinase 3 beta.

Table 3. Senile plaque and neurofibrillary tangle formation in humans, leopard cats and rodents.

Aβ protein (difference from human peptide)	Animals with identical Aβ amino acid sequences	SP formation	NFT formation	References
Human Aβ	Monkeys, Dogs, Bears	Argyrophilic plaques in aged individuals	Extremely rare, except in humans	[Johnstone 1991; Selkoe 1987]
Leopard cat Aβ (1 amino acid residue)	Novel	Granular Aβ deposits, No argyrophilic plaques	Often found in cases with Aβ deposits	Present study
Rodent Aβ (3 amino acid residues)	Rats, Mice	No reports of Aβ deposition	No reports of NFT	[Götz 2008]

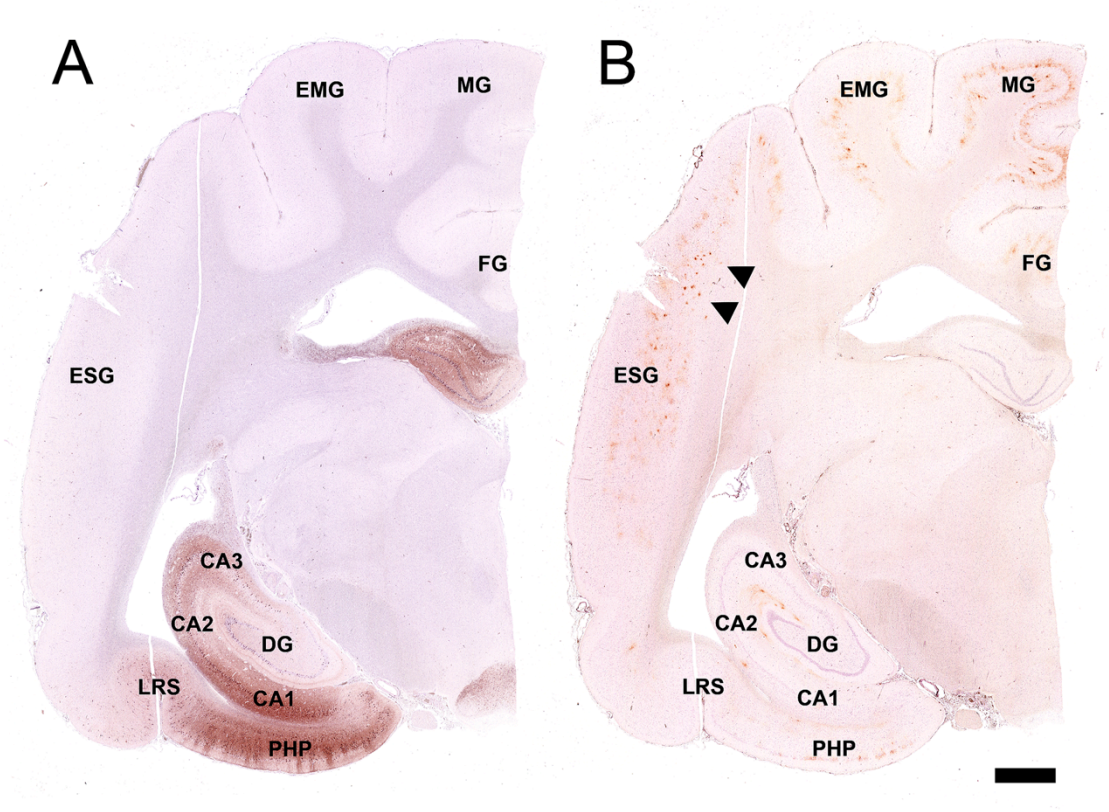

Figure 1. Distributions of hyperphosphorylated tau (A) and Aβ42 (B) in a leopard cat brain. (A) Hyperphosphorylated tau-positive cells were observed throughout the hippocampus and extended into the parahippocampal gyrus and the ectosylvian gyrus. (B) Aβ42 was deposited throughout the cerebral cortex as well as in the hippocampus. Speckled deposits of Aβ42 (arrowheads) were observed in a severely affected brain. Note that these deposits were not argyrophilic plaques. Bar = 2 mm. PHP: parahippocampal gyrus, DG: dentate gyrus, LRS: lateral rhinal sulcus, ESG: ectosylvian gyrus, EMG: ectomarginal gyrus, MG: marginal gyrus, FG: fornicatus gyrus.

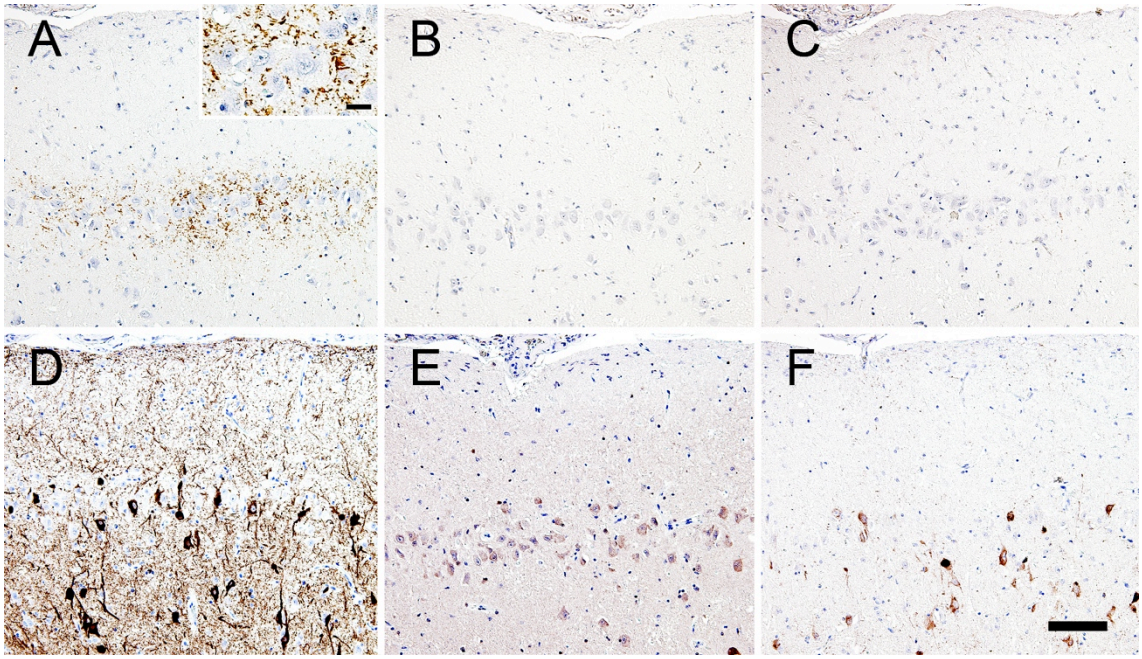

Figure 2. Sequential sections subjected to immunohistochemical examinations of Aβ and tau protein expression in the cerebral cortex. Aβ42 (A) was deposited in a granular pattern in the pyramidal cell layer of the parahippocampal gyrus (inset: high magnification, bar = 20μm), although staining for AβN1 (B) and AβpN3 (C) was negative on sequential sections. The neurons were intensely stained with anti-hyperphosphorylated tau (AT8) antibody (D). Both 3R-tau (E) and 4R-tau (F) are aggregated in the neuronal cell bodies on sequential sections. Bar = 100 μm.

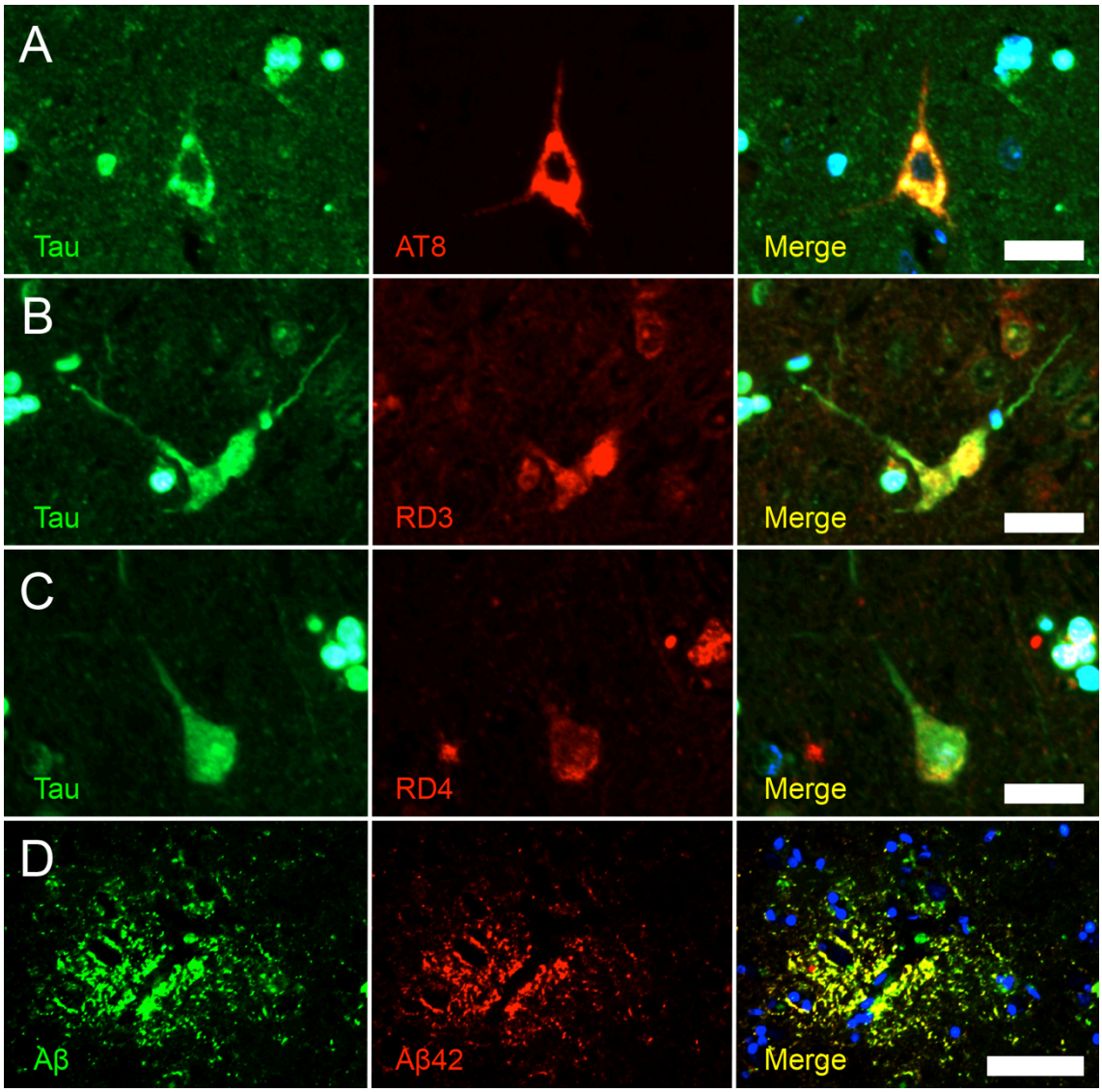

Figure 3. Double immunofluorescence staining of tau/hyperphosphorylated tau (AT100) (A), tau/3R-tau (B), tau/4R-tau (C), and Aβ/ Aβ42. (A, B, C) Hyperphosphorylated tau, 3R-tau and 4R-tau colocalized with pan tau-positive aggregates. Bar = 20 μm. (D) Granular staining of Aβ42 colocalized with pan Aβ. Bar = 100 μm.

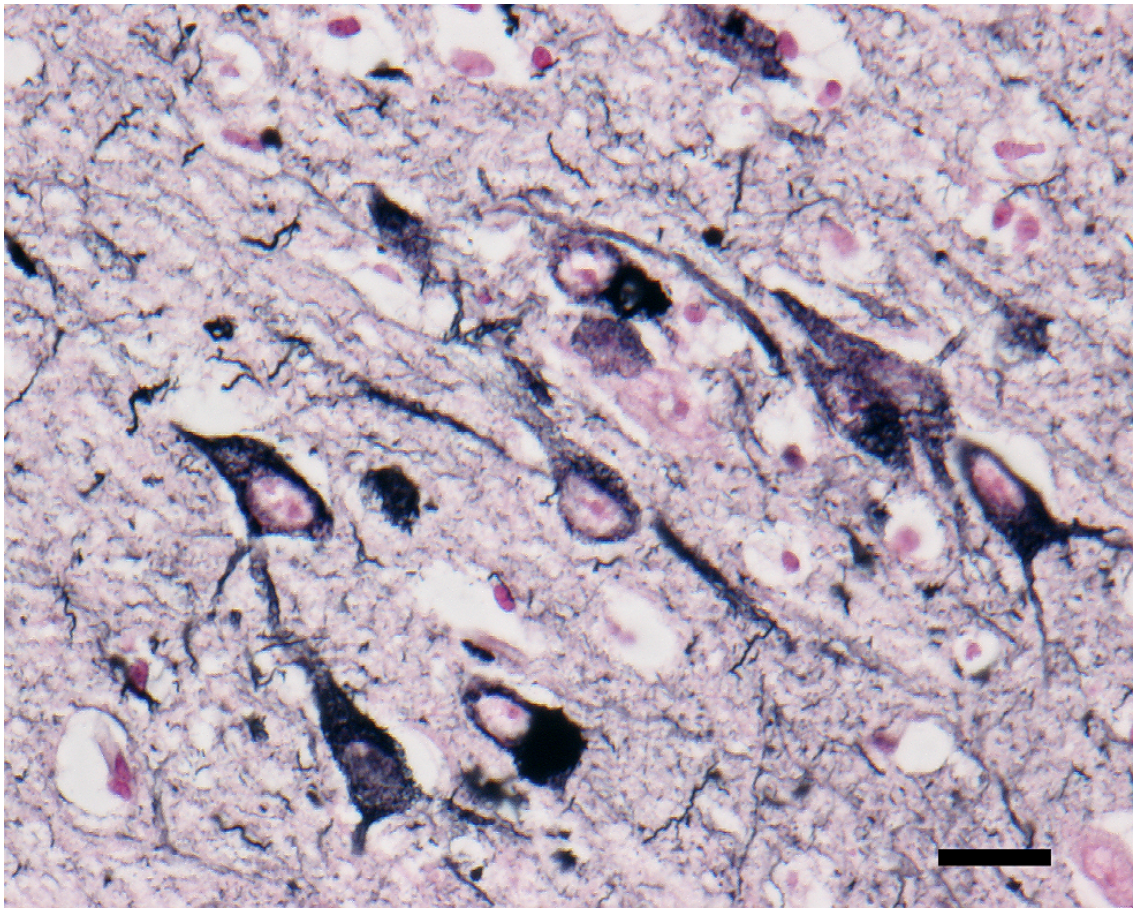

Figure 4. Gallyas-Braak staining. Argyrophilic NFTs and neuropil threads were abundantly observed in the areas containing hyperphosphorylated tau-positive cells. Bar = 100 μm. Inset: higher magnification of the affected neurons. Bar = 20 μm.

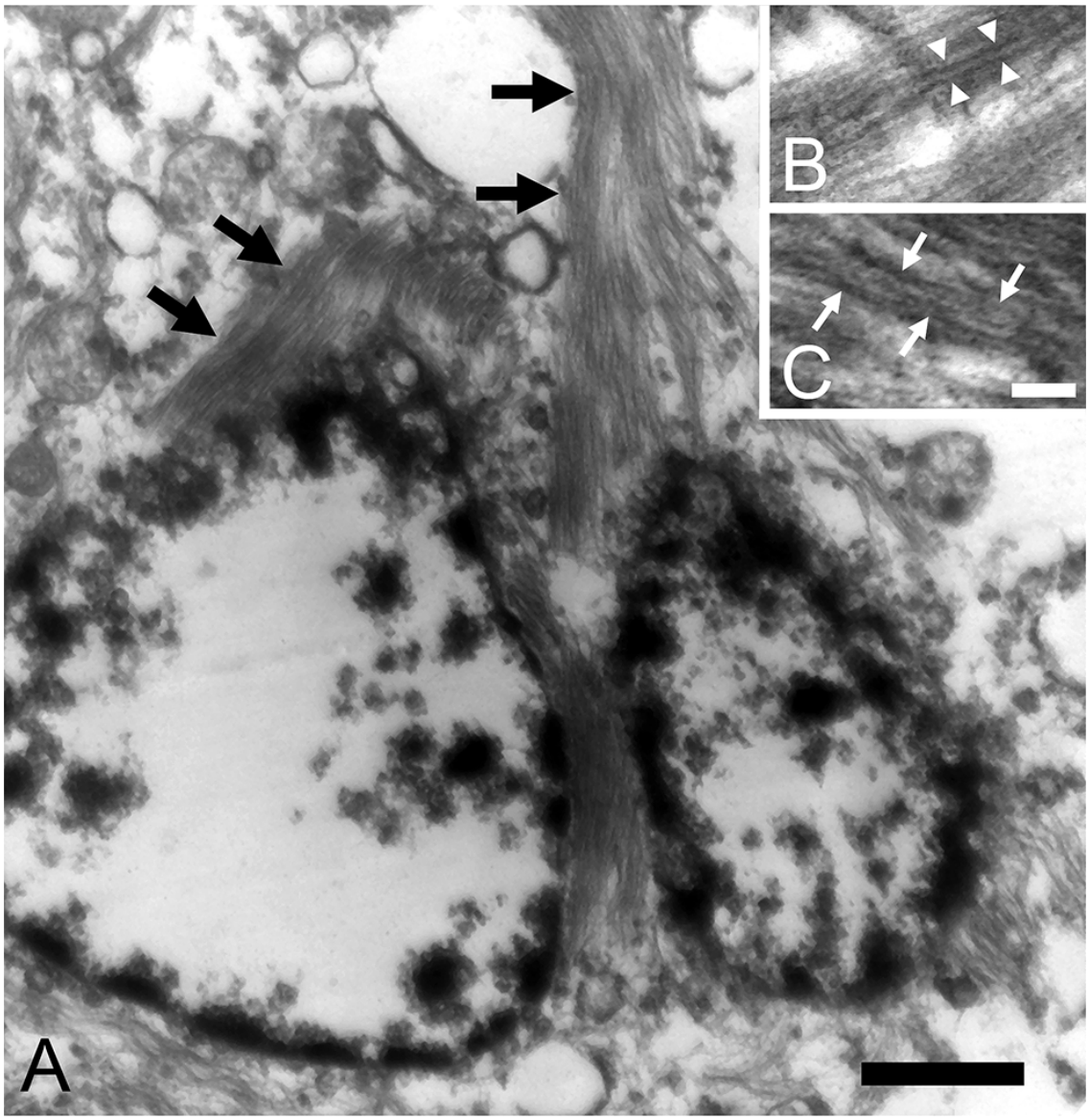

Figure 5. Electron micrographs of NFTs. (A) Some neuronal somata and neurites were filled with filamentous bundles (black arrows). Bar = 1 μm. (B, C) The filaments formed paired structures with diameters of 10-20 nm. Straight laminar filaments (white arrowheads) and constrictions (white arrows) suggesting helical structure. Bar =50 nm.

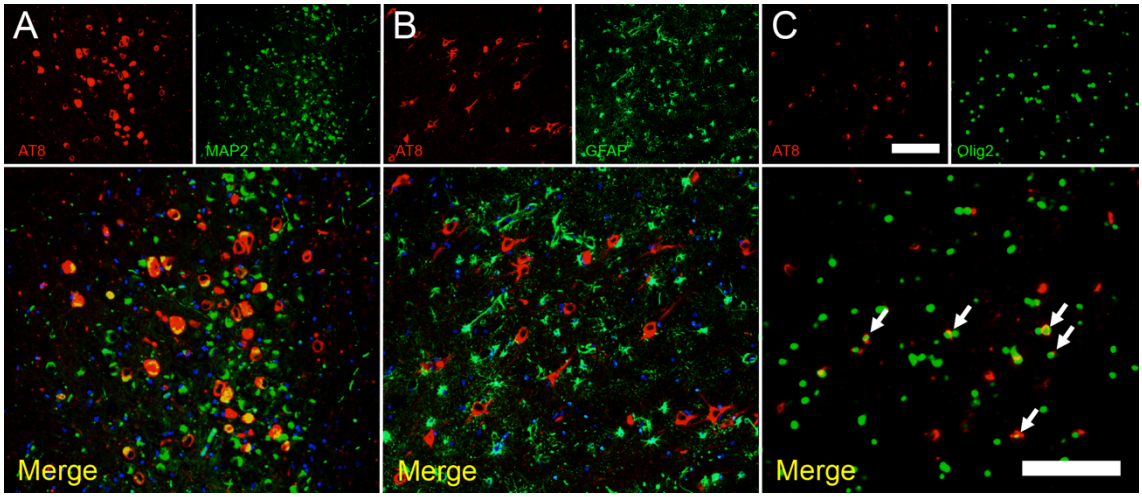

Figure 6. Double immunofluorescence staining of hyperphosphorylated tau (AT8)/MAP2 (A), AT8/GFAP (B), and AT8/Olig2 (C). Hyperphosphorylated tau was mainly localized in neuronal cells (MAP2+) and a few oligodendrocytes (Olig2+) (A, C), but not in astrocytes (GFAP+) (B). Bars = 100 μm.

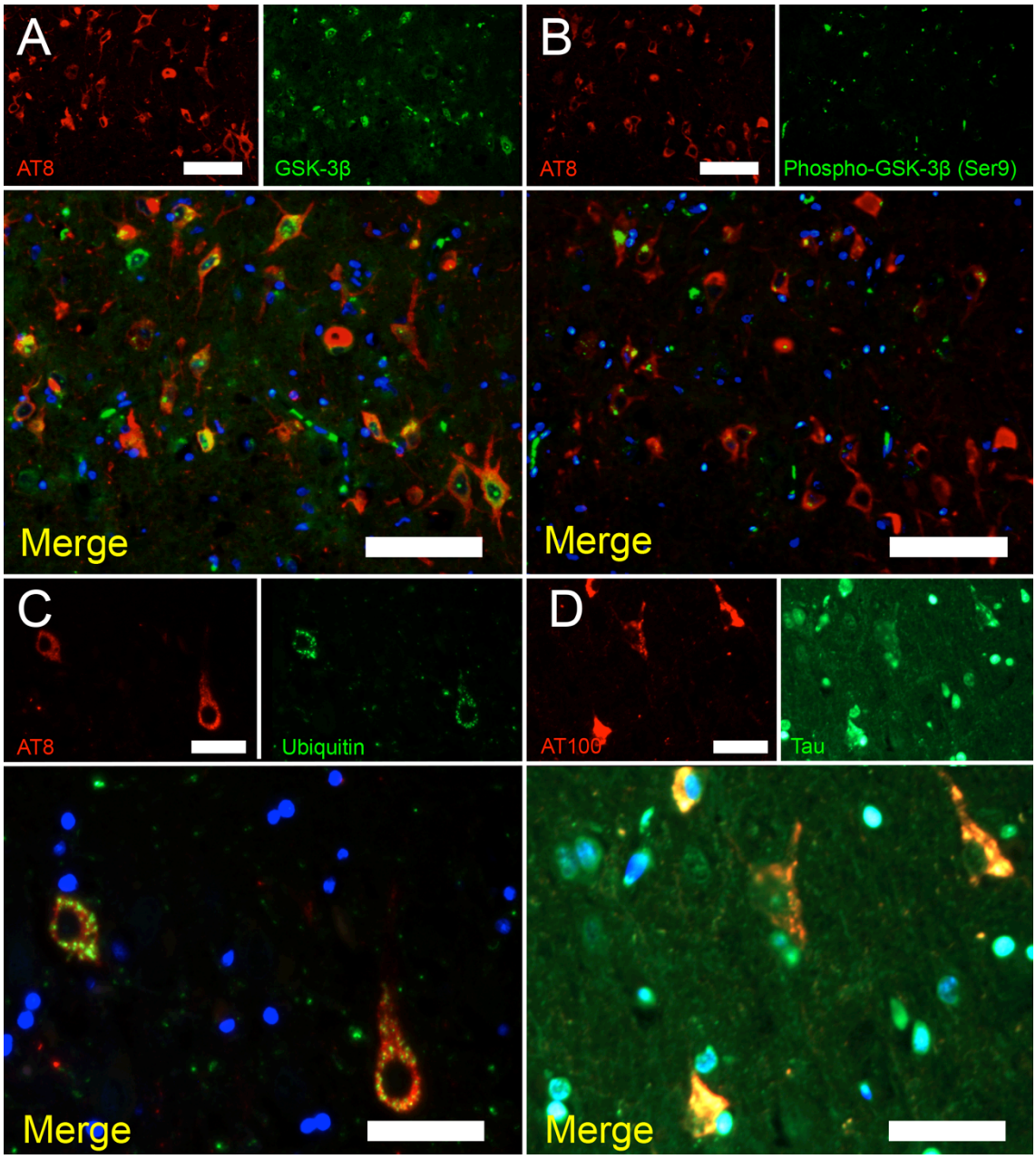

Figure 7. Double immunofluorescence staining of hyperphosphorylated tau (AT8)/GSK-3β (A), AT8/Phospho-GSK-3β (Ser9) (B), AT8/ubiquitin (C), and hyperphosphorylated tau (AT100)/tau (D). (A, B) AT8 colocalized with GSK-3β but not with phospho-GSK-3β (Ser9). Bars = 100μm. (C) Granular staining of ubiquitin was observed in the hyperphosphorylated tau-positive neurons. Bar = 50 μm. (D) AT100 colocalized with aggregated tau. Bar = 50 μm.

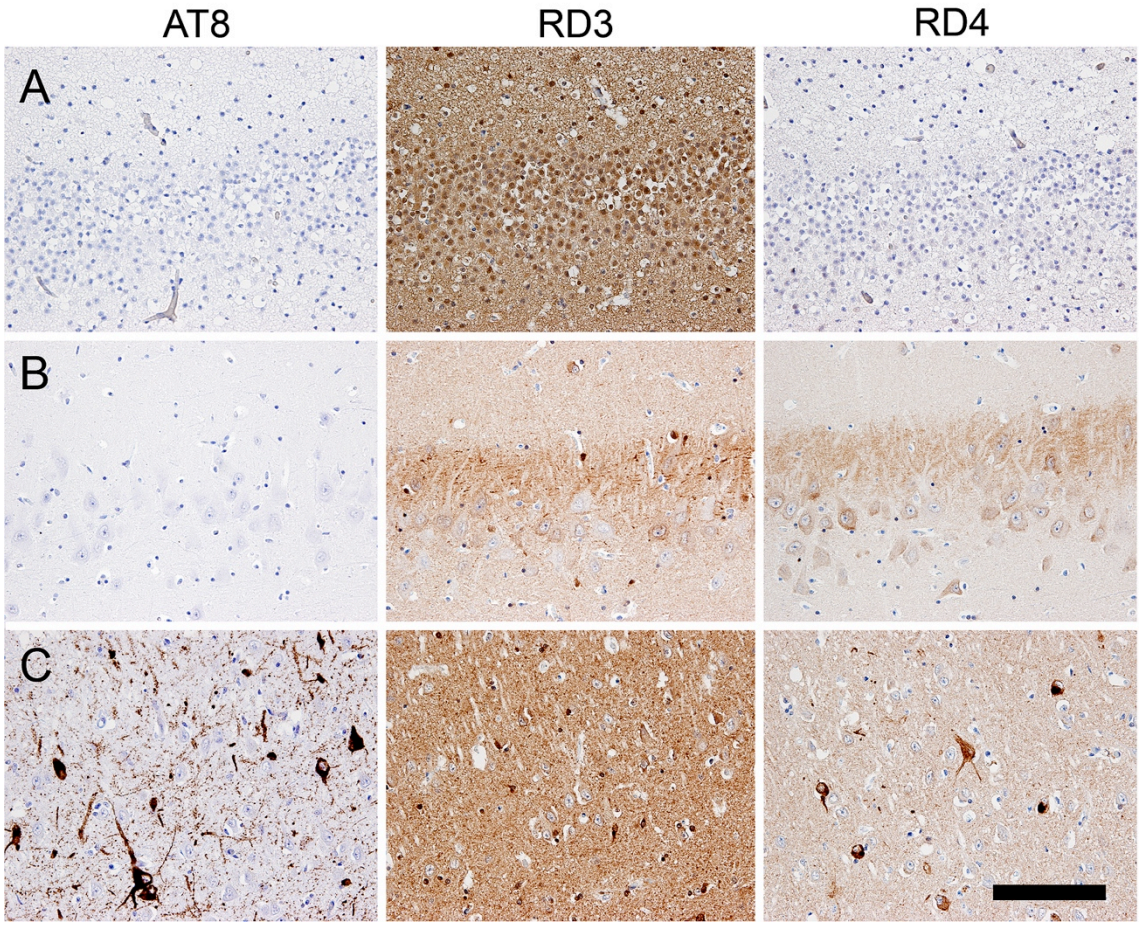

Figure 8. Sequential sections subjected to immunohistochemical staining of hyperphosphorylated tau (AT8), 3R-tau and 4R-tau in the CA1 region of a neonate brain (A), an adult brain without AT8-positive aggregates (B), and an adult brain with AT8-positive aggregates (C). (A) Only the 3R-tau isoform was expressed in the brain of the neonatal leopard cat. (B, C) In the adult brains, both the 3R-tau and 4R-tau isoforms were expressed regardless of the presence or absence of AT8-positive aggregates. Bar = 100 μm.

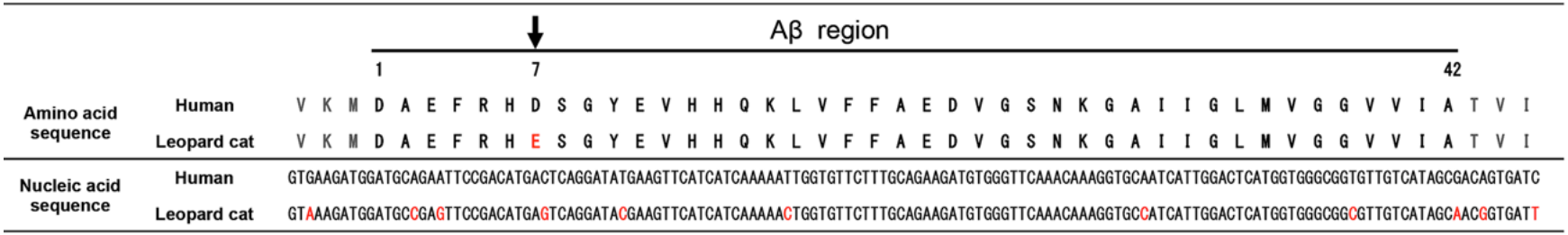

Figure 9. Nucleic acid and amino acid sequences of the leopard cat and human Aβ region. In humans, the 7th amino acid residue of the Aβ peptide is aspartic acid (D), while in leopard cats it is glutamic acid (E).

6. Abstract

Aβ deposits are seen in aged individuals in many of the mammalian species that possess the same Aβ amino acid sequence as humans. Conversely, NFT the other hallmark lesion of AD, are extremely rare in these animals. Aβ deposits were detected in the brains of Tsushima leopard cats (*Prionailurus bengalensis euptilurus*) that live exclusively on Tsushima Island, Japan. Aβ42 was deposited in a granular pattern in the neuropil of the pyramidal cell layer, but did not form argyrophilic senile plaques. These Aβ deposits were not immunolabeled with antibodies to the N-terminal of human Aβ. Sequence analysis of the amyloid precursor protein revealed an amino acid substitution at the 7th residue of the Aβ peptide. In comparison with other mammalian animals that do develop argyrophilic senile plaques, the author concluded that the alternative Aβ amino acid sequence of leopard cat is likely to be related to its distinctive deposition pattern in the brain. The distributions of hyperphosphorylated tau-positive cells and the two major isoforms of aggregated tau proteins were quite similar to those seen in Alzheimer's disease. In addition, the unphosphorylated form of GSK-3β colocalized with hyperphosphorylated tau within the affected neurons. In conclusion, this animal species develops AD-type NFTs without argyrophilic senile plaques.

Conclusion

Researches on the pathogenesis and treatment of AD have largely relied on transgenic mouse harboring the mutated gene of familial AD, and also on the monkey and the dog that possess the same Aβ aminoacid sequence to that of human and spontaneously develop SPs as they age (Table 1) [Braidy 2012; Götz 2008; Head 2013; Janus 2000; Janus 2001]. The monkey and the dog are indeed ideal animal models for studying age-dependent Aβ deposition in the cerebral parenchyma and blood vessel walls, however these animals rarely develop tau pathology, and moreover, neuronal cell death as observed in human AD patients does not occur in these animals.

In the present thesis, the author first studied the N-terminal subtypes of Aβ that compose SPs of the dog, monkey and bear in order to know whether SPs in these animals are actually related to AD or are age-related phenomena as seen in non-demented elderly (normal aging) human. As the result, the SPs of these animals were composed of N-terminally truncated Aβ (AβpN3), indicating that these animals develop AD-type SPs. Therefore, these animals can reproduce the initial step of AD (i.e. SP formation) as they age, although tau pathology, the next step of the amyloid cascade hypothesis of AD, is absent. The absence of tau pathology may be explained by the short life span of these animals. However, in the cat that shows small granular Aβ deposits and no SPs or CAA [Nakayama 2001], Aβ deposits were not labeled by neither anti-human AβN1 antibody nor anti-human AβpN3 antibody. This propensity was also observed in the leopard cat, an animal species that belong to the same family as the domestic cat (Felinae). The different N-terminal epitope and the low aggregability of

Aβ in Felinae species are probably due to the specific N-terminal aminoacid sequence that is conserved among these species (Table 1).

Next, the author described the pathological characteristics of vascular Aβ deposition in the brains of the squirrel monkey and the dog. Aβ 40 has a propensity to deposit in the arterioles, while Aβ42, which has a higher aggregability [Meisl 2014], is deposited in the capillaries that branches from the Aβ40 laden arterioles. In both animal species, capillary Aβ deposits were distributed as clusters in the deeper cortex and the subcortical WM, indicating that the vascular tree that is serving the local area is affected. As it has been described in the dog [Uchida 1992], dense-core plaque-like structures were often found adjacent to the Aβ-laden capillaries, appearing like a fruit of a tree. Since the production rate of Aβ by neurons does not differ with age and local area of the cerebral cortex, the above-mentioned findings may implicate a decreased efflux of ApoE-Aβ complex by the perivascular drainage system of the local vascular unit. This "Vascular tree hypothesis" is explained in Figure 1. Furthermore, in dogs, the WM myelin was substantially lost in correlation with capillary Aβ deposition Aβ-laden capillaries were often occluded, thus the vascular supply should be impaired in the deeper cerebrum (the WM). Such mild ischemia may induce oxidative damage to the myelin lipids. In fact, abundant peroxidate lipid-laden macrophages were found in the perivascular space in the WM of aged dogs with WM myelin loss. The author concludes that damaged myelin lipids are engulfed by macrophages and gathered around the vessels. This notion is in concordance with demyelinating disease such as MS [Kooi 2009]. Recently, the significance of cerebral WM myelin loss relating to

capillary CAA is disputed [Rolyan 2011; Thal 2009; Thal 2012]. The present study revealed that WM demyelination occurs in aged dogs as well as in aged humans, hence WM alteration may account for age-related behavioral changes of the dog. Moreover, dogs are useful animal model for CAA-related WM myelin loss as well as microhemorhage in AD patients [Uchida 1990].

In chapters 4 and 5, pathology of age-dependent NFT formation in the brains of domestic cat and the leopard cat was characterized. The affected cells, the distribution, the tau-isoforms and the activated kinase of NFTs were identical to that of human AD. The domestic cat was further studied, and intracellular Aβ oligomers were found in the hippocampus where NFTs were often developed. In addition, the hippocampal neurons were significantly decreased in aged cats with severe NFTs. Here, the author hypothesizes the mechanism of NFT formation in the cat that has a much shorter life span than human (Figure 2). The felid-type Aβ is resistant to develop SPs, but its oligomeric form induces hyperphosphorylation of tau proteins to develop NFTs. In fact, in other animal species that express human-type Aβ (i.e. monkeys and dogs), SPs may be gathering (buffering) toxic Aβ oligomers as "trash bins", preventing from proceeding to NFT formation. Exceptionally, we humans extended our life-span to overwhelm the buffering capacity of SPs, and proceed to NFT formation and neuronal loss due to the accumulated effect of Aβ oligomers. The results of the current thesis show a close topographical relation of intracellular Aβ, NFTs and neuronal loss in the hippocampus of the cat brain. However, no significant neuronal loss was observed in cat brains with intracellular Aβ but without NFTs. This

indicates the importance of NFTs in hippocampal neurodegeneration in aged cats, as well as in human AD brains.

Lastly, the present study has shown that, comparing the difference of age-related brain lesions among animal species not only will devote to seeking animal models but also will light the unrevealed pathology of human dementia from a novel point of view.

Table 1. Aβ and Tau amino acid homology and AD pathologies in human and animal.

Species	Aβ			Tau			Neuron loss
	Sequence vs. human	Oligomers	SP	Sequence vs. human	Isoforms	NFT	
Human	—	Yes	Yes	—	3R+4R (6)	Yes	Yes
Chimpanzee	100%	ND	Yes	100%	3R+4R (6)	No	No
Dog	100%	Yes	Yes	92%	3R+4R (4)	No	No
Cat	1 a.a. different	Yes	No	93%	3R+4R (6)	Yes	Yes
Mouse	3 a.a. different	No	No	89%	4R (4)	No	No

3R, 3-repeat; 4R, 4-repeat; (number of isoforms).

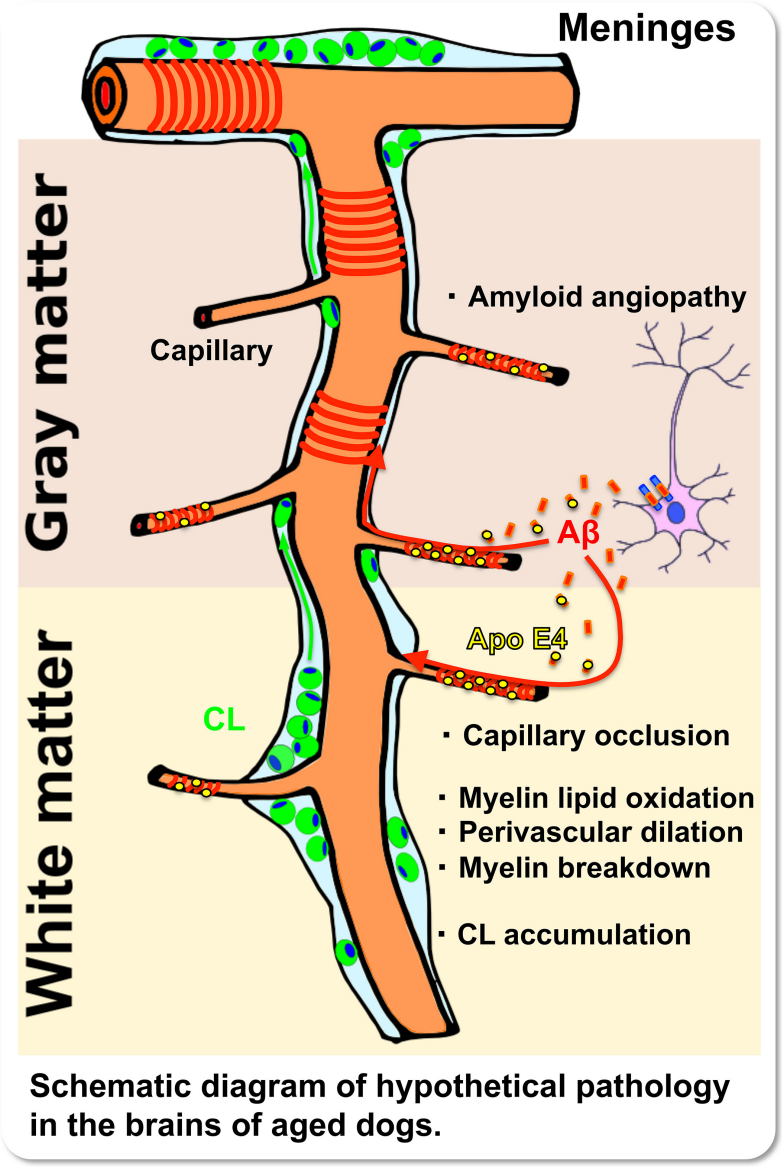
Meninges
Gray matter
White matter
Capillary
· Amyloid angiopathy
Aβ
Apo E4
CL
· Capillary occlusion
· Myelin lipid oxidation
· Perivascular dilation
· Myelin breakdown
· CL accumulation
Schematic diagram of hypothetical pathology in the brains of aged dogs.

Figure 1.

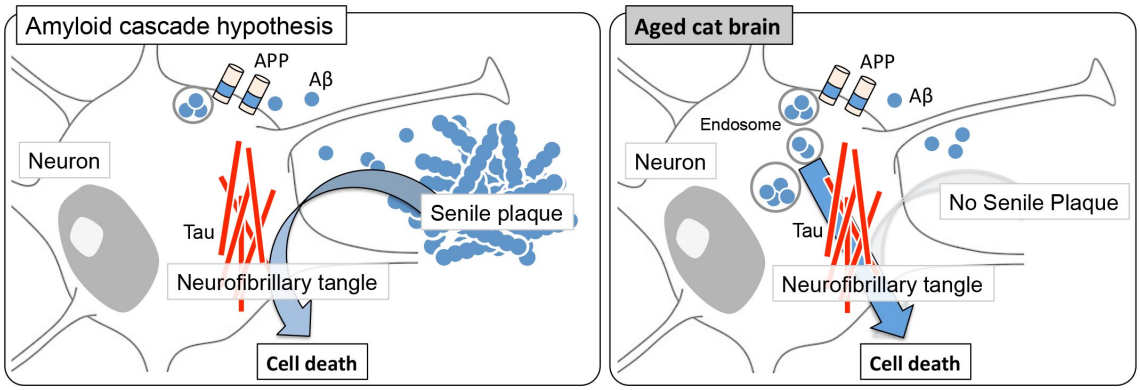
Amyloid cascade hypothesis
APP
Aβ
Neuron
Tau
Senile plaque
Neurofibrillary tangle
Cell death
Aged cat brain
APP
Aβ
Endosome
Neuron
No Senile Plaque
Tau
Neurofibrillary tangle
Cell death

Figure 2

Acknowledgements

I would like to express my sincere gratitude to Professor Hiroyuki Nakayama for guiding me through the long and winding study. I would also like to thank Associate Professor Kazuyuki Uchida for continuously providing invaluable advice, not only on my research but also on my career and personal life. I could not have gone thorough my research without the help of my colleagues Dr. Tomoyuki Harada, Dr. Mizue Ogawa, Dr. Satoshi Suzuki and all the members of the Department of Veterinary Pathology, the University of Tokyo.

I started studying pathology at the Department of Veterinary Pathology, Azabu University as an undergraduate student. I truly appreciate Professor Yumi Une for teaching me all the basis of veterinary pathology. I am grateful to Professor Yasuo Nomura for introducing me to Veterinary Pathology; Professor Kinji Shirota for training me as a pathologist and also giving helpful advice on my research; Associate Professor Junichi Kamiie for teaching me techniques for basic biological research. I would also like to thank Dr. Shin-ichi Nakamura and Dr. Naoyuki Aihara and the other members at the laboratory for studying together with me everyday until late at night.

At last, I truly appreciate my family and friends for all the support. Thank you.

References

1. Abbott A. Dementia: a problem for our age. Nature. 2011;475:S2-4.
2. Acero G, Manoutcharian K, Vasilevko V, Munguia ME, Govezensky T, Coronas G, Luz-Madrigal A, Cribbs DH, Gevorkian G. Immunodominant epitope and properties of pyroglutamate-modified abeta-specific antibodies produced in rabbits. J. Neuroimmunol. 2009;213:39-46.
3. Aizenstein HJ, Nebes RD, Saxton JA, Price JC, Mathis CA, Tsopelas ND, Ziolko SK, James JA, Snitz BE, Houck PR, Bi W, Cohen AD, Lopresti BJ, DeKosky ST, Halligan EM, Klunk WE. Frequent amyloid deposition without significant cognitive impairment among the elderly. Arch. Neurol. 2008;65:1509-1517.
4. Akiyama H, Kondo H, Ikeda K, Kato M, McGeer PL. Immunohistochemical localization of neprilysin in the human cerebral cortex: inverse association with vulnerability to amyloid beta-protein (Abeta) deposition. Brain Res. 2001;902:277-281.
5. Andorfer C, Kress Y, Espinoza M, de Silva R, Tucker KL, Barde YA, Duff K, Davies P. Hyperphosphorylation and aggregation of tau in mice expressing normal human tau isoforms. J. Neurochem. 2003;86:582-590.
6. Arima K. Ultrastructural characteristics of tau filaments in tauopathies: immuno-electron microscopic demonstration of tau filaments in tauopathies. Neuropathology. 2006;26:475-483.
7. Armstrong RA, Cairns NJ, Myers D, Smith CU, Lantos PL, Rossor MN. A comparison of beta-amyloid deposition in the medial temporal lobe in sporadic

Alzheimer's disease, down's syndrome and normal elderly brains. Neurodegeneration. 1996;5:35-41.

8. Attems J, Jellinger KA. The overlap between vascular disease and Alzheimer's disease--lessons from pathology. BMC Med. 2014;12:206.
9. Attems, J, Jellinger K, Thal DR, Van Nostrand W. Review: sporadic cerebral amyloid angiopathy. Neuropathol. Appl. Neurobiol. 2011;37:75-93.
10. Attems J, Lauda F, Jellinger KA. Unexpectedly low prevalence of intracerebral hemorrhages in sporadic cerebral amyloid angiopathy: an autopsy study. J. Neurol. 2008;255:70-76.
11. Attems J, Yamaguchi H, Saido TC, Thal DR. Capillary CAA and perivascular Abeta-deposition: two distinct features of Alzheimer's disease pathology. J. Neurol. Sci. 2010;299:155-162.
12. Bading JR, Yamada S, Mackic JB, Kirkman L, Miller C, Calero M, Ghiso J, Frangione B, Zlokovic BV. Brain clearance of Alzheimer's amyloid-beta40 in the squirrel monkey: a SPECT study in a primate model of cerebral amyloid angiopathy. J. Drug. Target. 2002;10:359-368.
13. Barber R, Scheltens P, Gholkar A, Ballard C, McKeith I, Ince P, Perry R, O'Brien J. White matter lesions on magnetic resonance imaging in dementia with Lewy bodies, Alzheimer's disease, vascular dementia, and normal aging. J. Neurol. Neurosurg. Psychiatry. 1999;67:66-72.
14. Bard F, Barbour R, Cannon C, Carretto R, Fox M, Games D, Guido T, Hoenow K, Hu K, Johnson-Wood K, Khan K, Kholodenko D, Lee C, Lee M, Motter R,

Nguyen M, Reed A, Schenk D, Tang P, Vasquez N, Seubert P, Yednock T. Epitope and isotype specificities of antibodies to beta -amyloid peptide for protection against Alzheimer's disease-like neuropathology. Proc. Natl. Acad. Sci. USA. 2003;100:2023-2028.

15. Bartzokis G. Age-related myelin breakdown: a developmental model of cognitive decline and Alzheimer's disease. Neurobiol. Aging 2004;25:5-18 author reply 49-62.
16. Benilova I, Karran E, De Strooper B. The toxic Aβ oligomer and Alzheimer's disease: an emperor in need of clothes. Nat. Neurosci. 2012;15:349-357.
17. Bennett DA, Gilley DW, Wilson RS, Huckman MS, Fox JH. Clinical correlates of high signal lesions on magnetic resonance imaging in Alzheimer's disease. J. Neurol. 1992;239:186-190.
18. Bennett DA, Schneider JA, Wilson RS, Bienias JL, Arnold SE. Neurofibrillary tangles mediate the association of amyloid load with clinical Alzheimer disease and level of cognitive function. Arch. Neurol. 2004;61:378-384.
19. Bernedo V, Insua D, Suarez ML, Santamarina G, Sarasa M, Pesini P. Beta-amyloid cortical deposits are accompanied by the loss of serotonergic neurons in the dog. J. Comp. Neurol. 2009;513:417-429.
20. Boche D, Zotova E, Weller RO, Love S, Neal JW, Pickering RM,Wilkinson D, Holmes C, Nicoll JAR. Consequence of Abeta immunization on the vasculature of human Alzheimer’s disease brain. Brain. 2008;131:3299-3310.
21. Borras D, Ferrer I, Pumarola M. Age-related changes in the brain of the dog. Vet.

Pathol. 1999:36;202-211.

22. Braak H, Braak E. Neuropathological stageing of Alzheimer-related changes. Acta Neuropathology. 1991;82:239-259.

23. Braak H, Braak E, Strothjohann M. Abnormally phosphorylated tau protein related to the formation of neurofibrillary tangles and neuropil threads in the cerebral cortex of sheep and goat. Neurosci. Lett. 1994;171:1-4.

24. Braidy N, Muñoz P, Palacios AG, Castellano-Gonzalez G, Inestrosa NC, Chung RS, Sachdev P, Guillemin GJ. Recent rodent models for Alzheimer's disease: clinical implications and basic research. J. Neural. Transm. 2012;119:173-95.

25. Brellou G, Vlemmas I, Lekkas S, Papaioannou N. Immunohistochemical investigation of amyloid beta-protein (abeta) in the brain of aged cats. Histol. Histopathol. 2005;20:725-731.

26. Brinkmalm G, Portelius E, Öhrfelt A, Mattsson N, Persson R, Gustavsson MK, Vite CH, Gobom J, Månsson JE, Nilsson J, Halim A, Larson G, Rüetschi U, Zetterberg H, Blennow K, Brinkmalm A. An online nano-LC-ESI-FTICR-MS method for comprehensive characterization of endogenous fragments from amyloid β and amyloid precursor protein in human and cat cerebrospinal fluid. J. Mass Spectrom. 2012;47:591-603.

27. Britschgi M, Olin CE, Johns HT, Takeda-Uchimura Y, LeMieux MC, Rufibach K, Rajadas J, Zhang H, Tomooka B, Robinson WH, Clark CM, Fagan AM, Galasko DR, Holtzman DM, Jutel M, Kaye JA, Lemere CA, Leszek J, Li G, Peskind ER, Quinn JF, Yesavage JA, Ghiso JA, Wyss-Coray T. Neuroprotective natural

antibodies to assemblies of amyloidogenic peptides decrease with normal aging and advancing Alzheimer's disease. Proc. Natl. Acad. Sci. USA. 2009;106:12145-12150.

28. Buée L, Delacourte A. Comparative biochemistry of tau in progressive supranuclear palsy, corticobasal degeneration, FTDP-17 and Pick's disease. Brain Pathol. 1999;9: 681-693.

29. Brown WR, Moody DM, Thore CR, Challa VR. Cerebrovascular pathology in Alzheimer's disease and leukoaraiosis. Ann. N. Y. Acad. Sci. 2000;903:39-45.

30. Calhoun ME, Burgermeister P, Phinney AL, Stalder M, Tolnay M, Wiederhold KH, Abramowski D, Sturchler-Pierrat C, Sommer B, Staufenbiel M, Jucker M. Neuronal overexpression of mutant amyloid precursor protein results in prominent deposition of cerebrovascular amyloid. Proc. Natl. Acad. Sci. USA. 1999;96:14088-14093.

31. Capucchio MT, Márquez M, Pregel P, Foradada L, Bravo M, Mattutino G, Torre C, Schiffer D, Catalano D, Valenza F, Guarda F, Pumarola M. Parenchymal and vascular lesions in ageing equine brains: histological and immunohistochemical studies. J. Comp. Pathol. 2010;142:61-73.

32. Carare RO, Bernardes-Silva M, Newman TA, Page AM, Nicoll JA, Perry VH, Weller RO. Solutes, but not cells, drain from the brain parenchyma along basement membranes of capillaries and arteries: significance for cerebral amyloid angiopathy and neuroimmunology. Neuropathol Appl Neurobiol 2008;34:131-144.

33. Caughey B, Lansbury PT. Protofibrils, pores, fibrils, and neurodegeneration:

separating the responsible protein aggregates from the innocent bystanders. Annu. Rev. Neurosci. 2003;26:267-298.

34. Chen WT, Hong CJ, Lin YT, Chang WH, Huang HT, Liao JY, Chang YJ, Hsieh YF, Cheng CY, Liu HC, Chen YR, Cheng IH. Amyloid-beta (Aβ) D7H mutation increases oligomeric Aβ42 and alters properties of Aβ-zinc/copper assemblies. PLoS. One. 2012;7:e35807.
35. Citron M. Strategies for disease modification in Alzheimer's disease. Nat. Rev. Neurosci. 2004;5:677-685.
36. Citron M, Diehl TS, Gordon G, Biere AL, Seubert P, Selkoe DJ. Evidence that the 42- and 40-amino acid forms of amyloid beta protein are generated from the beta-amyloid precursor protein by different protease activities. Proc. Natl. Acad. Sci. USA. 1996;93:13170-13175.
37. Colle M-, Hauw J-, Crespeau F, Uchihara T, Akiyama H, Checler F, Pageat P, Duykaerts C. Vascular and parenchymal Abeta deposition in the aging dog: correlation with behavior. Neurobiol. Aging 2000;21:695-704.
38. Collin RW, van Strien D, Leunissen JA, Martens GJ. Identification and expression of the first nonmammalian amyloid-beta precursor-like protein APLP2 in the amphibian Xenopus laevis. Eur. J. Biochem. 2004;271:1906-1912.
39. Cork LC, Powers RE, Selkoe DJ, Davies P, Geyer JJ, Price DL. Neurofibrillary tangles and senile plaques in aged bears. J. Neuropathol. Exp. Neurol. 1988;47:629-641.
40. Cork LC, Walker LC. Age-Related Lesions, Nervous System. In: Hunt RD, Jones

TC, Mohr U, editors. Nonhuman Primates Ⅱ. Berlin: Springer-Verlag. 1993;173-183.

41. Cotman CW, Head E, Muggenburg BA, Zicker S, Milgram NW. Brain aging in the canine: a diet enriched in antioxidants reduces cognitive dysfunction. Neurobiol. Aging. 2002; 23:809-818.

42. Coulson EJ, Paliga K, Beyreuther K, Masters CL. What the evolution of the amyloid protein precursor supergene family tells us about its function. Neurochem. Int. 2000;36:175-184.

43. Couchie D, Nunez J. Immunological characterization of microtubule-associated proteins specific for the immature brain. FEBS. Lett. 1985;188:331-335.

44. Couchiem D, Nunez J. Immunological characterization of microtubule-associated proteins specific for the immature brain. FEBS. Lett. 1985;188:331-335.

45. Cummings BJ, Head E, Afagh AJ, Milgram NW, Cotman CW. Beta-amyloid accumulation correlates with cognitive dysfunction in the aged canine. Neurobiol. Learn. Mem. 1996;66:11-23.

46. Cummings BJ, Head E, Ruehl W, Milgram NW, Cotman CW. The canine as an animal model of human aging and dementia. Neurobiol. Aging. 1996;17:259-268.

47. Cummings BJ, Su JH, Cotman CW, White R, Russell MJ. Beta-amyloid accumulation in aged canine brain: a model of early plaque formation in Alzheimer's disease. Neurobiol. Aging. 1993;14:547-560.

48. Czasch S, Paul S, Baumgartner W. A comparison of immunohistochemical and silver staining methods for the detection of diffuse plaques in the aged canine brain.

Neurobiol. Aging. 2006;27:293-305.

49. D'Andrea MR, Reiser PA, Polkovitch DA, Gumula NA, Branchide B, Hertzog BM, Schmidheiser D, Belkowski S, Gastard MC, Andrade-Gordon P. The use of formic acid to embellish amyloid plaque detection in Alzheimer's disease tissues misguides key observations. Neurosci. Lett. 2003;342:114-118.

50. Delacourte A, Robitaille Y, Sergeant N, Buée L, Hof PR. Specific pathological Tau protein variants characterize Pick's disease. J. Neuropathol. Exp. Neurol. 1996;55:159-168.

51. Delacourte A, Sergeant N, Wattez A, Gauvreau D, Robitaille Y. Vulnerable neuronal subsets in Alzheimer's and Pick's disease are distinguished by their tau isoform distribution and phosphorylation. Ann. Neurol. 1998;43:193-204.

52. de Silva R, Lashley T, Gibb G, Hanger D, Hope A, Reid A, Bandopadhyay R, Utton M, Strand C, Jowett T, Khan N, Anderton B, Wood N, Holton J, Revesz T, Lees A. Pathological inclusion bodies in tauopathies contain distinct complements of tau with three or four microtubule-binding repeat domains as demonstrated by new specific monoclonal antibodies. Neuropathol. Appl. Neurobiol. 2003;29:288-302.

53. Duyckaerts C, Potier MC, Delatour B. Alzheimer disease models and human neuropathology: similarities and differences. Acta Neuropathol. 2008;115:5-38.

54. Elfenbein HA, Rosen RF, Stephens SL, Switzer RC, Smith Y, Pare J, Mehta PD, Warzok R, Walker LC. Cerebral beta-amyloid angiopathy in aged squirrel monkeys. Histol. Histopathol. 2007;22:155-167.

55. Esch FS, Keim PS, Beattie EC, Blacher RW, Culwell AR, Oltersdorf T, McClure D, Ward PJ. Cleavage of amyloid beta peptide during constitutive processing of its precursor. Science. 1990;248:1122-1124.

56. Esiri MM, Nagy Z, Smith MZ, Barnetson L, Smith AD. Cerebrovascular disease and threshold for dementia in the early stages of Alzheimer's disease. Lancet. 1999;354:919-920.

57. Farris W, Schutz SG, Cirrito JR, Shankar GM, Sun X, George A, Leissring MA, Walsh DM, Qiu WQ, Holtzman DM, Selkoe DJ. Loss of neprilysin function promotes amyloid plaque formation and causes cerebral amyloid angiopathy. Am. J. Pathol. 2007;171:241-251.

58. Ferrer I. Cognitive impairment of vascular origin: neuropathology of cognitive impairment of vascular origin. J. Neurol. Sci. 2010;299:139-149.

59. Ferrer I. Defining Alzheimer as a common age-related neurodegenerative process not inevitably leading to dementia. Prog. Neurobiol. 2012;97:38-51.

60. Fotuhi M, Hachinski V, Whitehouse PJ. Changing perspectives regarding late-life dementia. Nat. Rev. Neurol. 2009;5:649-658.

61. Frank S, Clavaguera F, Tolnay M. Tauopathy models and human neuropathology: similarities and differences. Acta Neuropathol. 2008;115:39-53.

62. Frenkel D, Katz O, Solomon B. Immunization against Alzheimer's beta -amyloid plaques via EFRH phage administration. Proc. Natl. Acad. Sci. USA. 2000;97:11455-11459.

63. Frost JL, Le KX, Cynis H, Ekpo E, Kleinschmidt M, Palmour RM, Ervin FR,

Snigdha S, Cotman CW, Saido TC, Vassar RJ, St George-Hyslop P, Ikezu T, Schilling S, Demuth HU, Lemere CA. Pyroglutamate-3 amyloid-β deposition in the brains of humans, non-human primates, canines, and Alzheimer disease-like transgenic mouse models. Am. J. Pathol. 2013;183:369-381.

64. Fukami S, Watanabe K, Iwata N, Haraoka J, Lu B, Gerard NP, Gerard C, Fraser P, Westaway D, St George-Hyslop P, Saido TC. Abeta-degrading endopeptidase, neprilysin, in mouse brain: synaptic and axonal localization inversely correlating with Abeta pathology. Neurosci. Res. 2002;43:39-56.

65. Fukumoto H, Asami-Odaka A, Suzuki N, Shimada H, Ihara Y, Iwatsubo T. Amyloid beta protein deposition in normal aging has the same characteristics as that in Alzheimer's disease. predominance of A beta 42(43) and association of A beta 40 with cored plaques. Am. J. Pathol. 1996;148:259-265.

66. Fukumoto H, Tokuda T, Kasai T, Ishigami N, Hidaka H, Kondo M, Allsop D, Nakagawa M. High-molecular-weight beta-amyloid oligomers are elevated in cerebrospinal fluid of Alzheimer patients. FASEB. J. 2010;24:2716-2726.

67. Gauthier S, Reisberg B, Zaudig M, Petersen RC, Ritchie K, Broich K, Belleville S, Brodaty H, Bennett D, Chertkow H, Cummings JL, de Leon M, Feldman H, Ganguli M, Hampel H, Scheltens P, Tierney MC, Whitehouse P, Winblad B. Mild cognitive impairment. Lancet. 2006;367:1262-1270.

68. Gearing M, Tigges J, Mori H, Mirra SS. beta-Amyloid (A beta) deposition in the brains of aged orangutans. Neurobiol. Aging. 1997;18:139-146.

69. Goedert M, Jakes R. Expression of separate isoforms of human tau protein:

correlation with the tau pattern in brain and effects on tubulin polymerization. EMBO. J. 1990;9:4225-4230.

70. Goedert M, Spillantini MG. A century of Alzheimer's disease. Science. 2006;314:777-781.

71. Goedert M, Spillantini MG, Cairns NJ, Crowther RA. Tau proteins of Alzheimer paired helical filaments: abnormal phosphorylation of all six brain isoforms. Neuron. 1992;8:159-168.

72. Goedert M, Spillantini MG, Potier MC, Ulrich J, Crowther RA. Cloning and sequencing of the cDNA encoding an isoform of microtubule-associated protein tau containing four tandem repeats: differential expression of tau protein mRNAs in human brain. EMBO. J. 1989;8:393-399.

73. Gómez-Isla T, Hollister R, West H, Mui S, Growdon JH, Petersen RC, Parisi JE, Hyman BT. Neuronal loss correlates with but exceeds neurofibrillary tangles in Alzheimer's disease. Ann. Neurol. 1997;41:17-24.

74. Götz J, Ittner LM. Animal models of Alzheimer's disease and frontotemporal dementia. Nat. Rev. Neurosci. 2008;9:532-544.

75. Gouras GK, Tampellini D, Takahashi RH, Capetillo-Zarate E. Intraneuronal beta-amyloid accumulation and synapse pathology in Alzheimer's disease. Acta Neuropathol. 2010;119:523-541.

76. Grinberg LT, Heinsen H. Toward a pathological definition of vascular dementia. J. Neurol. Sci. 2010;299:136-138.

77. Gunn AP, Masters CL, Cherny RA. Pyroglutamate-abeta: Role in the natural

history of Alzheimer's disease. Int. J. Biochem. Cell. Biol. 2010;42:1915-1918.

78. Gunn-Moore D, Moffat K, Christie LA, Head E. Cognitive dysfunction and the neurobiology of ageing in cats. J. Small Anim. Pract. 2007;48:546-553.

79. Hampel H, Bürger K, Teipel SJ, Bokde AL, Zetterberg H, Blennow K. Core candidate neurochemical and imaging biomarkers of Alzheimer's disease. Alzheimers Dement. 2008;4:38-48.

80. Hardy J, Selkoe DJ. The amyloid hypothesis of Alzheimer's disease: progress and problems on the road to therapeutics. Science. 2002;297:353-356.

81. Hartig W, Goldhammer S, Bauer U, Wegner F, Wirths O, Bayer TA, Grosche J. Concomitant detection of beta-amyloid peptides with N-terminal truncation and different C-terminal endings in cortical plaques from cases with Alzheimer's disease, senile monkeys and triple transgenic mice. J. Chem. Neuroanat. 2010;40:82-92.

82. Härtig W, Klein C, Brauer K, Schüppel KF, Arendt T, Bigl V, Brückner G. Hyperphosphorylated protein tau is restricted to neurons devoid of perineuronal nets in the cortex of aged bison. Neurobiol. Aging. 2001;22:25-33.

83. Hasegawa M. Biochemistry and molecular biology of tauopathies. Neuropathology. 2006;26:484-490.

84. He W, Barrow CJ. The A beta 3-pyroglutamyl and 11-pyroglutamyl peptides found in senile plaque have greater beta-sheet forming and aggregation propensities in vitro than full-length A beta. Biochemistry. 1999;38:10871-10877.

85. Head E. A canine model of human aging and Alzheimer's disease. Biochim.

Biophys. Acta. 2013;1832:1384-1389.

86. Head E. Oxidative damage and cognitive dysfunction: antioxidant treatments to promote healthy brain aging. Neurochem. Res. 2009;34:670-678.

87. Head E. Neurobiology of the aging dog. Age. 2011;33:485-496.

88. Head E, Callahan H, Muggenburg BA, Cotman CW, Milgram NW. Visual-discrimination learning ability and beta-amyloid accumulation in the dog. Neurobiol. Aging. 1998;19:415-425.

89. Head E, Liu J, Hagen TM, Muggenburg BA, Milgram NW, Ames BN, Cotman CW. Oxidative damage increases with age in a canine model of human brain aging. J. Neurochem. 2002;82:375-381.

90. Head E, McCleary R, Hahn FF, Milgram NW, Cotman CW. Region-specific age at onset of beta-amyloid in dogs. Neurobiol Aging 2000;21:89-96.

91. Head E, Pop V, Vasilevko V, Hill M, Saing T, Sarsoza F, Nistor M, Christie LA, Milton S, Glabe C, Barrett E, Cribbs D. A two-year study with fibrillar beta-amyloid (abeta) immunization in aged canines: Effects on cognitive function and brain abeta. J. Neurosci. 2008;28:3555-3566.

92. Head E, Rofina J, Zicker S. Oxidative stress, aging, and central nervous system disease in the canine model of human brain aging. Vet. Clin. North Am. Small Anim. Pract. 2008;38:167-78.

93. Herzig MC, Van Nostrand WE, Jucker M. Mechanism of cerebral beta-amyloid angiopathy: murine and cellular models. Brain. Pathol. 2006;16:40-54.

94. Herzig MC, Winkler DT, Burgermeister P, Pfeifer M, Kohler E, Schmidt SD,

Danner S, Abramowski D, Sturchler-Pierrat C, Burki K, van Duinen SG, Maat-Schieman ML, Staufenbiel M, Mathews PM, Jucker M. Abeta is targeted to the vasculature in a mouse model of hereditary cerebral hemorrhage with amyloidosis. Nat. Neurosci. 2004;7:954-960.

95. Holzer M, Craxton M, Jakes R, Arendt T, Goedert M. Tau gene (MAPT) sequence variation among primates. Gene. 2004;341:313-322.

96. Hooper C, Killick R, Lovestone S. The GSK3 hypothesis of Alzheimer's disease. J. Neurochem. 2008;104:1433-1439.

97. Iadecola C. The overlap between neurodegenerative and vascular factors in the pathogenesis of dementia. Acta. Neuropathol. 2010;20:287-296.

98. Ide T, Uchida K, Kagawa Y, Suzuki K, Nakayama H. Pathological and immunohistochemical features of subdural histiocytic sarcomas in 15 dogs. J. Vet. Diagn. Invest. 2011;23:127-132.

99. Ihara M, Polvikoski TM, Hall R, Slade JY, Perry RH, Oakley AE, Englund E, O'Brien JT, Ince PG, Kalaria RN. Quantification of myelin loss in frontal lobe white matter in vascular dementia, Alzheimer's disease, and dementia with Lewy bodies. Acta. Neuropathol. 2010;119:579-589.

100. Ikeda K, Akiyama H, Arai T, Nishimura T. Glial tau pathology in neurodegenerative diseases: their nature and comparison with neuronal tangles. Neurobiol. Aging. 1998;19:S85-91.

101. Ittner LM, Götz J. Amyloid-β and tau--a toxic pas de deux in Alzheimer's disease. Nat. Rev. Neurosci. 2011;12:65-72.

102. Iwamoto N, Nishiyama E, Ohwada J, Arai H. Distribution of amyloid deposits in the cerebral white matter of the Alzheimer's disease brain: relationship to blood vessels. Acta. Neuropathol. 1997;93:334-340.

103. Iwata N, Tsubuk, S, Takaki Y, Shirotani K, Lu B, Gerard NP, Gerard C, Hama E, Lee HJ, Saido TC. Metabolic regulation of brain Abeta by neprilysin. Science. 2001;292:1550-1552.

104. Iwata N, Tsubuki S, Takaki Y, Watanabe K, Sekiguchi M, Hosoki E, Kawashima-Morishima M, Lee HJ, Hama E, Sekine-Aizawa Y, Saido TC. Identification of the major Abeta1-42-degrading catabolic pathway in brain parenchyma: suppression leads to biochemical and pathological deposition. Nat. Med. 2000;6:143-150.

105. Iwatsubo T, Odaka A, Suzuki N, Mizusawa H, Nukina N, Ihara Y. Visualization of A beta 42(43) and A beta 40 in senile plaques with end-specific A beta monoclonals: evidence that an initially deposited species is A beta 42(43). Neuron. 1994;13:45-53.

106. Jack CR Jr, Knopman DS, Jagust WJ, Petersen RC, Weiner MW, Aisen PS, Shaw LM, Vemuri P, Wiste HJ, Weigand SD, Lesnick TG, Pankratz VS, Donohue MC, Trojanowski JQ. Tracking pathophysiological processes in Alzheimer's disease: an updated hypothetical model of dynamic biomarkers. Lancet Neurol. 2013;12:207-216.

107. Jakes R, Novak M, Davison M, Wischik CM. Identification of 3- and 4-repeat tau isoforms within the PHF in Alzheimer's disease. EMBO. J. 1991;10:2725-2729.

108. Janus C, Westaway D. Transgenic mouse models of Alzheimer's disease. Physiol. Behav. 2001;73:873-886.

109. Janus C, Pearson J, McLaurin J, Mathews PM, Jiang Y, Schmidt SD, Chishti MA, Horne P, Heslin D, French J, Mount HT, Nixon RA, Mercken M, Bergeron C, Fraser PE, St George-Hyslop P, Westaway D. A beta peptide immunization reduces behavioural impairment and plaques in a model of Alzheimer's disease. Nature. 2000;408:979-982.

110. Jarrett JT, Berger EP, Lansbury PT Jr. The carboxy terminus of the beta amyloid protein is critical for the seeding of amyloid formation: implications for the pathogenesis of Alzheimer's disease. Biochemistry. 1993;32:4693-4697.

111. Jimenez S, Torres M, Vizuete M, Sanchez-Varo R, Sanchez-Mejias E, Trujillo-Estrada L, Carmona-Cuenca I, Caballero C, Ruano D, Gutierrez A, Vitorica J. Age-dependent accumulation of soluble amyloid beta (Abeta) oligomers reverses the neuroprotective effect of soluble amyloid precursor protein-alpha (sAPP(alpha)) by modulating phosphatidylinositol 3-kinase (PI3K)/Akt-GSK-3beta pathway in Alzheimer mouse model. J. Biol. Chem. 2011;286:18414-18425.

112. Johnson WE, Eizirik E, Pecon-Slattery J, Murphy WJ, Antunes A, Teeling E, O'Brien SJ. The late Miocene radiation of modern Felidae: a genetic assessment. Science. 2006;311:73-77.

113. Johnstone EM, Chaney MO, Norris FH, Pascual R, Little SP. Conservation of the sequence of the Alzheimer's disease amyloid peptide in dog, polar bear and five

other mammals by cross-species polymerase chain reaction analysis. Brain Res. Mol. Brain Res. 1991;10:299-305.

114. Jucker M, Walker LC. Pathogenic protein seeding in Alzheimer disease and other neurodegenerative disorders. Ann. Neurol. 2011;70:532-540.

115. Kasai T, Tokuda T, Taylor M, Nakagawa M, Allsop D. Utilization of a multiple antigenic peptide as a calibration standard in the BAN50 single antibody sandwich ELISA for Aβ oligomers. Biochem. Biophys. Res. Commun. 2012;422:375-380.

116. Kawarabayashi T, Shoji M, Younkin LH, Wen-Lang L, Dickson DW, Murakami T, Matsubara E, Abe K, Ashe KH, Younkin SG. Dimeric amyloid beta protein rapidly accumulates in lipid rafts followed by apolipoprotein E and phosphorylated tau accumulation in the Tg2576 mouse model of Alzheimer's disease. J. Neurosci. 2004;24:3801-3809.

117. Kayed R, Canto I, Breydo L, Rasool S, Lukacsovich T, Wu J, Albay R 3rd, Pensalfini A, Yeung S, Head E, Marsh JL, Glabe C. Conformation dependent monoclonal antibodies distinguish different replicating strains or conformers of prefibrillar Aβ oligomers. Mol. Neurodegener. 2010;5:57.

118. Kayed R, Head E, Thompson JL, McIntire TM, Milton SC, Cotman CW, Glabe CG. Common structure of soluble amyloid oligomers implies common mechanism of pathogenesis. Science. 2003;300:486-489

119. Kiatipattanasakul W, Nakamura S, Hossain MM, Nakayama H, Uchino T, Shumiya S, Goto N, Doi K. Apoptosis in the aged dog brain. Acta. Neuropathol. 1996;92:242-248.

120. Kimotsuki T, Nagaoka T, Yasuda M, Tamahara S, Matsuki N, Ono K. Changes of magnetic resonance imaging on the brain in beagle dogs with aging. J. Vet. Med. Sci. 2005;67:961-967.

121. Kimura N, Nakamura S, Goto N, Narushima E, Hara I, Shichiri S, Saitou K, Nose M, Hayashi T, Kawamura S, Yoshikawa Y. Senile plaques in an aged western lowland gorilla. Exp. Anim. 2001;50:77-81.

122. Kooi EJ, van Horssen J, Witte ME, Amor S, Bo L, Dijkstra CD, van der Valk P, Geurts JJ. Abundant extracellular myelin in the meninges of patients with multiple sclerosis. Neuropathol. Appl. Neurobiol. 2009;35:283-295.

123. Kumar-Singh S, Pirici D, McGowan E, Serneels S, Ceuterick C, Hardy J, Duff K, Dickson D, Van Broeckhoven C. Dense-core plaques in Tg2576 and PSAPP mouse models of Alzheimer's disease are centered on vessel walls. Am. J. Pathol. 2005;167: 527-543.

124. LaFerla FM, Green KN, Oddo S. Intracellular amyloid-beta in Alzheimer's disease. Nat. Rev. Neurosci. 2007;8:499-509.

125. LaFerla FM, Troncoso JC, Strickland DK, Kawas CH, Jay G. Neuronal cell death in Alzheimer's disease correlates with apoE uptake and intracellular Abeta stabilization. J. Clin. Invest. 1997;100:310-320.

126. Langui D, Girardot N, El Hachimi KH, Allinquant B, Blanchard V, Pradier L, Duyckaerts C. Subcellular topography of neuronal Abeta peptide in APPxPS1 transgenic mice. Am. J. Pathol. 2004;165:1465-1477.

127. Leroy K, Yilmaz Z, Brion JP. Increased level of active GSK-3beta in Alzheimer's

disease and accumulation in argyrophilic grains and in neurones at different stages of neurofibrillary degeneration. Neuropathol. Appl. Neurobiol. 2007;33:43-55.

128. Lesné S, Koh MT, Kotilinek L, Kayed R, Glabe CG, Yang A, Gallagher M, Ashe KH. A specific amyloid-beta protein assembly in the brain impairs memory. Nature. 2006;440:352-357.

129. Lesné SE, Sherman MA, Grant M, Kuskowski M, Schneider JA, Bennett DA, Ashe KH. Brain amyloid-β oligomers in ageing and Alzheimer's disease. Brain. 2013;136:1383-1398.

130. Levy E, Amorim A, Frangione B, Walker LC. beta-Amyloid precursor protein gene in squirrel monkeys with cerebral amyloid angiopathy. Neurobiol. Aging. 1995;16:805-808.

131. Lintl P, Braak H. Loss of intracortical myelinated fibers: a distinctive age-related alteration in the human striate area. Acta Neuropathol. 1983;61:178-182.

132. Liu F, Gong CX. Tau exon 10 alternative splicing and tauopathies. Mol. Neurodegener. 2008;3:8.

133. Ma QL, Yang F, Rosario ER, Ubeda OJ, Beech W, Gant DJ, Chen PP, Hudspeth B, Chen C, Zhao Y, Vinters HV, Frautschy SA, Cole GM. Beta-amyloid oligomers induce phosphorylation of tau and inactivation of insulin receptor substrate via c-Jun N-terminal kinase signaling: suppression by omega-3 fatty acids and curcumin. J. Neurosci. 2009;29:9078-9089.

134. Marcello A, Wirths O, Schneider-Axmann T, Degerman-Gunnarsson M, Lannfelt L, Bayer TA. Reduced levels of IgM autoantibodies against N-truncated

pyroglutamate abeta in plasma of patients with Alzheimer's disease. Neurobiol. Aging. 2011;32:1379-1387.

135. Masters CL, Simms G, Weinman NA, Multhaup G, McDonald BL, Beyreuther K. Amyloid plaque core protein in Alzheimer disease and down syndrome. Proc. Natl. Acad. Sci. USA. 1985;82:4245-4249.

136. Masuda R, Yoshida MC. Two Japanese wildcats, the Tsushima cat and the Iriomote cat, show the same mitochondrial DNA lineage as the leopard cat Felis bengalensis. Zoolog. Sci. 1995;12:655-659.

137. Matsas R, Kenny AJ, Turner AJ. An immunohistochemical study of endopeptidase-24.11 ("enkephalinase") in the pig nervous system. Neuroscience. 1986;18:991-1012.

138. Mattsson N, Olsson M, Gustavsson MK, Kosicek M, Malnar M, Månsson JE, Blomqvist M, Gobom J, Andreasson U, Brinkmalm G, Vite C, Hecimovic S, Hastings C, Blennow K, Zetterberg H, Portelius E. Amyloid-β metabolism in Niemann-Pick C disease models and patients. Metab. Brain Dis. 2012;27:573-585.

139. McMillan P, Korvatska E, Poorkaj P, Evstafjeva Z, Robinson L, Greenup L, Leverenz J, Schellenberg GD, D'Souza I. Tau isoform regulation is region- and cell-specific in mouse brain. J. Comp. Neurol. 2008;511:788-803.

140. Meisl G, Yang X, Hellstrand E, Frohm B, Kirkegaard JB, Cohen SI, Dobson CM, Linse S, Knowles TP. Differences in nucleation behavior underlie the contrasting aggregation kinetics of the Aβ40 and Aβ42 peptides. Proc. Natl. Acad. Sci. U S A. 2014;111:9384-9389.

141. Meli G, Lecci A, Manca A, Krako N, Albertini V, Benussi L, Ghidoni R, Cattaneo A. Conformational targeting of intracellular Aβ oligomers demonstrates their pathological oligomerization inside the endoplasmic reticulum. Nat. Commun. 2014;5:3867.

142. Millan Y, Mascort J, Blanco A, Costa C, Masian D, Guil-Luna S, Pumarola M, Martin de Las Mulas J. Hypomyelination in three Weimaraner dogs. J. Small Anim. Pract. 2010;51:594-598.

143. Miners JS, Van Helmond Z, Chalmers K, Wilcock G, Love S, Kehoe PG. Decreased expression and activity of neprilysin in Alzheimer disease are associated with cerebral amyloid angiopathy. J. Neuropathol. Exp. Neurol. 2006;65:1012-1021.

144. Miyawaki K, Nakayama H, Nakamura S, Uchida K, Doi K. Three-dimensional structures of canine senile plaques. Acta Neuropathol. 2001;102:321-328.

145. Mutsuga M, Chambers JK, Uchida K, Tei M, Makibuchi T, Mizorogi T, Takashima A, Nakayama H. Binding of curcumin to senile plaques and cerebral amyloid angiopathy in the aged brain of various animals and to neurofibrillary tangles in Alzheimer's brain. J. Vet. Med. Sci. 2012;74:51-7.

146. Nakamura S, Nakayama H, Goto N, Ono F, Sakakibara I, Yoshikawa Y. Histopathological studies of senile plaques and cerebral amyloidosis in cynomolgus monkeys. J. Med. Primatol. 1998;27:244-252.

147. Nakamura S, Nakayama H, Goto N, Ono-Ochikubo F, Sakakibara I, Yoshikawa Y. Histopathological studies on senile plaques and cerebral amyloid angiopathy in

aged cynomolgus monkeys. Exp. Anim. 1995;43:711-718.

148. Nakamura S, Nakayama H, Kiatipattanasakul W, Uetsuka K, Uchida K, Goto N. Senile plaques in very aged cats. Acta Neuropathol. 1996;91:437-439.

149. Nakamura S, Nakayama H, Uetsuka K, Sasaki N, Uchida K, Goto N. Senile plaques in an aged two-humped (Bactrian) camel (Camelus bactrianus). Acta Neuropathol. 1995;90:415-418.

150. Nakayama H, Katayama K, Ikawa A, Miyawaki K, Shinozuka J, Uetsuka K, Nakamura S, Kimura N, Yoshikawa Y, Doi K. Cerebral amyloid angiopathy in an aged great spotted woodpecker (Picoides major). Neurobiol. Aging. 1999;20:53-56.

151. Nakayama H, Kiatipattanasakul W, Nakamura S, Miyawaki K, Kikuta F, Uchida K, Kuroki K, Makifuchi T, Yoshikawa Y, Doi K. Fractal analysis of senile plaque observed in various animal species. Neurosci. Lett. 2001;297:195-8.

152. Nakayama H, Uchida K, Doi K. A comparative study of age-related brain pathology--are neurodegenerative diseases present in nonhuman animals ? Med. Hypotheses. 2004;63:198-202.

153. Nishimura M, Tomimoto H, Suenaga T, Namba Y, Ikeda K, Akiguchi I, Kimura J. Immunocytochemical characterization of glial fibrillary tangles in Alzheimer's disease brain. Am. J. Pathol. 1995;146:1052-1058.

154. Nussbaum JM, Schilling S, Cynis H, Silva A, Swanson E, Wangsanut T, Tayler K, Wiltgen B, Hatami A, Rönicke R, Reymann K, Hutter-Paier B, Alexandru A, Jagla W, Graubner S, Glabe CG, Demuth HU, Bloom GS. Prion-like behaviour and

tau-dependent cytotoxicity of pyroglutamylated amyloid-β. Nature. 2012;485:651-655.

155. Oddo S, Caccamo A, Shepherd JD, Murphy MP, Golde TE, Kayed R, Metherate R, Mattson MP, Akbari Y, LaFerla FM. Triple-transgenic model of Alzheimer's disease with plaques and tangles: intracellular Abeta and synaptic dysfunction. Neuron. 2003;39:409-421.

156. Oddo S, Caccamo A, Smith IF, Green KN, LaFerla FM. A dynamic relationship between intracellular and extracellular pools of Abeta. Am. J. Pathol. 2006;168:184-194.

157. Ogomori K, Kitamoto T, Tateishi J, Sato Y, Suetsugu M, Abe M. Beta-protein amyloid is widely distributed in the central nervous system of patients with Alzheimer's disease. Am. J. Pathol. 1989;134:243-251.

158. Ohyagi Y, Tsuruta Y, Motomura K, Miyoshi K, Kikuchi H, Iwaki T, Taniwaki T, Kira J. Intraneuronal amyloid beta42 enhanced by heating but counteracted by formic acid. J. Neurosci. Methods. 2007;159:134-1138.

159. Oikawa N, Kimura N, Yanagisawa K. Alzheimer-type tau pathology in advanced aged nonhuman primate brains harboring substantial amyloid deposition. Brain Res. 2010;1315:137-149.

160. Ono K, Condron MM, Teplow DB. Effects of the English (H6R) and Tottori (D7N) familial Alzheimer disease mutations on amyloid beta-protein assembly and toxicity. J. Biol. Chem. 2010;285:23186-23197.

161. Opii WO, Joshi G, Head E, Milgram NW, Muggenburg BA, Klein JB, Pierce WM,

Cotman CW, Butterfield DA. Proteomic identification of brain proteins in the canine model of human aging following a long-term treatment with antioxidants and a program of behavioral enrichment: relevance to Alzheimer's disease. Neurobiol. Aging. 2008; 29:51-70.

162. Papaioannou N, Tooten PCJ, van Ederen AM, Bohl JRE, Rofina J, Tsangaris T, Gruys E. Immunohistochemical investigation of the brain of aged dogs. I. Detection of neurofibrillary tangles and and of 4-hydroxynonenal protein, an oxidative damage product, in senile plaques. Amyloid. 2001;8:11-21.

163. Petersen RC, Smith GE, Waring SC, Ivnik RJ, Tangalos EG, Kokmen E. Mild cognitive impairment: Clinical characterization and outcome. Arch. Neurol. 1999;56:303-308.

164. Philipson O, Lord A, Gumucio A, O'Callaghan P, Lannfelt L, Nilsson LN. Animal models of amyloid-beta-related pathologies in Alzheimer's disease. FEBS. J. 2010;277:1389-1409.

165. Piccini A, Russo C, Gliozzi A, Relini A, Vitali A, Borghi R, Giliberto L, Armirotti A, D'Arrigo C, Bachi A, Cattaneo A, Canale C, Torrassa S, Saido TC, Markesbery W, Gambetti P, Tabaton M. Beta-amyloid is different in normal aging and in Alzheimer disease. J. Biol. Chem. 2005;280:34186-34192.

166. Podlisny MB, Tolan DR, Selkoe DJ. Homology of the amyloid beta protein precursor in monkey and human supports a primate model for beta amyloidosis in Alzheimer's disease. Am. J. Pathol. 1991;138:1423-1435.

167. Pohl T, Zimmer M, Mugele K, Spiess J. Primary structure and functional

expression of a glutaminyl cyclase. Proc Natl Acad Sci USA 1991;88:10059-10063.

168. Portelius E, Bogdanovic N, Gustavsson MK, Volkmann I, Brinkmalm G, Zetterberg H, Winblad B, Blennow K. Mass spectrometric characterization of brain amyloid beta isoform signatures in familial and sporadic Alzheimer's disease. Acta Neuropathol. 2010;120:185-193.

169. Preston SD, Steart PV, Wilkinson A, Nicoll JA, Weller RO. Capillary and arterial cerebral amyloid angiopathy in Alzheimer's disease: defining the perivascular route for the elimination of amyloid beta from the human brain. Neuropathol. Appl. Neurobiol. 2003;29:106-117.

170. Prophet EB, Mills B, Arrington JB, Sobin LH. Laboratory Methods in Histotechnology, first ed., American Registry of Pathology, Washington D. C. 1992.

171. Pugliese M, Carrasco JL, Gomez-Anson B, Anrade C, Zamora A, Rodriguez MJ, Mascort J, Mahy N. Magnetic resonance imaging of cerebral involutional changes in dogs as markers of aging: An innovative tool adapted from a human visual rating scale. Vet J. 2010;186:166-171.

172. Pugliese M, Mascort J, Mahy N, Ferrer I. Diffuse beta-amyloid plaques and hyperphosphorylated tau are unrelated processes in aged dogs with behavioral deficits. Acta Neuropathol. 2006;112:175-183.

173. Reeves RH. Down's syndrome. A complicated genetic insult. Lancet. 2001;358:Suppl, S23.

174. Revesz T, Ghiso J, Lashley T, Plant G, Rostagno A, Frangione B, Holton JL. Cerebral amyloid angiopathies: a pathologic, biochemical, and genetic view. J Neuropathol. Exp. Neurol. 2003;62:885-898.

175. Roertgen KE, Parisi JE, Clark HB, Barnes DL, O'Brien TD, Johnson KH. A beta-associated cerebral angiopathy and senile plaques with neurofibrillary tangles and cerebral hemorrhage in an aged wolverine (Gulo gulo). Neurobiol. Aging. 1996;17:243-247.

176. Rofina J, van Andel I, van Ederen AM, Papaioannou N, Yamaguchi H, Gruys E, Canine counterpart of senile dementia of the Alzheimer type: amyloid plaques near capillaries but lack of spatial relationship with activated microglia and macrophages. Amyloid. 2003;10: 86-96.

177. Rofina JE, van Ederen AM, Toussaint MJ, Secreve M, van der Spek A, van der Meer I, Van Eerdenburg FJ, Gruys E. Cognitive disturbances in old dogs suffering from the canine counterpart of Alzheimer's disease. Brain Res. 2006;1069:216-226.

178. Rofina JE, Singh K, Skoumalova-Vesela A, van Ederen AM, van Asten AJAM, Wilhelm J, Gruys E. Histochemical accumulation of oxidative damage products is associated with Alzheimer-like pathology in the canine. Amyloid. 2004;11:90-100.

179. Roher AE, Kuo YM, Esh C, Knebel C, Weiss N, Kalback W, Luehrs DC, Childress JL, Beach TG, Weller RO, Kokjohn TA. Cortical and leptomeningeal cerebrovascular amyloid and white matter pathology in Alzheimer's disease. Mol. Med. 2003;9:112-122.

180. Roher AE, Lowenson JD, Clarke S, Woods AS, Cotter RJ, Gowing E, Ball MJ. beta-Amyloid-(1-42) is a major component of cerebrovascular amyloid deposits: implications for the pathology of Alzheimer disease. Proc. Natl. Acad. Sci. USA. 1993;90:10836-10840.

181. Rolyan H, Feike AC, Upadhaya AR, Waha A, Van Dooren T, Haass C, Birkenmeier G, Pietrzik CU, Van Leuven F, Thal DR. Amyloid-beta protein modulates the perivascular clearance of neuronal apolipoprotein E in mouse models of Alzheimer's disease. J. Neural. Transm. 2011;118:699-712.

182. Roques BP, Noble F, Dauge V, Fournie-Zaluski MC, Beaumont A. Neutral endopeptidase 24.11: structure, inhibition, and experimental and clinical pharmacology. Pharmacol. Rev. 1993;45:87-146.

183. Rosen RF, Farberg AS, Gearing M, Dooyema J, Long PM, Anderson DC, Davis-Turak J, Coppola G, Geschwind DH, Paré JF, Duong TQ, Hopkins WD, Preuss TM, Walker LC. Tauopathy with paired helical filaments in an aged chimpanzee. J. Comp. Neurol. 2008;509(3):259-270.

184. Russo C, Saido TC, DeBusk LM, Tabaton M, Gambetti P, Teller JK. Heterogeneity of water-soluble amyloid beta-peptide in Alzheimer's disease and down's syndrome brains. FEBS. Lett. 1997;409:411-416.

185. Russo C, Violani E, Salis S, Venezia V, Dolcini V, Damonte G, Benatti U, D'Arrigo C, Patrone E, Carlo P, Schettini G. Pyroglutamate-modified amyloid beta-peptides--AbetaN3(pE)--strongly affect cultured neuron and astrocyte survival. J. Neurochem. 2002;82:1480-1489.

186. Ryan L, Walther K, Bendlin BB, Lue LF, Walker DG, Glisky EL. Age-related differences in white matter integrity and cognitive function are related to APOE status. Neuroimage. 2011;54:1565-1577.

187. Saido TC, Iwata N. Metabolism of amyloid beta peptide and pathogenesis of Alzheimer's disease. Towards presymptomatic diagnosis, prevention and therapy. Neurosci. Res. 2006;54:235-253.

188. Saido TC, Yamao-Harigaya W, Iwatsubo T, Kawashima S. Amino- and carboxyl-terminal heterogeneity of beta-amyloid peptides deposited in human brain. Neurosci. Lett. 1996;215:173-176.

189. Saito T, Matsuba Y, Mihira N, Takano J, Nilsson P, Itohara S, Iwata N, Saido TC. Single App knock-in mouse models of Alzheimer's disease. Nat. Neurosci. 2014;17:661-663.

190. Sanders HM, Lust R, Teller JK. Amyloid-beta peptide Abetap3-42 affects early aggregation of full-length Abeta1-42. Peptides. 2009;30:849-854.

191. Sarasa L, Gallego C, Monleon I, Olvera A, Canudas J, Montanes M, Pesini P, Sarasa M. Cloning, sequencing and expression in the dog of the main amyloid precursor protein isoforms and some of the enzymes related with their processing. Neuroscience. 2010;171:1091-1101.

192. Sarasa M, Pesini P. Natural non-trasgenic animal models for research in Alzheimer's disease. Curr. Alzheimer Res. 2009;6:171-178.

193. Schilling S, Appl T, Hoffmann T, Cynis H, Schulz K, Jagla W, Friedrich D,

Wermann M, Buchholz M, Heiser U, von Horsten S, Demuth HU. Inhibition of glutaminyl cyclase prevents pGlu-abeta formation after intracortical/hippocampal microinjection in vivo/in situ. J. Neurochem. 2008;106:1225-1236.

194. Schilling S, Lauber T, Schaupp M, Manhart S, Scheel E, Böhm G, Demuth HU. On the seeding and oligomerization of pGlu-amyloid peptides (in vitro). Biochemistry. 2006;45:12393-12399.

195. Schilling S, Wasternack C, Demuth HU. Glutaminyl cyclases from animals and plants: A case of functionally convergent protein evolution. Biol. Chem. 2008;389: 983-991.

196. Schilling S, Zeitschel U, Hoffmann T, Heiser U, Francke M, Kehlen A, Holzer M, Hutter-Paier B, Prokesch M, Windisch M, Jagla W, Schlenzig D, Lindner C, Rudolph T, Reuter G, Cynis H, Montag D, Demuth HU, Rossner S. Glutaminyl cyclase inhibition attenuates pyroglutamate abeta and Alzheimer's disease-like pathology. Nat. Med. 2008;14:1106-1111.

197. Schultz C, Dehghani F, Hubbard GB, Thal DR, Struckhoff G, Braak E, Braak H. Filamentous tau pathology in nerve cells, astrocytes, and oligodendrocytes ofaged baboons. J. Neuropathol. Exp. Neurol. 2000;59:39-52.

198. Selkoe DJ. The molecular pathology of Alzheimer's disease. Neuron. 1991;6:487-498.

199. Selkoe DJ. Resolving controversies on the path to Alzheimer's therapeutics. Nat. Med. 2011;17:1060-1065.

200. Selkoe DJ, Bell DS, Podlisny MB, Price DL, Cork LC. Conservation of brain

amyloid proteins in aged mammals and humans with Alzheimer's disease. Science. 1987;235:873-877.

201. Serizawa S, Chambers JK, Une Y. Beta Amyloid Deposition and Neurofibrillary Tangles Spontaneously Occur in the Brains of Captive Cheetahs (Acinonyx jubatus). Vet. Pathol. 2012;49:304-312.

202. Seubert P, Vigo-Pelfrey C, Esch F, Lee M, Dovey H, Davis D, Sinha S, Schlossmacher M, Whaley J, Swindlehurst C. Isolation and quantification of soluble Alzheimer's beta-peptide from biological fluids. Nature. 1992;359:325-327.

203. Shimada A, Kuwamura M, Awakura T, Umemura T, Takada K, Ohama E, Itakura C. Topographic relationship between senile plaques and cerebrovascular amyloidosis in the brain of aged dogs. J. Vet. Med. Sci. 1992;54:137-144.

204. Shimada A, Kuwamura M, Umemura T, Takada K, Ohama E. Itakura C. Modified Bielschowsky and immunohistochemical studies on senile plaques in aged dogs. Neurosci. Lett. 1991;129:25-28.

205. Shirotani K, Tsubuki S, Iwata N, Takaki Y, Harigaya W, Maruyama K, Kiryu-Seo S, Kiyama H, Iwata H, Tomita T, Iwatsubo T, Saido TC. Neprilysin degrades both amyloid beta peptides 1-40 and 1-42 most rapidly and efficiently among thiorphan- and phosphoramidon-sensitive endopeptidases. J. Biol. Chem. 2001;276:21895-21901.

206. Shoji M, Golde TE, Ghiso J, Cheung TT, Estus S, Shaffer LM, Cai XD, McKay DM, Tintner R, Frangione B. Production of the Alzheimer amyloid beta protein by

normal proteolytic processing. Science. 1992;258:126-129.

207. Sisodia SS, Koo EH, Beyreuther K, Unterbeck A, Price DL. Evidence that beta-amyloid protein in Alzheimer's disease is not derived by normal processing. Science. 1990;248:492-495.

208. Skoumalova A, Rofina J, Schwippelova Z, Gruys E, Wilhelm J. The role of free radicals in canine counterpart of senile dementia of the Alzheimer type. Exp. Gerontol. 2003;38:711-719.

209. Smith CD, Snowdon D, Markesbery WR. Periventricular white matter hyperintensities on MRI: correlation with neuropathologic findings. J. Neuroimaging. 2000;10:13-16.

210. Solomon B. Alzheimer's disease and immunotherapy. Curr. Alzheimer Res. 2004;1: 149-163.

211. Solomon B, Koppel R, Frankel D, Hanan-Aharon E. Disaggregation of Alzheimer beta-amyloid by site-directed mAb. Proc. Natl. Acad. Sci. USA. 1997;94:4109-4112.

212. Staekenborg SS, Koedam EL, Henneman WJ, Stokman P, Barkhof F, Scheltens P, van der Flier WM. Progression of mild cognitive impairment to dementia: contribution of cerebrovascular disease compared with medial temporal lobe atrophy. Stroke. 2009;40:1269-1274.

213. Stephan A, Wermann M, von Bohlen A, Koch B, Cynis H, Demuth HU, Schilling S. Mammalian glutaminyl cyclases and their isoenzymes have identical enzymatic characteristics. FEBS. J 2009;276:6522-6536.

214. Struble RG, Price DL Jr, Cork LC, Price DL. Senile plaques in cortex of aged normal monkeys. Brain Res. 1985;361:267-275.

215. Sykes PA, Watson SJ, Temple JS, Bateman RC Jr. Evidence for tissue-specific forms of glutaminyl cyclase. FEBS. Lett. 1999;455:159-161.

216. Takahashi E, Kuribayashi H, Chambers JK, Imamura E, Une Y. Senile plaques and cerebral amyloid angiopathy in an aged California sea lion (Zalophus californianus). *Amyloid.* 2014;21:211-215.

217. Takahashi RH, Milner TA, Li F, Nam EE, Edgar MA, Yamaguchi H, Beal MF, Xu H, Greengard P, Gouras GK. Intraneuronal Alzheimer abeta42 accumulates in multivesicular bodies and is associated with synaptic pathology. Am. J. Pathol. 2002;161:1869-1879.

218. Takashima A, Murayama M, Murayama O, Kohno T, Honda T, Yasutake K, Nihonmatsu N, Mercken M, Yamaguchi H, Sugihara S, Wolozin B. Presenilin 1 associates with glycogen synthase kinase-3beta and its substrate tau. Proc. Natl. Acad. Sci. U S A. 1998;95:9637-9641.

219. Takeuchi Y, Uetsuka K, Murayama M, Kikuta F, Takashima A, Doi K, Nakayama H. Complementary distributions of amyloid-beta and neprilysin in the brains of dogs and cats. Vet. Pathol. 2008;45:455-466.

220. Tapp PD, Head K, Head E, Milgram NW, Muggenburg BA, Su MY. Application of an automated voxel-based morphometry technique to assess regional gray and white matter brain atrophy in a canine model of aging. Neuroimage. 2006;29:234-244.

221. Tapp PD, Siwak CT, Estrada J, Head E, Muggenburg BA, Cotman CW, Milgram NW. Size and reversal learning in the beagle dog as a measure of executive function and inhibitory control in aging. Learn Mem. 2003;10:64-73.

222. Tapp PD, Siwak CT, Estrada J, Holowachuk D, Milgram NW. Effects of age on measures of complex working memory span in the beagle dog (canis familiaris) using two versions of a spatial list learning paradigm. Learn Mem 2003;10:148-160.

223. Tapp PD, Siwak CT, Gao FQ, Chiou JY, Black SE, Head E, Muggenburg BA, Cotman CW, Milgram NW, Su MY. Frontal lobe volume, function, and beta-amyloid pathology in a canine model of aging. J. Neurosci. 2004;24:8205-8213.

224. Tekirian TL. Commentary: Abeta N- terminal isoforms: Critical contributors in the course of AD pathophysiology. J. Alzheimers Dis. 2001;3:241-248.

225. Tekirian TL, Cole GM, Russell MJ, Yang F, Wekstein DR, Patel E, Snowdon DA, Markesbery WR, Geddes JW. Carboxy terminal of beta-amyloid deposits in aged human, canine, and polar bear brains. Neurobiol. Aging. 1996;17:249-257.

226. Thal DR, Capetillo-Zarate E, Larionov S, Staufenbiel M, Zurbruegg S, Beckmann N. Capillary cerebral amyloid angiopathy is associated with vessel occlusion and cerebral blood flow disturbances. Neurobiol. Aging. 2009;30:1936-1948.

227. Thal DR, Ghebremedhin E, Rub U, Yamaguchi H, Del Tredici K, Braak H. Two types of sporadic cerebral amyloid angiopathy. J. Neuropathol. Exp. Neurol. 2002;61:282-293.

228. Thal DR, Grinberg LT, Attems J. Vascular dementia: different forms of vessel disorders contribute to the development of dementia in the elderly brain. Exp. Gerontol. 2012;47:816-824.

229. Thal DR, Larionov S, Abramowski D, Wiederhold KH, Van Dooren T, Yamaguchi H, Haass C, Van Leuven F, Staufenbiel M, Capetillo-Zarate E. Occurrence and co-localization of amyloid beta-protein and apolipoprotein E in perivascular drainage channels of wild-type and APP-transgenic mice. Neurobiol. Aging. 2007;28:1221-1230.

230. Thal DR, Rüb U, Orantes M, Braak H. Phases of A beta-deposition in the human brain and its relevance for the development of AD. Neurology. 2002;58:1791-1800.

231. Togo T, Sahara N, Yen SH, Cookson N, Ishizawa T, Hutton M, de Silva R, Lees A, Dickson DW. Argyrophilic grain disease is a sporadic 4-repeat tauopathy. J. Neuropathol. Exp. Neurol. 2002;61:547-556.

232. Tolnay M, Probst A. REVIEW: tau protein pathology in Alzheimer's disease and related disorders. Neuropathol. Appl. Neurobiol. 1999;25:171-187.

233. Tomiyama T, Asano S, Furiya Y, Shirasawa T, Endo N, Mori H. Racemization of Asp23 residue affects the aggregation properties of Alzheimer amyloid beta protein analogues. J. Biol. Chem. 1994;269:10205-10208.

234. Tomiyama T, Matsuyama S, Iso H, Umeda T, Takuma H, Ohnishi K, Ishibashi K, Teraoka R, Sakama N, Yamashita T, Nishitsuji K, Ito K, Shimada H, Lambert MP, Klein WL, Mori H. A mouse model of amyloid beta oligomers: their contribution

to synaptic alteration, abnormal tau phosphorylation, glial activation, and neuronal loss in vivo. J. Neurosci. 2010;30:4845-4856.

235. Trembath D, Ervin JF, Broom L, Szymanski M, Welsh-Bohmer K, Pieper C, Hulette CM. The distribution of cerebrovascular amyloid in Alzheimer's disease varies with ApoE genotype. Acta Neuropathol. 2007;113:23-31.

236. Turner AJ. Proteolytic enzymes. In: Barrett AJ editor. Proteolytic enzymes : aspartic and metallo peptidases. San Diego: Academic Press. 1995;1080-1085.

237. Uchida K, Miyauchi Y, Nakayama H, Goto N. Amyloid angiopathy with cerebral hemorrhage and senile plaque in aged dogs. Nihon Juigaku Zasshi. 1990;52:605-611.

238. Uchida K, Nakayama H, Goto N. Pathological studies on cerebral amyloid angiopathy, senile plaques and amyloid deposition in visceral organs in aged dogs. J. Vet. Med. Sci. 1991;53:1037-1042.

239. Uchida K, Nakayama H, Tateyama S, Goto N. Immunohistochemical analysis of constituents of senile plaques and cerebro-vascular amyloid in aged dogs. J. Vet. Med. Sci. 1992;54:1023-1029.

240. Uchida K, Tani Y, Uetsuka K, Nakayama H, Goto N. Immunohistochemical studies on canine cerebral amyloid angiopathy and senile plaques. J. Vet. Med. Sci. 1992;54:659-667.

241. Uchida K, Yoshino T, Yamaguchi R, Tateyama S, Kimoto Y, Nakayama H, Goto N. Senile plaques and other senile changes in the brain of an aged American black bear. Vet. Pathol. 1995;32:412-414.

242. Uh J, Lewis-Amezcua K, Martin-Cook K, Cheng Y, Weiner M, Diaz-Arrastia R, Devous MSr, Shen D, Lu H. Cerebral blood volume in Alzheimer's disease and correlation with tissue structural integrity. Neurobiol. Aging. 2010;31:2038-2046.

243. Umeda T, Maekawa S, Kimura T, Takashima A, Tomiyama T, Mori H. Neurofibrillary tangle formation by introducing wild-type human tau into APP transgenic mice. Acta Neuropathol. 2014; 127:685-698.

244. Vanderstichele H, De Meyer G, Andreasen N, Kostanjevecki V, Wallin A, Olsson A, Blennow K, Vanmechelen E. Amino-truncated beta-amyloid42 peptides in cerebrospinal fluid and prediction of progression of mild cognitive impairment. Clin. Chem. 2005;51:1650-1660.

245. Varadarajan S, Yatin S, Aksenova M, Butterfield DA. Review: Alzheimer's amyloid beta-peptide-associated free radical oxidative stress and neurotoxicity. J. Struct. Biol. 2000;130:184-208.

246. Vassar R, Bennett BD, Babu-Khan S, Kahn S, Mendiaz EA, Denis P, Teplow DB, Ross S, Amarante P, Loeloff R, Luo Y, Fisher S, Fuller J, Edenson S, Lile J, Jarosinski MA, Biere AL, Curran E, Burgess T, Louis JC, Collins F, Treanor J, Rogers G, Citron M. Beta-secretase cleavage of Alzheimer's amyloid precursor protein by the transmembrane aspartic protease BACE. Science. 1999;286:735-741.

247. Walker LC. Animal models of cerebral beta-amyloid angiopathy. Brain Res. Brain Res. Rev. 1997;25:70-84.

248. Walker LC, Kitt CA, Schwam E, Buckwald B, Garcia F, Sepinwall J, Price DL.

Senile plaques in aged squirrel monkeys. Neurobiol. Aging. 1987;8:291-296.

249. Walker LC, Masters C, Beyreuther K, Price DL. Amyloid in the brains of aged squirrel monkeys. Acta Neuropathol. 1990;80:381-387.

250. Walsh DM, Minogue AM, Sala Frigerio C, Fadeeva JV, Wasco W, Selkoe DJ. The APP family of proteins: similarities and differences. Biochem. Soc. Trans. 2007; 35:416-420.

251. Walsh DM, Selkoe DJ. Deciphering the molecular basis of memory failure in Alzheimer's disease. Neuron. 2004;44:181-193.

252. Wang DS, Lipton RB, Katz MJ, Davies P, Buschke H, Kuslansky G, Verghese J, Younkin SG, Eckman C, Dickson DW. Decreased neprilysin immunoreactivity in Alzheimer disease, but not in pathological aging. J. Neuropathol. Exp. Neurol. 2005;64:378-385.

253. Weller RO, Djuanda E, Yow HY, Carare RO. Lymphatic drainage of the brain and the pathophysiology of neurological disease. Acta Neuropathol. 2009;117:1-14.

254. Weller RO, Massey A, Newman TA, Hutchings M, Kuo YM, Roher AE. Cerebral amyloid angiopathy: amyloid beta accumulates in putative interstitial fluid drainage pathways in Alzheimer's disease. Am. J. Pathol. 1998;153:725-733.

255. Weller RO, Subash M, Preston SD, Mazanti I, Carare RO. Perivascular drainage of amyloid-beta peptides from the brain and its failure in cerebral amyloid angiopathy and Alzheimer's disease. Brain Pathol. 2008;18:253-266.

256. Wilhelmus MM, Otte-Holler I, van Triel JJ, Veerhuis R, Maat-Schieman ML, Bu G, de Waal RM, Verbeek MM. Lipoprotein receptor-related protein-1 mediates

amyloid-beta-mediated cell death of cerebrovascular cells. Am. J. Pathol. 2007;171:1989-1999.

257. Wirths O, Breyhan H, Cynis H, Schilling S, Demuth HU, Bayer TA. Intraneuronal pyroglutamate-abeta 3-42 triggers neurodegeneration and lethal neurological deficits in a transgenic mouse model. Acta Neuropathol. 2009;118:487-496.

258. Wisniewski HM, Ghetti B, Terry RD. Neuritic (senile) plaques and filamentous changes in aged rhesus monkeys. J. Neuropathol. Exp. Neurol. 1973;32:566-584.

259. Wisniewski T, Sigurdsson EM. Murine models of Alzheimer's disease and their use in developing immunotherapies. Biochim. Biophys. Acta. 2010;1802:847-859.

260. Xu J, Chen S, Ahmed SH, Chen H, Ku G, Goldberg MP, Hsu CY. Amyloid-beta peptides are cytotoxic to oligodendrocytes. J. Neurosci. 2001;21:RC118.

261. Yamada T, Sasaki H, Furuya H, Miyata T, Goto I, Sakaki Y. Complementary DNA for the mouse homolog of the human amyloid beta protein precursor. Biochem. Biophys. Res. Commun. 1987;149:665-671.

262. Yamaguchi H, Ishiguro K, Uchida T, Takashima A, Lemere CA, Imahori K. Preferential labeling of Alzheimer neurofibrillary tangles with antisera for tau protein kinase (TPK) I/glycogen synthase kinase-3 beta and cyclin-dependent kinase 5, a component of TPK II. Acta Neuropathol. 1996;92:232-241.

263. Yamamoto Y, Ihara M, Tham C, Low RW, Slade JY, Moss T, Oakley AE, Polvikoski T, Kalaria RN. Neuropathological correlates of temporal pole white matter hyperintensities in CADASIL. Stroke. 2009;40:2004-2011.

264. Yasojima K, Akiyama H, McGeer EG, McGeer PL. Reduced neprilysin in high

plaque areas of Alzheimer brain: a possible relationship to deficient degradation of beta-amyloid peptide. Neurosci. Lett. 2001;297:97-100.

265. Yoshida M. Cellular tau pathology and immunohistochemical study of tau isoforms in sporadic tauopathies. Neuropathology. 2006;26:457-470.

266. Yoshino T, Uchida K, Tateyama S, Yamaguchi R, Nakayama H, Goto N. A retrospective study of canine senile plaques and cerebral amyloid angiopathy. Vet. Pathol. 1996;33:230-234.

267. Zicker SC, Ward P, Head E. Dogs of different breeds are apolipoprotein E4 homozygous by PCR-RFLP. J. Vet. Intern. Med. 2008;22:811.